An optical study of uniaxial stress effects on point defects in diamond.

Foy, C P

An Optical Study of Uniaxial Stress Effects on Point Defects in Diamond

A thesis submitted for the degree of Doctor of Philosophy in the University of London

by

Colleen Patricia Foy

Wheatstone Physics Laboratory, Kings' College, University of London.

February 1980

For John

ABSTRACT

Diamond is very unusual in that it is sufficiently simple to be regarded as a fundamental material and yet has great commercial value.From the point of view of basic science, atomic-sized defects in diamond can be regarded as the prototypes of defects in all other covalent crystals, so a detailed study of them will have far reaching applications.Before any model of a defect centre can be made, its symmetry must be known.Various experimental methods exist for determining the symmetry of a centre and this thesis describes the use of uniaxial stress measurements.The application of uniaxial stress can lift the degeneracy, both orientational and electronic, at a defect centre and this removal of the degeneracy can be detected by observation of the splitting of optical absorption and luminescence lines in the spectrum of each defect.This thesis reports the application of uniaxial stress analysis to four different defect centres in diamond, all of which had been created by electron irradiation.

The main defect centre studied was the GR centre which is produced in all types of diamond; the work reported here has yielded furhter information about the ground and excited states of this interesting centre, including its Jahn-Teller properties.The higher energy GR 2-8 lines have also been investigated and their stress behaviour explained.

The zero phonon lines at 2.639eV. and 2.672eV. produced in type II diamonds and known as TR12 and TR13 have been investigated in both absorption and luminescence and the symmetry of the optical centre at which they occur confirmed.Some further information on the energy levels at this centre is also given.

Lastly, uniaxial stress measurements have been made on two

hitherto unreported zero phonon lines produced at 1.795eV. and 2.358eV. in type Ib diamonds.

The work reported in this thesis further illustrates the usefulness of uniaxial stress analysis which has already been successfully used in the investigation of many defect centres.

ACKNOWLEDGEMENTS

My warmest thanks go to Dr. Gordon Davies who has supervised this work and who has always cheerfully given help and advice.I would also like to thank Dr. E. C. Lightowlers and Dr. A. T. Collins for their advice and helpful suggestions for the experimental aspects of this work.Discussions with Dr. A. Mainwood and Dr. K. O'Donnell have been stimulating and fruitful and Dr. M. O. Henry has not only helped with such exercises as transferring liquid helium but has also been a constant source of cheerfulness and humour.

Thanks also go to the technical staff of the Physics Research Department who have always been ready to help with any apparatus problems.

I thank my fellow postgraduate students for sharing the ups and downs of my research work and lastly I thank the S.R.C. for providing the studentship that enabled me to do this work.

PUBLICATIONS

Most of the work described in Chapter III is to be published in the Journal of Physics, C13.Some of the contents of Chapter IV are also to be published by the same journal.The work on the GR2-3 lines has been published in the Journal of Physics, C11, and that on the GR4-8 lines in the Journal of Physics, C13.

A paper on the GR2-4 lines was read at the Diamond Conference, Oxford, in 1978 and papers on the optical properties of the GR1 system and on the TR12 and TR13 lines were read at the Diamond Conference, Cambridge, in 1979.

CONTENTS

FIGURE CAPTIONS

Throughout this work, π denotes "electric vector of the light parallel to stress", and σ denotes the perpendicular polarisation.Where necessary σ_{hkl} is used for "electric vector along the hkl axis".
In the stress response diagrams crosses show the π polarisation, circles the σ polarisation where •• show the $\sigma_{1\bar{1}0}$ polarisation and ∘∘ the σ_{001} polarisation.In the diagrams of sample spectra bold lines represent π polarisation, dotted lines represent σ polarisation.

CHAPTER I

An Outline of the Properties of Defects in Diamond

Introduction:

Diamond can be regarded as the prototype of the Group IV semiconductors; the optical properties of the defects in diamond are at present understood in far greater detail than the corresponding properties of defects in silicon or germanium.In this chapter we present a brief outline of defect creation by electron irradiation and discuss the importance of the symmetry of defect systems.We also list the various experimental methods which have been used to investigate these symmetries, paying particular attention to uniaxial stress techniques.

1.The Classification of Diamond.

Every owner of a gem quality diamond likes to feel that her diamond is unique; indeed, jewellery advertisements constantly tell us that no two diamonds are alike.In favour of this assertion is the fact that diamond is a natural mineral and likely to be of the order of 10^9 years old so that over the years radiation damage may have occurred, imperfections may have been created, diffusion of impurities may have taken place, so that each diamond may well be different from all others.

It is the impurity content of diamond which provides a means of classifying diamonds into a few "types", even though the impurities are only present as small fractions of an atomic percent.Within each "type" the diamonds contain the same impurities in similar proportions and show qualitatively the same behaviour. The "type" classification generally used for diamond is based on the variations in shape of the impurity-induced infra-red absorption spectrum at wavenumbers below about 1400cm^{-1} (that is, wavelengths

greater than 7.14μm.).Using this basis diamonds have been classified as type I, with subgroups IaA, IaB, Ib, and type II, with subgroups IIa, IIb; type I diamonds contain nitrogen as the major impurity whereas in type II diamonds nitrogen is only weakly present.

It is now generally accepted that the nitrogen in type Ia diamonds is present in two forms which are identifiable from their infra-red spectra; these forms are called the A and B forms (Sutherland et al, 1954).Both these forms are known to be non-paramagnetic, indicating that they contain even numbers of nitrogen atoms to allow spin-pairing. The evidence is that both the A and B forms are substitutional nitrogen aggregates.Davies (1977a) has shown that the A aggregate is composed of a pair of nearest neighbour substitutional nitrogen atoms; the exact form of the B aggregate has not yet been established but the indications are that it contains an even number of nitrogen atoms with not more than about eight atoms per aggregate (Davies, 1977b).

Only about 0.1% of natural diamond is of type Ib, whereas about 98% is of type Ia (Dyer et al, 1965).E.s.r. work (Smith et al, 1959) has confirmed that the nitrogen in type Ib diamond is in the form of single substitutional nitrogen atoms.Virtually all commercially produced synthetic diamond is of type Ib and it is interesting to note that the isolated substitutional impurity in synthetic diamond may be transformed into the A-aggregate form by heating at high temperatures (Chrenko et al, 1977); this is an indication that the aggregated nitrogen in natural diamonds has formed during the long time spent at the high temperatures present deep in the earth's crust.

Kaiser and Bond (1959) were the first to recognise nitrogen as the major impurity in many diamonds, and for many years after their discovery the nitrogen in diamond was considered to be responsible for the platelets lying in (100) planes.Evans and Phaal (1962) have

shown that the lattice on either side of the platelets is under compression; the resulting strain field is responsible for the X-ray spikes along the (100) directions in reciprocal space reported by Hoerni and Wooster (1955).Sobolev et al (1968) could find no correlation between the optical absorption at 7.8μm. (the strength of this gives a measure of the nitrogen content) and the integrated X-ray spike intensity.This showed that the platelets were not composed mainly of nitrogen.Evans (1973) has proposed that the platelets are associated with the precipitation of interstitial carbon atoms.

Large natural type IIb diamonds are rare.The characteristic property of type IIb diamonds is that they are p-type semiconducting. Custers (1952) discovered semiconducting diamond when his type II specimen exhibited phosphorescence after irradiation with ultra-violet light; he also found that his crystal was a poor insulator when compared with other diamonds.He called his type of diamond type IIb in order to distinguish it from the insulating type IIa.The properties of type IIb diamonds indicate that only one species of defect is the acceptor centre.For some years this was assumed to be aluminium since aluminium is present in most diamonds and various workers had shown that the aluminium concentration in several type IIb diamonds was almost equal to the acceptor concentrations in the same specimens. However, Collins and Williams (1971) made Hall effect and resistivity measurements on type IIb diamond; the resistivity measurements were characteristic of a single acceptor centre and the Hall effect data gave the concentration of donors and acceptors.They then used slow neutron activation analysis to measure the concentration of aluminium in their samples and this was found to be much lower that the acceptor concentration.They therefore concluded that the aluminium was not the acceptor centre.Boron was the only group III element

that neutron activation analysis did not eliminate as the possible acceptor.It is therefore now generally accepted that boron is the acceptor in type IIb diamonds.

Compared with type I diamonds ,type IIb diamonds have low impurity concentrations; it is for this reason that they were used in the analysis of the GR band to be described later, since impurities such as nitrogen give rise to significant broadening of sharp zero phonon lines.

The classification of type IIa diamond is not so clear cut as the previous cases.Type IIa diamond is defined as that which has no detectable infra-red absorption below about 1332cm^{-1} (that is, below about 0.16eV.).The type IIa specimens analysed, however, contain concentrations of nitrogen which are at least two orders of magnitude greater than in type IIb diamonds, so the type IIa classification will probably disappear once higher sensitivity methods of detecting A and B nitrogen have been developed.

2.Defects in Diamond.

The perfect diamond lattice consists of carbon atoms covalently bonded by sp^3 orbitals; there is a perfect tetrahedral environment for each atom.The lattice is face-centred cubic with each lattice point shared by a basis of two carbon atoms, each displaced $\pm$(1/8, 1/8,1/8) along the body diagonal.This perfect lattice cannot absorb radiation with the direct production of 1 phonon since there is no first order change in electric dipole moment produced by any vibrational mode (Lax and Bernstein, 1955).However, absorption involving two phonons can occur.This can be explained as follows: one phonon breaks the translational symmetry of the crystal, allowing local fluctuations of the charges on each atom.Radiation can couple to these instantaneous dipoles and so can be absorbed with the creation of a second phonon. The introduction of a defect into a perfect lattice also breaks the

translational symmetry; the defect modifies the electron energy levels from the perfect lattice band structure, giving rise to localised electron orbitals centred on the defect.There are two extreme examples of defects: a) those whose properties are characterised by the defect itself, with only a weak crystal field perturbation from the rest of the lattice, and b) those whose properties are governed by the lattice with only a minor "central cell" correction for the chemical nature of the defect.Most defects in diamond are intermediate between these two extremes.

A defect centre in a cubic crystal is characterised by its point symmetry group, which is a subgroup of the cubic group of the crystal.Its symmetry elements must coincide with the elements of the same or higher symmetry in the crystal.The possible defect symmetry groups in a cubic crystal can be classified into eight symmetry systems.Each system is distinguished by a smallest common set of symmetry elements with particular orientations in the crystal.The eight symmetry systems are: cubic (T, O, T_h, T_d, O_h) whose symmetry axes must coincide with the lattice axes; triclinic (C_1 or S_2) for which there are no restrictions on defect orientation; tetragonal (D_{4h}, $D_4, C_{4v}, D_{2d}, C_{4h}, S_4, C_4$); trigonal ($D_{3d}, D_3, C_{3v}, S_6, C_3$); rhombic I (D_{2h}, D_2, C_{2v}); rhombic II (D_{2h}, D_2, C_{2v}); monoclinic I (C_{2h}, C_2, C_{1h}); monoclinic II (C_{2h}, C_2, C_{1h}).Six of the eight possible symmetry systems are shown schematically in figure 1.1 (after Kaplyanskii, 1964a). Orientation degeneracy occurs at centres in cubic crystals which have non-cubic symmetry but degeneracy can also occur in a strictly cubic field.This type of degeneracy can occur with respect to states of the host crystal or in the local state levels of individual defects situated in the lattice in a cubic field.The methods of resolving these degeneracies will be discussed in section 1.4.

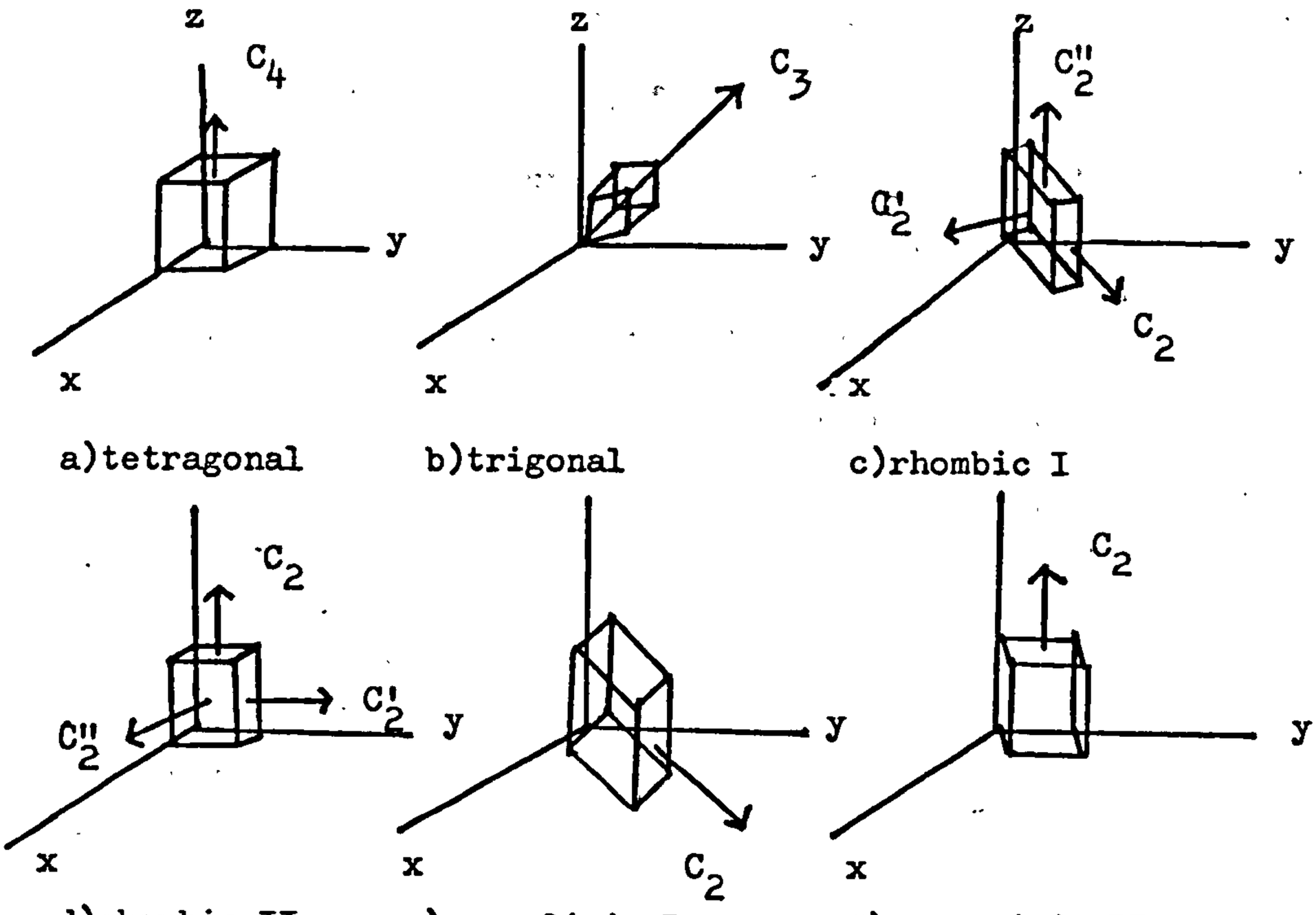

a)tetragonal b)trigonal c)rhombic I

d)rhombic II e)monoclinic I f)monoclinic II

Figure 1.1

3.Defect Production by Electron Irradiation.

If a detailed study of defects is to be made the defects must be present in sufficiently high concentration.Several techniques can be used to increase the defect concentration above the thermal equilibrium value; in this work electron irradiation was used to create the defect centres, though neutrons and gamma rays could also have been used.

Defect production by energetic particles depends on both the nature and energy of the incident particle and on the bonding and crystal structure of the irradiated solid.An incident particle can share its energy with an atom in the solid, which, as a result, may be ejected from its normal lattice site, leaving behind a vacancy; this atom may then go into an interstitial site.The displacement energy, E_d, represents the sum of the energy needed to overcome the binding energy of an atom in its lattice site, the energy required to

overcome the opposition of the lattice to the movement of the displaced atom and the energy regained in establishing bonds at whatever lattice site the atom comes to rest.If an atom in a lattice site does not gain sufficient energy from an incident particle it will not be displaced but instead the energy will be dissipated through vibrational motion. This simple picture implies that E_d has a discrete value in crystalline solids; if this were the case then the probability displacement curve would be a step function, as shown in figure 1.2.

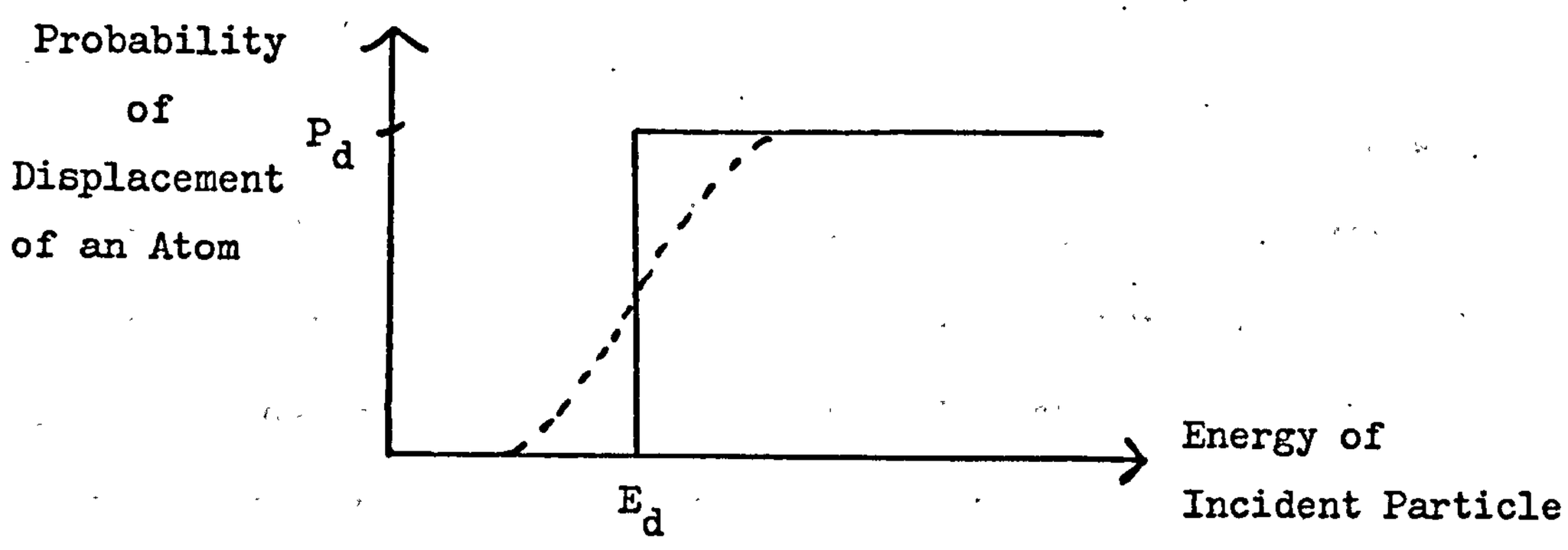

Figure 1.2

Thermal vibrations broaden this curve appreciably but more important are the effects of the ordered crystal lattice on the displacement process; E_d thus becomes a function of both temperature and crystal symmetry.These effects give a curve similar to the dotted curve in figure 1.2, and E_d can be taken as the energy transfered to an atom when the probability for displacement in an arbitrary direction and at a given temperature is $\frac{1}{2}$.

E_d can be found experimentally by comparing the computed curve for defect production as a function of primary electron energy with an observed parameter change.The theoretical curve for defect production may be found, for example, by the methods given by Mitchell (1965).Clark et al (1961) have compared the computed curve with the experimental results for the growth of the GR band in

diamond and have obtained a best fit with $E_d \sim 80eV$.

Apart from an initial impact of an incident particle with an atom subsequent collisions may also cause displacements.The primary knock-on events are often very energetic and they can therefore cause further events as they move through the lattice; the most important of these are electron excitation and ionisation together with the production of further knock-ons.The energy of a displaced atom is therefore degraded by interactions with other atoms until the energy available is less than E_d; the displaced atom then comes to rest in an interstitial site dissipating its remaining energy by exciting lattice vibrations.

The effects of electron irradiation and neutron and gamma ray irradiation of diamond are very similar; the only real difference between the two types of bombardment is that neutron and gamma ray irradiation damage gives optical centres that are more highly perturbed by nearby centres than the centres resulting from electron damage.This is a result of the tendency for multiple damage to occur during neutron and gamma ray irradiation; in particular, gamma ray irradiation works via an intermediate process whereby, for example, e^- and e^+ pairs are created and these go on to cause the damage.

All the diamonds used in the experiments described in this thesis had been irradiated at room temperature with electrons from the Reading University Van der Graaff accelerator.The dose was typically of the order of $2x10^{21}m^{-2}$ 2MeV electrons at a current density of approximately $0.15Am^{-2}$, and the crystals were 1mm. or 2mm. cubes.

Using the values for displacement cross-sections given by Mitchell (1965) an estimate of the density of the displaced atoms, n_d, can be made:

n_d=(number of incident electrons m^{-2})x(number of atoms m^{-3})
x(displacement cross-section)

$$n_d = n_e \times n_a \times \sigma_d \qquad 1.1$$

Now, $n_e = 2\times10^{21}$ m^{-2} and, for diamond,

$n_a = 1.65\times10^{29}$ m^{-3}.

For E_d= 80eV. and 2MeV. electrons, $\sigma_d = 4.79\times10^{-28}$ m^2. Thus

$$n_d = (2\times10^{21}) \times (1.65\times10^{29}) \times (4.79\times10^{-28})$$

$$n_d = 1.5807\times10^{23}$$

i.e. this radiation can displace $\sim 1.6 \times 10^{23}$ atoms per metre^3.

One of the visible effects of radiation damage in diamond is a possible colour change caused by the absorbing properties of the defect which has been created.In particular, electron irradiation of type IIb diamond creates the GR bands which absorb both red and ultra-violet light leaving a window in the blue part of the spectrum.Diamonds containing the GR band are therefore blue or bluish-green.

4.The Removal of Degeneracy in Defect Systems.

Defect centres can be broadly classified into three types in terms of their possible degeneracies.These are: i) anisotropic centres possessing purely orientational degeneracy, i.e. having non-degenerate or Kramers doublet energy levels, ii) centres of cubic symmetry in cubic crystals where only electronic degeneracy is involved, and iii) trigonal and tetragonal centres where both orientation and electronic degeneracy are present.In order to investigate these centres it is necessary to introduce some perturbation which will lift the degeneracy.The theory of the removal of degeneracy by uniaxial stress perturbations will be given in Chapter 2; in this section an outline of the basic experimental methods of lifting degeneracy and thus determining symmetry is presented.

The four main methods used are; i) the Zeeman effect, ii) polarisation of luminescence, iii) the Stark effect, iv) uniaxial stress.Polarisation of luminescence differs from the other three methods

in that no specific perturbation is applied to lift the degeneracy.In this method polarised excitation light is used to preferentially excite some centres; providing there is no reorientation of the excited centres any luminescence from them will be anisotropic (Feofilov, 1954).This technique cannot be applied to non-emissive centres and cannot give the direction of a transition (i.e. it cannot distinguish whether a transition is, for example, A to E or E to A); also, if centres can reorient in a time comparable with the emission lifetime, the crystal loses its anisotropy and the method fails.This problem is not present with techniques which apply a perturbation to lift the degeneracy; in these experiments the isotropy of the lattice is destroyed by making centres with different orientations with respect to the applied field absorb light at different frequencies.The effect of uniaxial stress on orientational degeneracy is to make some orientations more favourable than others.Degeneracy in the initial state may be distinguished from that in the final state by temperature dependence measurements of stress-split components.Unfortunately stress splittings cannot distinguish between models of centres which differ only in their inversion symmetry and so results of this type of experiment may suggest a higher symmetry for the centre than is actually valid.Also, external stresses can only align defects so that they have a common axis rather than a common orientation along the axis.One important aspect of stress work which is relevant to the analysis of the GR bands discussed in Chapter 3 is that the magnitude of the splittings of the spectral lines caused by the applied stress give the electron-lattice coupling coefficients.

The maximum orbital degeneracy possible for a defect centre in diamond is 3; the angular momentum quantum number is therefore small and fairly simple Zeeman splitting patterns are produced when a

magnetic field is applied across a specimen.Zeeman spectroscopy also gives spin information on a defect, which the other methods mentioned here do not.Unfortunately the magnitude of the magnetic fields required to produce Zeeman splitting in diamond are very large so this technique is not widely used.The perturbation caused by an electric field applied along a z-axis, say, in a crystal can be written as

$$V_E = eEz$$

In this expression V_E has odd parity and its expectation value is therefore zero in any state which has definite parity, that is, V_E has zero expectation value for any state of a defect which has inversion symmetry.There is therefore no linear Stark effect for defects with inversio: symmetry.(There is no linear Stark effect if the linear coupling is zero, either.) In these centres the quadratic Stark effect can still occur so these electric field perturbations allow centres without inversion symmetry to be identified.The Stark effect is generally difficult to detect since the line widths involved are usually much larger than the shifts caused by the electric field.However, Kaplyanskii et al (1970) have developed a method for testing the inversion symmetry of a centre by observing the Stark effect on the zero phonon line of the centre. When an electric field of frequency f is applied a component in the differential absorption is observed at 2f.The spectral shape resembles the second derivative of the zero phonon line when there is a linear Stark effect but the first derivative for a quadratic effect.This technique has recently been applied to several centres in diamond (Davies and Manson, 1979).

5.Uniaxial Stress Experiments.

In the present work uniaxial stress experiments were used to investigate the symmetries and properties of various defects; these experiments are fairly straightforward to perform, the bulk of the

work being in the subsequent analysis.The samples used were 1mm. or 2mm. cubes which had been carefully cut to have (001)(110)($1\bar{1}0$) or (111)($1\bar{1}0$)($11\bar{2}$) faces.When the stress was applied it could therefore be applied parallel to one of these faces.All the samples had been irradiated as described earlier.

The experiments were usually performed with the samples held at liquid nitrogen temperature in the stress cell shown in figure 1.3 (this cell was designed by Dr.E.C.Lightowlers); the cell was placed in the liquid nitrogen dewar as shown.An oil ram pressed on a long steel rod which was in contact with a steel piston; the sample was placed centrally between two steel pistons.A double layer of metal foil measuring about 3mm.x3mm. was glued to the surface of each piston using low temperature varnish to ensure that the stress was evenly distributed to the diamond.The temperature of the sample was that of the boil-off gas from the liquid nitrogen and the temperature was kept steady by ensuring that the liquid nitrogen level in the inner container remained fairly constant.Using this apparatus stresses of up to 3GPa. were applied to the samples.

In all the uniaxial stress absorption experiments light from a 100w. tungsten filament lamp passed through the sample in a direction perpendicular to the applied stress; the electric vector of the light could therefore be resolved parallel or perpendicular to the stress direction by using a polaroid filter.The light transmitted by the sample was received by a 1m. Jarrall Ash monochromator fitted with an E.M.I. photomultiplier.The d.c. signal was displayed on strip chart for analysis.Several absorption experiments were performed with the samples held at 10K and for these experiments the stress cell was placed in a helium gas flow dewar.

The splittings of the spectral lines caused by the uniaxial

The Stress Cell and Nitrogen Dewar.

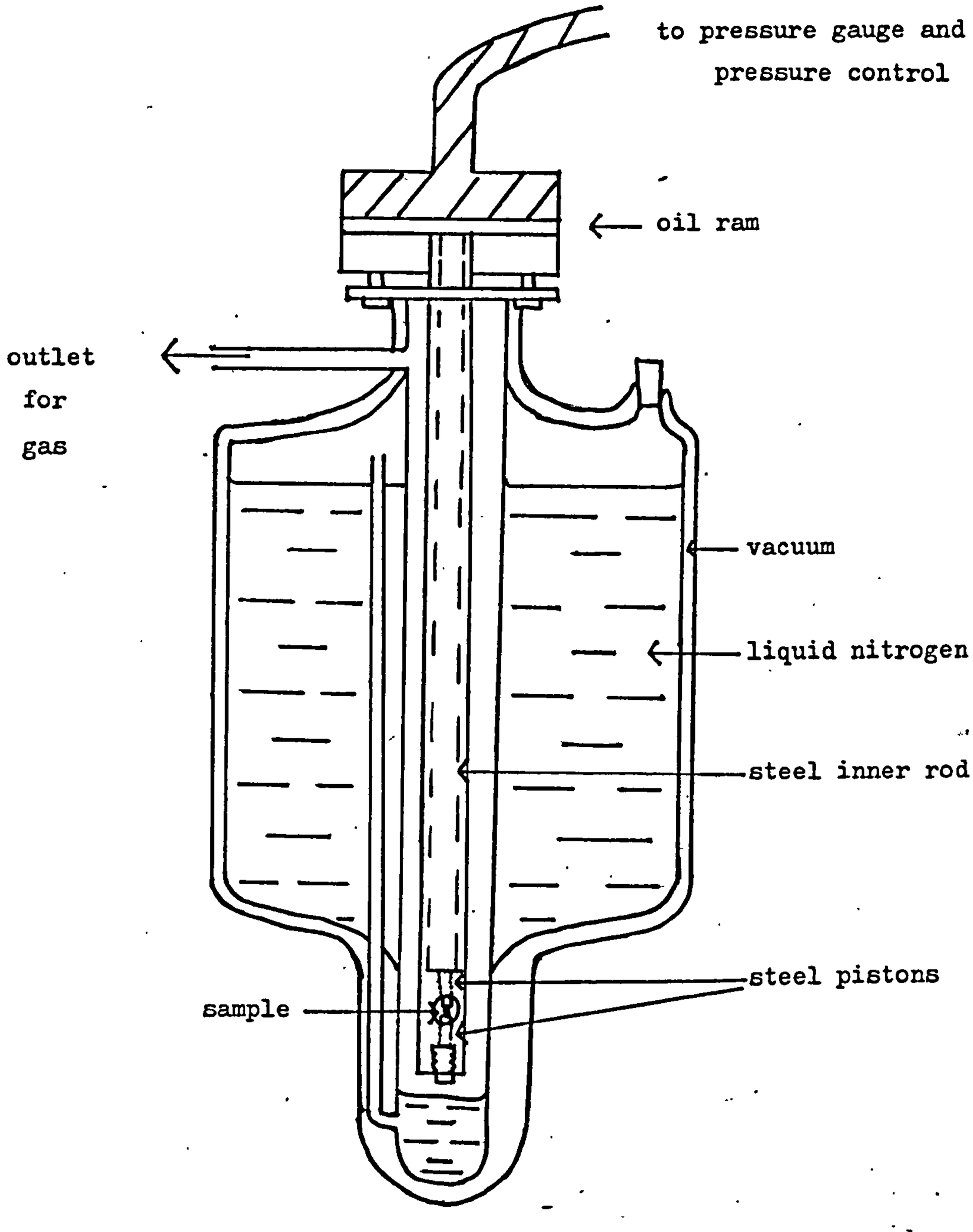

Figure 1.3

stresses were usually greater than the widths of the lines, making this method of analysis an accurate and useful one.

CHAPTER II

Some Theoretical Aspects of Optical Transitions in Diamond

Introduction:

A defect atom has its electronic structure determined by linear combinations of the atomic orbitals of itself and its neighbours.It is therefore, to some extent, a molecular complex encased in a lattice. Any treatment of an optical transition must also take account of its effect on the lattice.In this chapter we describe how the Born-Oppenheimer approximation and the Franck-Condon Principle enable a description of the electron-lattice coupling to be given.We briefly describe the Jahn-Teller Principle and outline the theory necessary for the uniaxial stress analysis.

1.Phonons and Electron-lattice Coupling.

When an electron at a defect centre is excited by the absorption of light, the centre becomes unstable and will therefore try to lower its energy.It can do this by emitting a photon but this deexcitation process has a lifetime of the order of 10 nanoseconds.The characteristic time for lattice vibrations is 10^{-12} to 10^{-13} seconds, so that lattice relaxation with the creation of phonons is the most favourable deexcitation process.

The Hamiltonian for a defect centre is of the form:

$$H = T_e + T_n + V(r,R) \qquad 2.1$$

where T_e and T_n are the electron and nuclear kinetic energy terms and the potential energy term, V(r,R), contains the nuclear repulsion, electron repulsion, and electron-nuclear attraction terms.If this full Hamiltonian were used in the problems involving electronic transitions at defects, the wavefunctions would be very complicated indeed.In order to simplify calculations, therefore, the adiabatic approximation is used.In this approximation, the electronic motion is taken to be much

faster than the nuclear motion so that a nucleus at a defect centre "sees" a potential determined by the entire electron cloud, not by any instantaneous position of the electrons.(This difference in electronic and nuclear motions can be understood by considering electronic transition energies and phonon energies; the former are typically a few electron-volts whereas phonon energies, which give a measure of the nuclear vibrational energies, are of the order of 10's of meV.)The ideas of the adiabatic approximation are used to formulate the Born-Oppenheimer wavefunction for the centre (Born and Oppenheimer, 1927):

$$\Psi(r,R) = \chi^n(R)\psi^n(r,R) \qquad 2.2$$

the r are the electron coordinates and R the nuclear coordinates.χ^n is the vibrational wavefunction in the n^{th} electronic state and ψ^n is the electronic wavefunction.If light is absorbed by a defect with the excitation of an electron then the electron moves from the n^{th} electronic state to the m^{th}, say.The matrix element for the transition is then

$$\int \Psi^n(r,R) \cdot e\underline{r} \cdot \Psi^m(r,R)^* \, drdR \qquad 2.3$$

where $e\underline{r}$ is the perturbation produced by the light.Using the Born-Oppenheimer wavefunction this becomes

$$\int (\chi^n(R)\psi^n(r,R)) e\underline{r} (\chi^m(R)\psi^m(r,R))^* drdR \qquad 2.4$$

Using the Condon approximation, which asserts that the integral over the electronic coordinates is essentially independent of R, equation 2.4 can be factorised to

$$\int \psi^n(r) e\underline{r} \psi^m(r)^* dr \int \chi^n(R)\chi^m(R)^* dR \qquad 2.5$$

Thus the electronic transition can be expressed in terms of an electronic matrix element and a nuclear overlap integral.

When an electron is excited by absorbing light there is a finite probability that no vibrational mode will be excited; this case gives the "zero-phonon" line, where there is no displacement or broadening due to energy transfer to lattice modes.The zero-phonon transition

therefore occurs between the ground vibrational states of the initial and final states.When electron-lattice coupling is significant the transition matrix element is reduced from the corresponding purely electronic case.From equation 2.5 it can be seen that this reduction factor is a vibrational overlap integral.(This reduction of the matrix elements by the electron-lattice coupling analogous to the Ham effect in Jahn-Teller coupling).

The relaxation that occurs when an electron at a defect is excited is opposed by the rest of the lattice; the total energy at the centre is then

$$\mathcal{E} = E_0 - cQ + kQ^2 \qquad 2.6$$

in the approximation where only linear electron-lattice coupling is considered.E_0 is the energy absorbed from the incident photon, Q is a coordinate describing the lattice relaxation and c is the electron-lattice coupling parameter, kQ^2 is the elastic restoring force.(In the harmonic approximation with linear coupling, each mode vibrates independently of all others and it is therefore possible to describe the interaction in terms of just one mode, as in equation 2.6; if more than one mode is considered similar results are obtained (Pryce, 1966))

Equation 2.6 can be rewritten as

$$\mathcal{E} = E_0 + k(Q - c/2k)^2 - c^2/4k \qquad 2.7$$

by completing the square in Q.As with a simple harmonic oscillator the energy is still parabolic in Q, so the centre still vibrates harmonically but now the vibrations occur about an equilibrium position $Q_0 = c/2k$. The electron-lattice coupling has lowered the energy by an amount $c^2/4k$ which is generally of the same order of magnitude as phonon energies and therefore results in phonons being involved in electric dipole transitions.

A configuration coordinate diagram provides a clear method of

describing what can happen during an electronic transition.This diagram shows the total potential energy as a function of a single "effective" mode Q for two different electronic states, and is given in figure 2.1.The Franck-Condon Principle (Franck, 1925, Condon, 1928) is usually involved when using this diagram.According to this, electronic transitions occur with no change in nuclear configuration; a cycle of absorption and emission of light might therefore be as follows:

At low temperatures the defect system will be in the lowest state,A; absorption occurs primarily to B the excited state with the same configuration.As previously explained, non-radiative processes occur rapidly and the system can therefore relax to C with the release of energy $S\hbar\omega$, where S, the "Huang-Rhys factor", is the mean number of quanta, each of energy $\hbar\omega$, emitted.Emission of light will occur

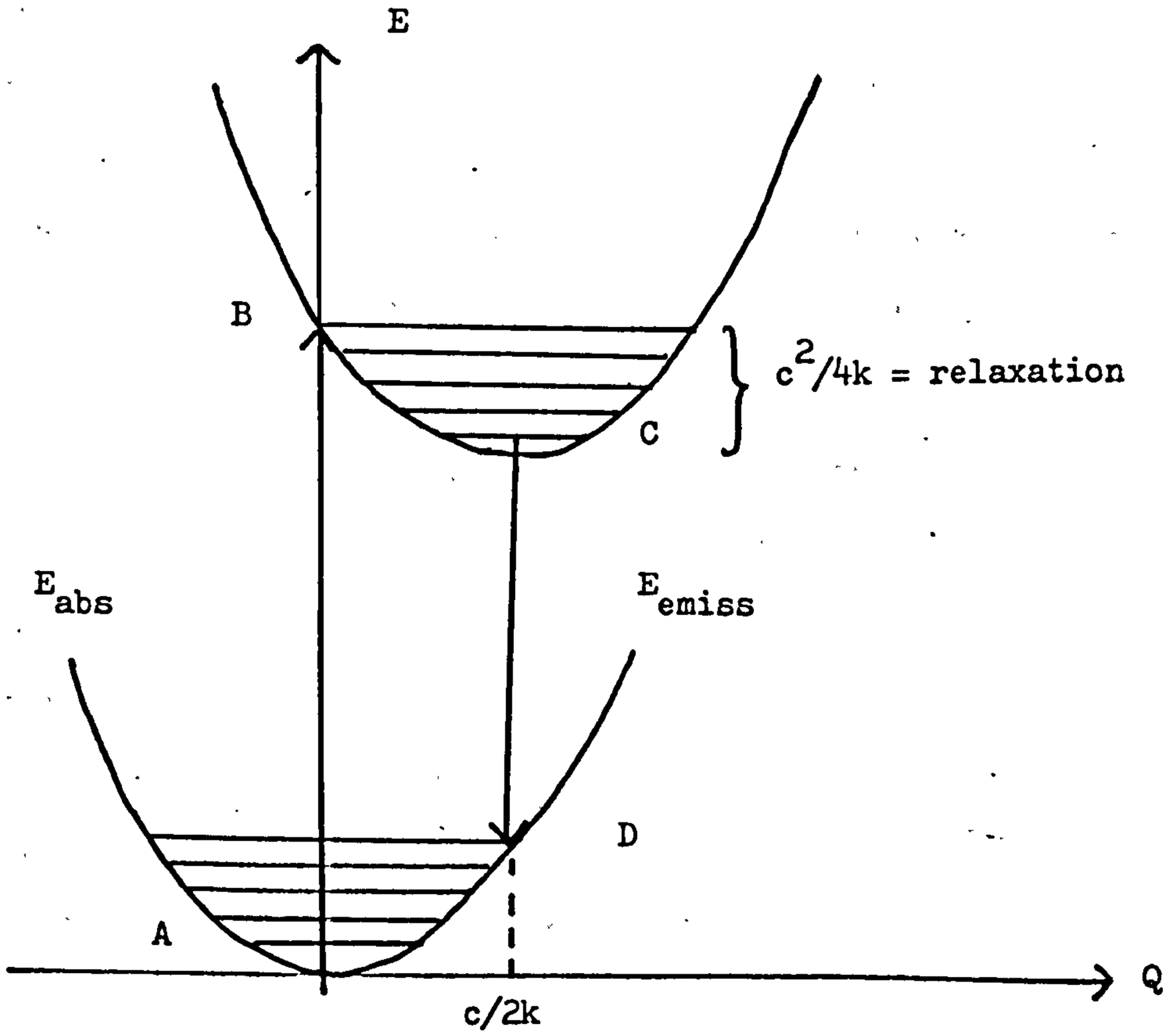

Figure 2.1

primarily in a transition to D at constant configuration.Finally, non-radiative processes will take the system back to its initial state A with the emission of phonon energy $S\hbar\omega$.

As can be seen from equation 2.5, the transition probability for such a transition depends on the overlap of the vibrational wavefunctions in the initial and the final states.In the ground state, A, the vibrational wavefunction is concentrated near $Q = Q_0$.Most of the excited states have their wavefunctions centred near the classical turning points which lie on the upper energy curve; of these, the ones that overlap most strongly with the initial state A are those with turning points at B.The basic point of the Franck-Condon Principle is that only these states need be considered.The principle is used to predict the "most probable transition" which in the above example is from A to B.If the electron-lattice coupling is weak, however, (i.e. c/2k is small) the most probable transition will be the zero-phonon transition from A to C.

The theory of optical spectra resulting from linear electron-lattice coupling is well established (see Pryce, 1966, Fitchen, 1968) One of its conclusions is that the absorption spectrum consists of a series of lines at $E_p = E_0 + p\hbar\omega$, where E_0 is the energy of the zero-phonon line and $p = (n-m)$ indicates the net change in vibrational level, or the number of vibrational quanta excited in the transitions; $\omega$is the frequency of vibration in the case where all the coupled modes have the same frequency.The transition probability for a transition involving p quanta is then

$$W_p = \frac{e^{-S} \cdot S^p}{p!} \qquad (\text{at } T = 0K) \qquad 2.8$$

where S is also given by

$$S = \frac{c^2/4k}{\hbar\omega} = \frac{\text{relaxation energy}}{\text{energy of vibrational quantum}} \qquad 2.9$$

as mentioned earlier.For the zero-phonon line the transition probability is thus

$$W_0 = e^{-S}$$

The magnitude of S depends on the strength of the electron-lattice coupling and this therefore determines the fraction of the total intensity of the transition which appears in the zero-phonon line. For $S > 5$ the zero-phonon line is usually too weak to be seen, since the intensity is now mostly in the multi-phonon sideband.(An exception to this can be found in the ultra-violet absorption edge produced by the A aggregates of nitrogen in Type Ia diamonds- see Davies and Nazare, 1979).

Another of the conclusions of linear electron-lattice coupling theory is that the emission spectrum should be a mirror image of the absorption spectrum at low temperatures.If there is quadratic coupling, however, this is no longer the case; for quadratic coupling equation 2.6 contains a further term in Q^2:

$$\mathcal{E} = E_0 - cQ + kQ^2 + KQ^2 = E_0 - cQ + (k+K)Q^2 \qquad 2.10$$

This means that the effective force constant of the lattice is changed from k to (k+K), i.e. the frequency of the vibration of atoms near the defect is changed.This makes the energy spacing of the vibronic levels different in the ground and excited states.

The effects of quadratic coupling also appear in the temperature dependence of the spectrum.If the energy spacing of the vibronic levels is different in the ground and excited states, then transitions from thermally excited levels will no longer coincide with those from the lowest vibronic level of the ground state.This gives a temperature dependent shift in the energy of the centroid of the zero-phonon line and an increased width with temperature.Thus observation of the spectrum will indicate whether linear or quadratic coupling is present and will

also indicate the strength of the coupling.

2.The Jahn-Teller Effect.

The previous discussion of electron-lattice coupling dealt with non-degenerate states; in this case linear coupling simply displaces the normal modes without affecting their frequencies.The situation is more complicated if the electronic state is degenerate.The Jahn-Teller theorem states that if a defect is in a state which has electronic degeneracy then there will always be a distortion which lowers the symmetry of the defect and thereby removes the degeneracy and lowers the energy.The only exceptions to this case are linear systems which are stable against bending and Kramers degeneracy which can only be removed by a magnetic field.As an illustration of the Jahn-Teller effect a tetrahedral optical centre, point group T_d, is considered. The vibrational modes in this group transform as A_1 (1 dimensional), E (2 dimensional), or T_2 (3 dimensional).The Hamiltonian for a centre in which all these modes are active would be

$$H=H_e+\frac{(p_A^2}{2m_A}+\frac{p_\theta^2+p_\varepsilon^2}{2m_E}+\frac{p_x^2+p_y^2+p_z^2}{2m_T})+$$
$$(k_A Q_A^2+k_E(Q_\theta^2+Q_\varepsilon^2)+k_T(Q_x^2+Q_y^2+Q_z^2))+$$
$$(c_A Q_A+c_{E\theta}Q_\theta+c_{E\varepsilon}Q_\varepsilon+c_{Tx}Q_x+c_{Ty}Q_y+c_{Tz}Q_z) \quad 2.11$$

where H_e is the electronic Hamiltonian and the terms in brackets are the kinetic energy of the vibrational modes, the potential energy of the vibrational modes, and the electron-lattice coupling terms respectively.For simplicity only the coupling of a doubly degenerate electronic state with E modes of vibration will be considered.The coupling of the operators $c_{E\theta}$ and $c_{E\varepsilon}$ to a doubly degenerate electronic state can be found from Griffiths (1964):

coupling of $c_{E\theta}$:-

	θ	ε
θ	-1	0
ε	0	1

coupling of $c_{E\varepsilon}$:-

	θ	ε
θ	0	1
ε	1	0

This means that $(\varepsilon|c_\theta|\varepsilon) = C$, say, $(\theta|c_\theta|\theta) = -C$, $(\theta|c_\varepsilon|\theta) = 0$ etc. From this and from equation 2.11 the determinental equation for the effects of E modes of vibration on doubly degenerate electronic states can be constructed:

$$\begin{vmatrix} k(Q_\theta^2 + Q_\varepsilon^2) - CQ_\theta - V & CQ_\varepsilon \\ CQ_\varepsilon & k(Q_\theta^2 + Q_\varepsilon^2) + CQ_\theta - V \end{vmatrix} = 0 \qquad 2.12$$

This has the solution $V = k(Q_\theta^2 + Q_\varepsilon^2) \pm C\sqrt{Q_\theta^2 + Q_\varepsilon^2}$ which, if $p = \sqrt{Q_\theta^2 + Q_\varepsilon^2}$, becomes

$$V = kp^2 \pm Cp = k(p \pm c/2k)^2 - c^2/4k \qquad 2.13$$

It can be seen, then, that the coupling has removed the electronic degeneracy, giving two potential energy surfaces for the coupled states as shown in figure 2.2.The minimum value for the potential energy now occurs for a finite distortion and is depressed by an amount $c^2/4k$. By an analysis similar to that given above it can be shown (see for e.g. Stoneham, 1975) that a triply degenerate electronic state coupled to E modes gives three potential energy surfaces.

To summarize, the Jahn-Teller effect causes defects to take

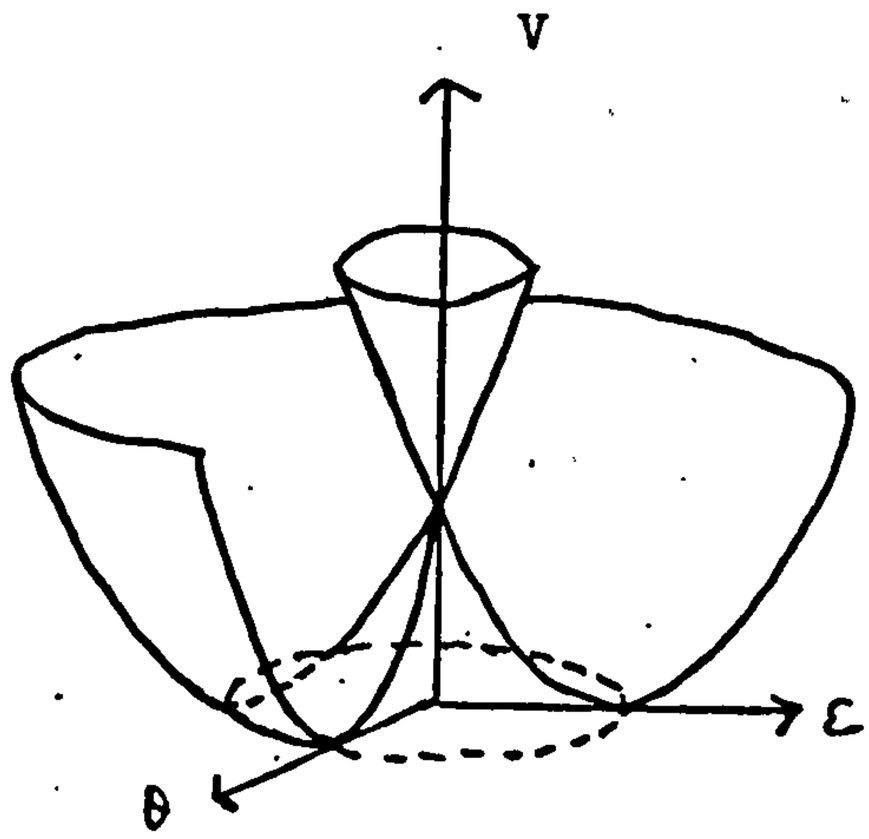

Figure 2.2

one of a number of equivalent configurations related to the symmetry operations of the undistorted lattice.The defect may make transitions between these different configurations.If the mean transition time is much longer than the characteristic time of the experiment being performed on the system then the experiment will indicate a permanent lowering of site symmetry; this is called the static Jahn-Teller effect. The dynamic Jahn-Teller effect occurs when the mean transition time is shorter than the characteristic time of the experiment and the average lowering of the site symmetry is zero.The ground state of the GR centre undergoes a Jahn-Teller distortion and this will be treated more fully in chapter III.

3.Theoretical Aspects of Uniaxial Stress Analysis.

Since zero-phonon lines are quite narrow, uniaxial stress experiments are usually performed on them rather than on broad bands where the splittings are difficult to detect.In uniaxial stress analysis the important quantities are the number of split components, and the energy, intensity and polarisation of each stress split component. (The application of hydrostatic pressure does not cause a splitting of the zero-phonon line because it does not reduce the crystal symmetry; the splittings caused by uniaxial stress are due to this reduction of symmetry).The effects of uniaxial stress are slightly different for the three basic categories of defect.For anisotropic defects, which are the most common, the splitting arises only because the different orientations in the unstressed crystal are no longer equivalent in the stressed crystal.There is a different transition energy for each of the inequivalent orientations.The defect can generally be assigned to one of the seven possible anisotropic symmetry systems mentioned in section 1.2 simply by analysing this "piezo-spectroscopic" splitting. However, for anisotropic defects of trigonal or tetragonal symmetry

the stress may lift both electronic and orientational degeneracies. The stress splitting pattern and any stress-induced dichroism may then give the character of the electronic degeneracy and indicate whether it occurs in the ground state, the excited state, or both.With the third type of defect, that with cubic symmetry, uniaxial stress removes the electronic degeneracy and this causes a different set of stress splitting patterns.

The specific analysis relevant to each of the defect systems studied in this thesis will be given in the chapter dealing with that defect, so only a brief outline of the derivations will be given here. When stress is applied to a defect the change in potential at the defect can be represented by an operator V.This operator can be expanded in terms of the symmetry components that transform as the various representations of the point group of the centre.For a non-degenerate state ψ_1, the first order energy shift under the perturbation V is

$$\delta = (\psi_1 | V | \psi_1) \qquad 2.14$$

but only the totally symmetric A_1 component of V which transforms in the same way as the centre under symmetry operations will contribute to the shift.This symmetric component, V_{A_1}, can be written in the linear form

$$V_{A_1} = \sum_{ij} (a_{ij} s_{ij}) \qquad 2.15$$

$\{s_{ij}\}$ is the stress tensor and its tensor property means that if a uniaxial stress, P, is applied to the crystal along an arbitrary direction, the elements of the stress tensor will be given by

$$s_{ij} = P \cos (P,i) \cos (P,j) \qquad 2.16$$

where (P,i) is the angle between the direction of P and the axis labelled by i.(see Kapljanskii, 1964a)The $\{a_{ij}\}$ are the coupling tensors.The shift in energy for a transition between non-degenerate

states ψ_1 and ψ_2 can be expressed as

$$= A_{xx}\varepsilon_{xx} + A_{yy}\varepsilon_{yy} + A_{zz}\varepsilon_{zz} + 2A_{xy}\varepsilon_{xy} + 2A_{yz}\varepsilon_{yz} + 2A_{zx}\varepsilon_{zx}$$

where $A_{ij} = (a^1_{ij} - a^2_{ij})$, a^1_{ij} refers to ψ_1 and a^2_{ij} refers to ψ_2 2.17

The coefficients A_{ij} can usually be reduced to a small number of independent components using the condition that they must be invariant under the symmetry operations of the centre.More detail in the specific use of this theory will be given in chapter V.

If a state with orbital degeneracy is involved in the zero-phonon transition, this degeneracy may be lifted by components of the stress which which do not have the symmetry of the defect.In this case degenerate perturbation theory must be used to calculate the stress shifts.Hughes and Runciman (1967) have calculated the stress splittings and intensities of lines for anisotropic trigonal and tetragonal centres which possess both orientational and electronic degeneracy.In this section an outline of the removal of electronic degeneracy in cubic centres will be presented.The specific use of this theory in the analysis of the GR centre will be given in chapter III.

Since the elastic deformation in the crystal is small ($\sim 10^{-3}$) the stress perturbation operator can be written in the linear form (Kaplyanskii, 1964b)

$$V = \sum_{ij} V_{ij}\,\varepsilon_{ij} \qquad 2.18$$

However in calculating the first order energy shifts of the states of a defect it is necessary to calculate the matrix elements of V between wavefunctions which form the basis for irreducible representations of the point symmetry group of the defect.It is therefore better to express V in symmetry form by choosing linear combinations of the ε_{ij} such that the resulting set, $\varepsilon_{\Gamma r}$, transform according to the r^{th} basis vector of the irreducible representation Γ.V can then be written

$$V = \sum_{\Gamma,r} A_{\Gamma r}\,\varepsilon_{\Gamma r} \qquad 2.19$$

The ε_{ij} form equation 2.18 transform like the bilinear forms xy etc. and in cubic symmetry the bilinear forms span the symmetric part of $T_1 \times T_1$ which contains the irreducible representations A_1,E and T_2 having the quadratic basis functions

$$A_1 = x^2 + y^2 + z^2$$

$$E = 2z^2 - x^2 - y^2, \sqrt{3}\,(x^2 - y^2)$$

$$T_2 = yz,\ zx,\ xy \qquad 2.20$$

Thus V can be written

$$V = V_A\,(\varepsilon_{xx}+\varepsilon_{yy}+\varepsilon_{zz}) + V_E\,(2\varepsilon_{zz}-\varepsilon_{xx}-\varepsilon_{yy}) + V_E\sqrt{3}(\varepsilon_{xx}-\varepsilon_{yy}) + V_{yz}\varepsilon_{yz} + V_{zx}\varepsilon_{zx} + V_{xy}\varepsilon_{xy} \qquad 2.21$$

The effect of the perturbation V on a three-fold degenerate T level, say, can then be found by solving a determinant of the form

$$\begin{vmatrix} & Tx & Ty & Tz \\ Tx & V_{11}+W & V_{12} & V_{13} \\ Ty & V_{21} & V_{22}+W & V_{23} \\ Tz & V_{31} & V_{32} & V_{33}+W \end{vmatrix} = 0 \qquad 2.22$$

where $V_{11} = (Tx|V|Tx)$, $V_{12} = (Tx|V|Ty)$ etc.

This theory can be extended to include situations where different levels are mixed together by the stress perturbation.For example, the effect of stress on the E, A ground state levels of the GR centre can be found by solving a determinant of the form

$$\begin{vmatrix} & \Theta & \mathcal{E} & A_1 & A_2 \\ \Theta & V_{11}+W & V_{12} & V_{13} & V_{14} \\ \mathcal{E} & V_{21} & V_{22}+W & V_{23} & V_{24} \\ A_1 & V_{31} & V_{32} & V_{33}+W & V_{34} \\ A_2 & V_{41} & V_{42} & V_{43} & V_{44}+W \end{vmatrix} = 0 \qquad 2.23$$

where $V_{11} = (\Theta|V|\Theta)$, $V_{21} = (\mathcal{E}|V|\Theta)$ etc.

The theory outlined in this chapter forms the basis for all the analyses in the following chapters.

CHAPTER III

The GR Centre, I

Introduction:

The GR centre in diamond has been extensively studied and yet there is still much to be learnt about it.Two main points of interest are, firstly, that the GR1 band is a transition between two electronic states which both undergo dynamic Jahn-Teller distortions and secondly, the higher energy GR 2-8 lines which occur at the GR centre do not yet have a satisfactory explanation.In this chapter we report experimental and theoretical work on the GR ground state and the GR1 transition; we also give the first complete high resolution GR1 luminescence spectrum.

1.Previous Work on the GR Centre.

The GR bands, shown in figure 3.1, are created in all types of diamond by electron, neutron or gamma ray irradiation (Clark et al, 1956a).In the present work the defect centres giving rise to them were created by electron irradiation as described in chapter I.The GR band consists of a prominent zero-phonon line at 1.673eV., called the GR1 line, a satellite line at 1.665eV., and vibronic structure extending to about 2.6eV.(The GR 2-8 lines shown in figure 3.1 are also thought to be electronic transitions at the GR defect; these sharp lines will be considered in detail in chapter IV).Although the system can be produced by irradiation of all types of diamond it is found that the GR1 zero-phonon line is sharpest in type IIb diamonds for reasons outlined in chapter I.Most of the work on the GR centre has therefore been done using these semiconducting diamonds.

Dyer and Ferdinando (1966) made a comparison of the strengths of the GR bands in type IIb and type IIa diamonds as a function of electron dose under identical conditions and found that the GR band grew steadily throughout irradiation in type IIa diamonds whereas there was an

The GR1 absorption spectrum

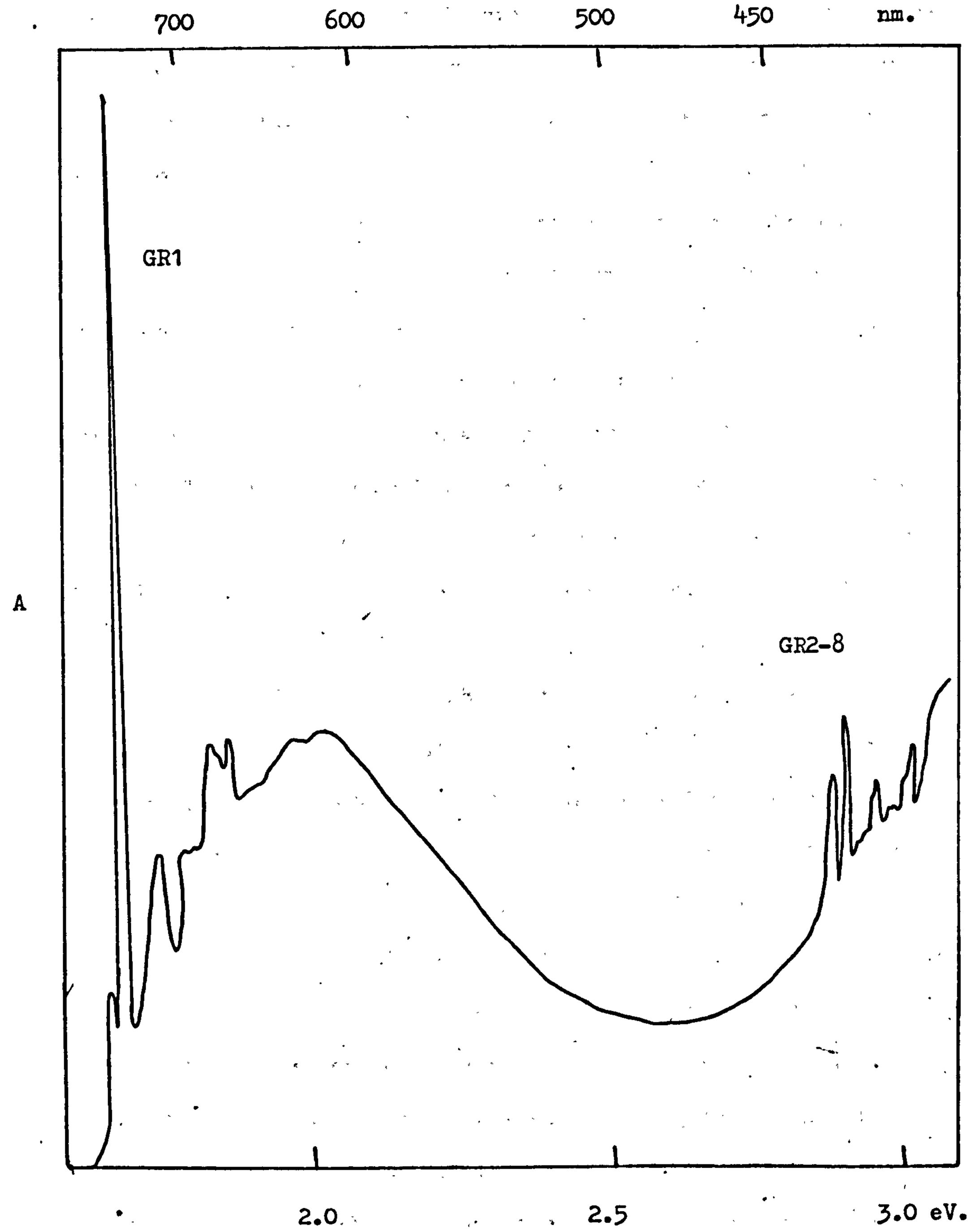

Figure 3.1

initial induction for the IIb crystals.These authors also reported that the GR centre was not present in type IIb diamonds until all the acceptor centres had been compensated and this led Mitchell (1967) to propose that the GR band was associated with a neutral or negatively charged donor centre.Interstitials are mobile at quite low temperatures whereas vacancies are stable to much higher temperatures.The GR centre is stable to very high temperatures (~1200K) so this led Mitchell (1967) to infer that the GR defect is a vacant lattice site.The conclusion that the GR centre was not present until all the acceptor centres were compensated has been shown to be wrong (Collins, 1974) Nevertheless, work by Clark and Walker (1973) showed that the GR centre possessed tetrahedral symmetry and the only intrinsic defects which possess this symmetry are the vacant atomic site and the interstitial carbon atom.The description of the neutral vacancy given by Coulson and Kearsley (1957) has been found to agree very closely with the properties of the GR band so it is now generally accepted that the GR centre is the neutral vacancy (see also Lowther and Stoneham, 1978)

In 1971 Clark and Walker showed that the 1.665eV. and the 1.673eV. lines originate from ground states 8meV. apart.The detailed uniaxial stress work of Clark and Walker (1973) on these lines showed that the zero-phonon line was an E to T transition and the 1.665eV. line was an A to T transition, as shown in figure 3.2.Davies and Penchina (1974) confirmed this analysis and extended it to give a quantitative description of the E and A ground states under stress.It should be noted that uniaxial stress experiments cannot distinguish between A_1 to T_2 and A_2 to T_1 transitions; the assignments A_1 to T_2 have been adopted for the GR centre but all the experimental results described here could be interpreted in exactly the same way if the subscripts (1 and 2) of all the irreducible representations were simultaneously

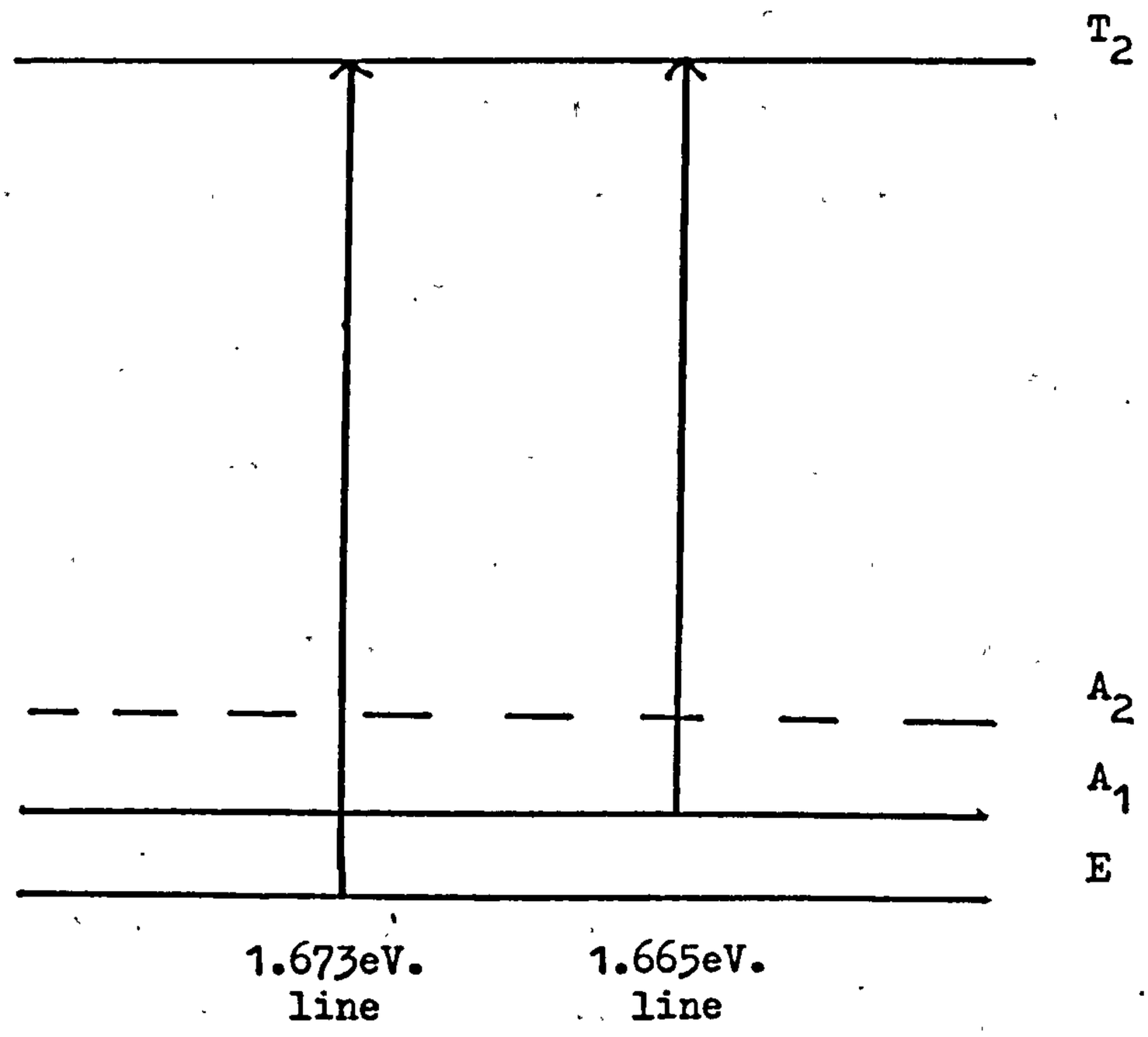

Figure 3.2

interchanged.

One of the problems concerning the GR1 ground state was that none of the theoretical treatments predicted an A_1 electronic state close to the E electronic state, as indicated experimentally. However, also Hannoo t Stoneham (1968), Douglas t Runciman (1947) Stoneham (1977) and Lowther (1976) showed that the E, A ground states derive from a single electronic E state coupled to lattice vibrations of e symmetry. Thus, as would be expected for a degenerate state, the E ground state undergoes a Jahn-Teller distortion. This distortion is dynamic since the overall T_d symmetry of the centre is maintained.

2. The GR1 Ground State.

As described earlier the GR1 ground state has been shown to consist of an E and an A_1 level, the A_1 level being derived from the coupling of the E state to e modes of vibration. Jahn-Teller theory

(see e.g. O'Brien, 1964) predicts an A_2 vibronic level to lie somewhat above the A_1 level (see figure 3.2).Stoneham (1977) estimates the A_2 level to lie about 20meV. above the E zero-phonon level.Transitions between A_2 and the first excited T_2 state, the level involved in the GR1 transition, are electric dipole forbidden.However, the GR2 level transforms as T_1 (Walker et al, 1974) and, on symmetry grounds at least, the A_2 to T_1 transition is allowed.It was therefore decided to search the transmission spectrum about 20meV. below the GR2 line and a weak transition at 2.8633eV. was observed.This is 17meV. below the GR 2 line.In order to confirm that this transition did originate from the proposed A_2 level the variation of its intensity relative to the GR2 line as a function of temperature was investigated.The apparatus used (Maeda, 1965) is shown in figure 3.3.The sample was mounted in

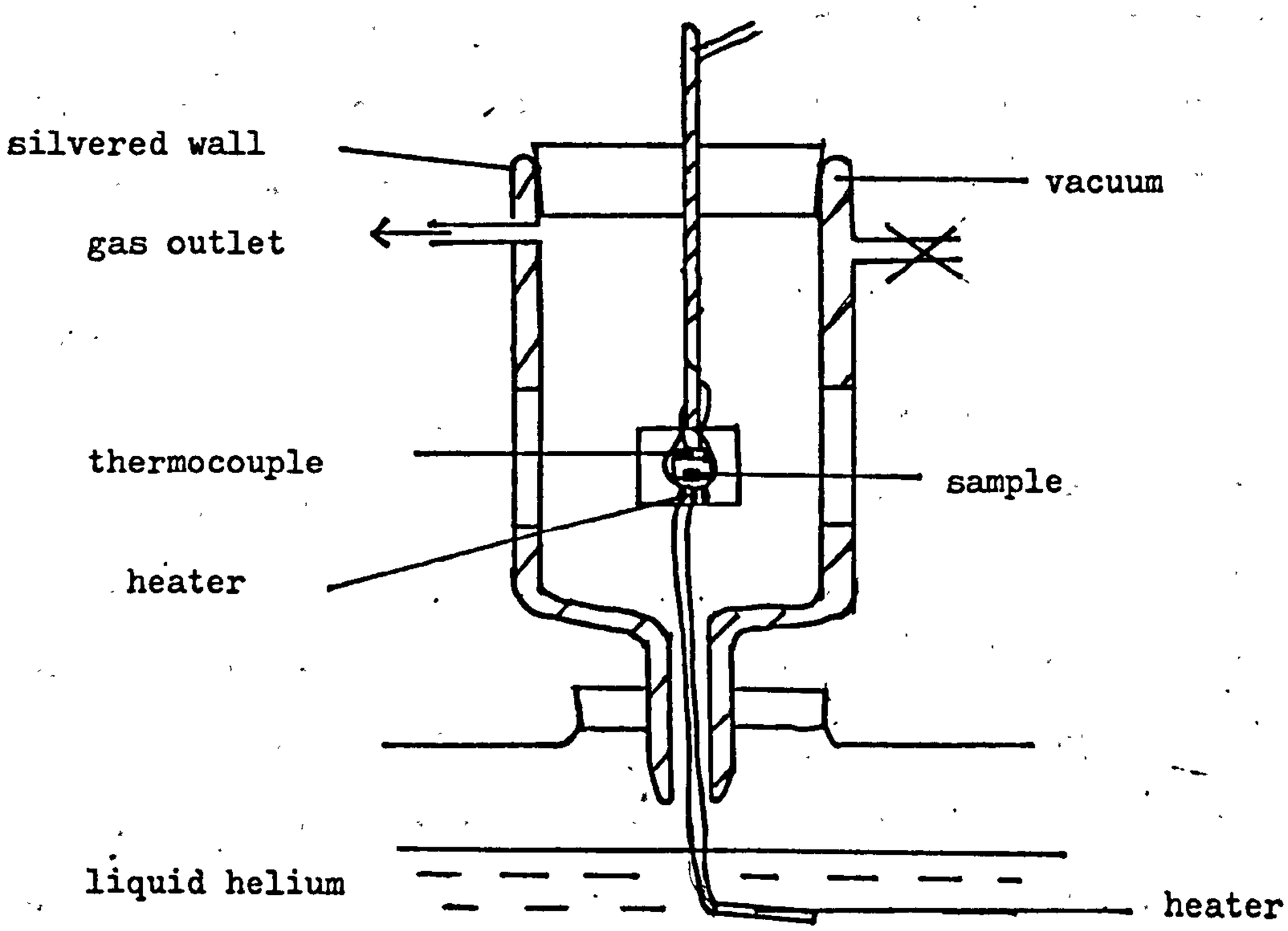

Figure 3.3

helium boil-off gas.The temperature of the diamond was controlled using two small heaters; one was submerged in liquid helium and therefore controlled the boil-off rate, the other was attached to the diamond mount and acted as a fine control of the temperature, which was measured using a chromel-constantan thermocouple..

Figure 3.4b shows that the relative intensity of the A_2 transition to the GR2 transition follows a simple Boltzman distribution law:

$$\frac{A_2 \text{ transition intensity}}{\text{GR2 intensity}} \propto e^{-\Delta/kT} \qquad 3.1$$

with an activation energy Δ= 17.1meV. as determined by a least squares fit.Thus the intensity of the new transition relative to GR2 decreases at low temperature consistent with a ground state splitting $\sim$17meV. This places the A_2 state 17 meV. above the E state in agreement with Stoneham's prediction.This result is significant for the interpretation of the Jahn-Teller properties of the GR centre discussed in section 3.5.It also completes the mapping of the lowest three levels of the GR centre.

3.The GR1 Transition.

The effects of uniaxial stresses up to 1.6GPa. on the 1.673 and 1.665eV. lines are understood quantitatively (Clark and Walker, 1973, Davies and Penchina, 1974).In the present work stresses up to 3GPa. were applied, as described in chapter I, in order to cofirm that the existing theory applies at these higher stresses, and to try to detect some interaction between the E ground state and the A_2 vibronic level.The energies of the stress-split components of the 1.673 and 1.665eV. lines are shown in figure 3.5.It should be noted that the existence of the 1.665eV. line is evidence for e-mode coupling in the T_2 electronic state (Lowther, 1975).Without this coupling

a)

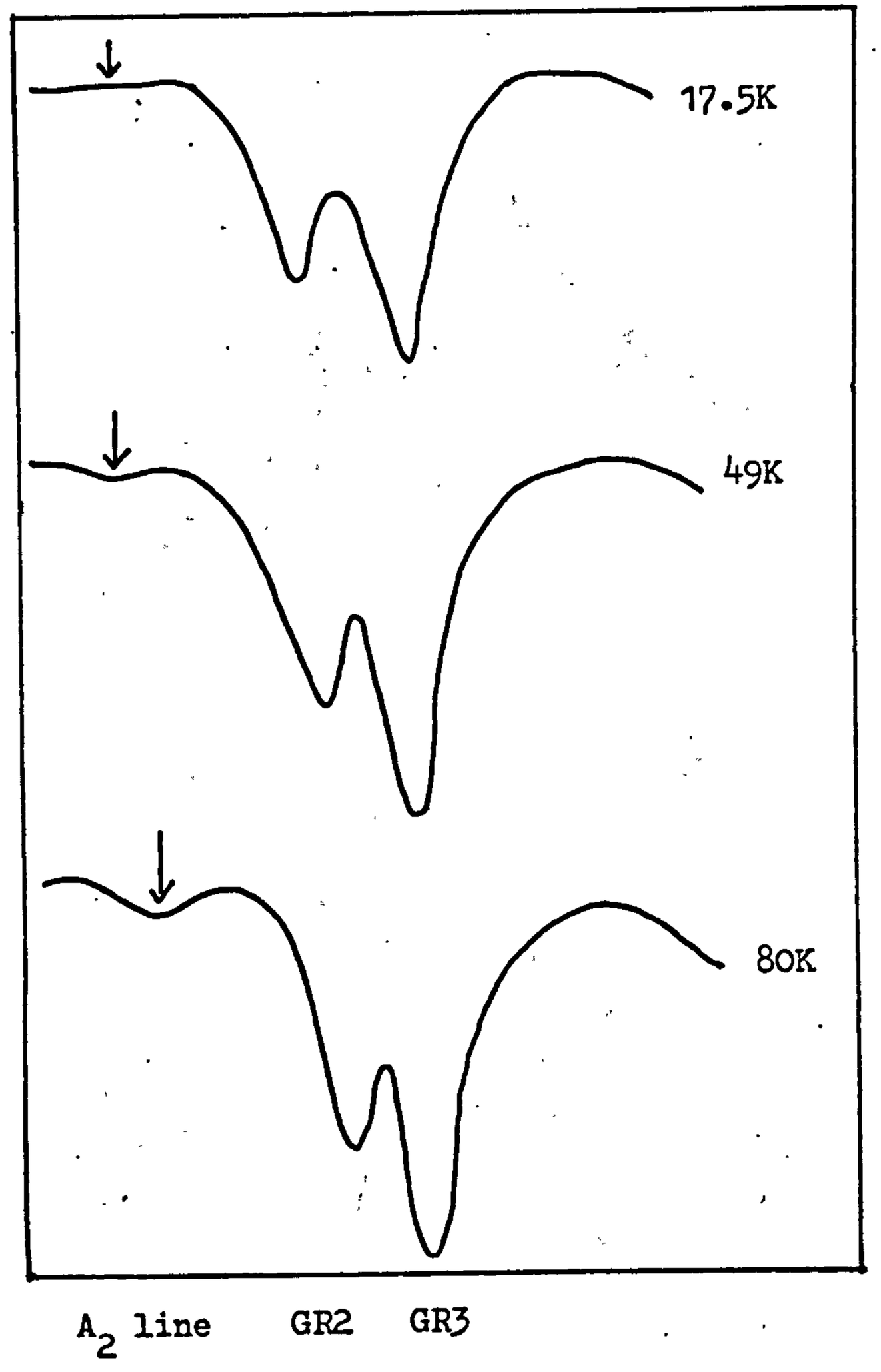
17.5K
49K
80K
A2 line
GR2
GR3

b)

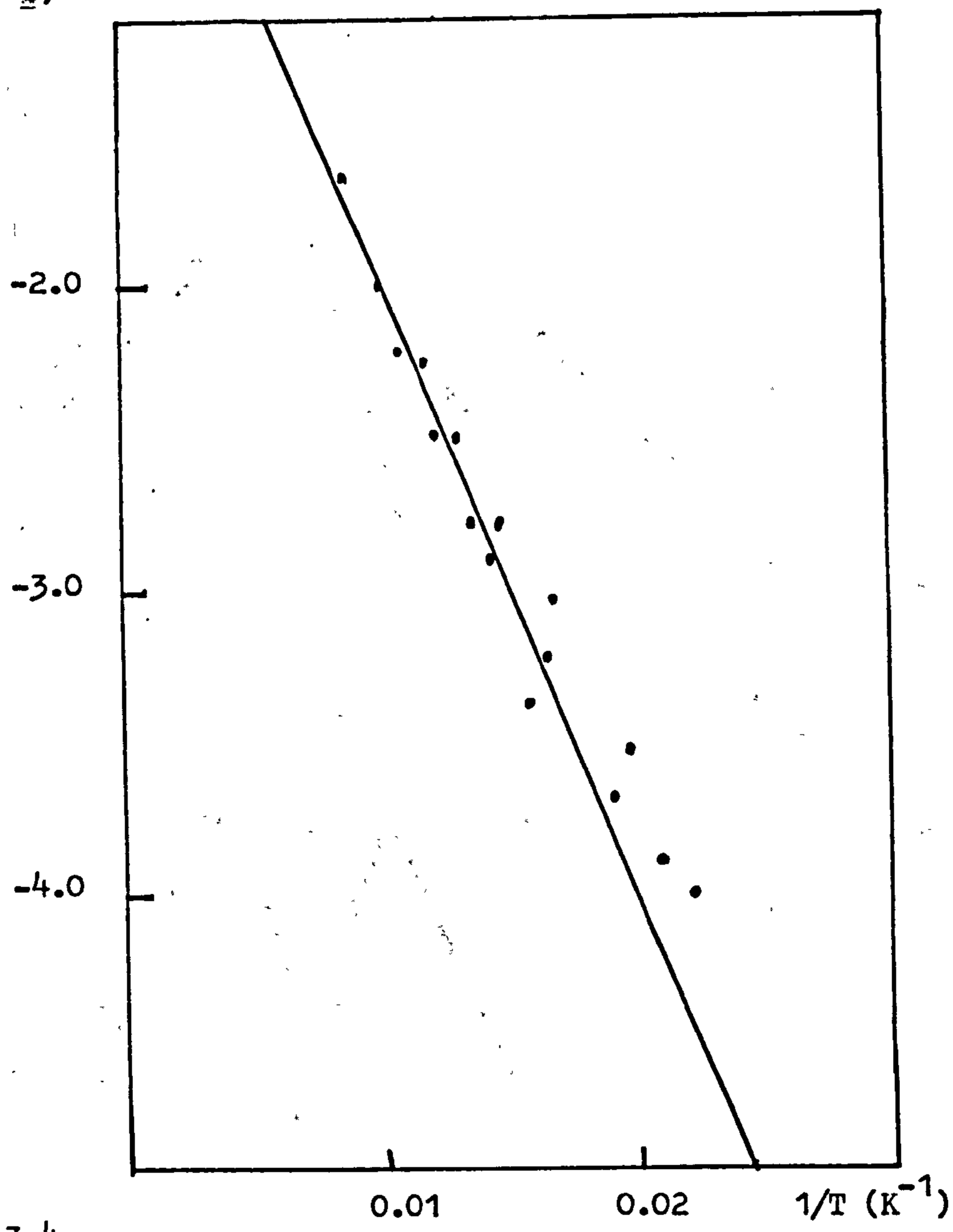
-2.0
-3.0
-4.0
ln (intensity ratio)
0.01
0.02
1/T (K-1)

Figure 3.4

The GR1 stress-split components.

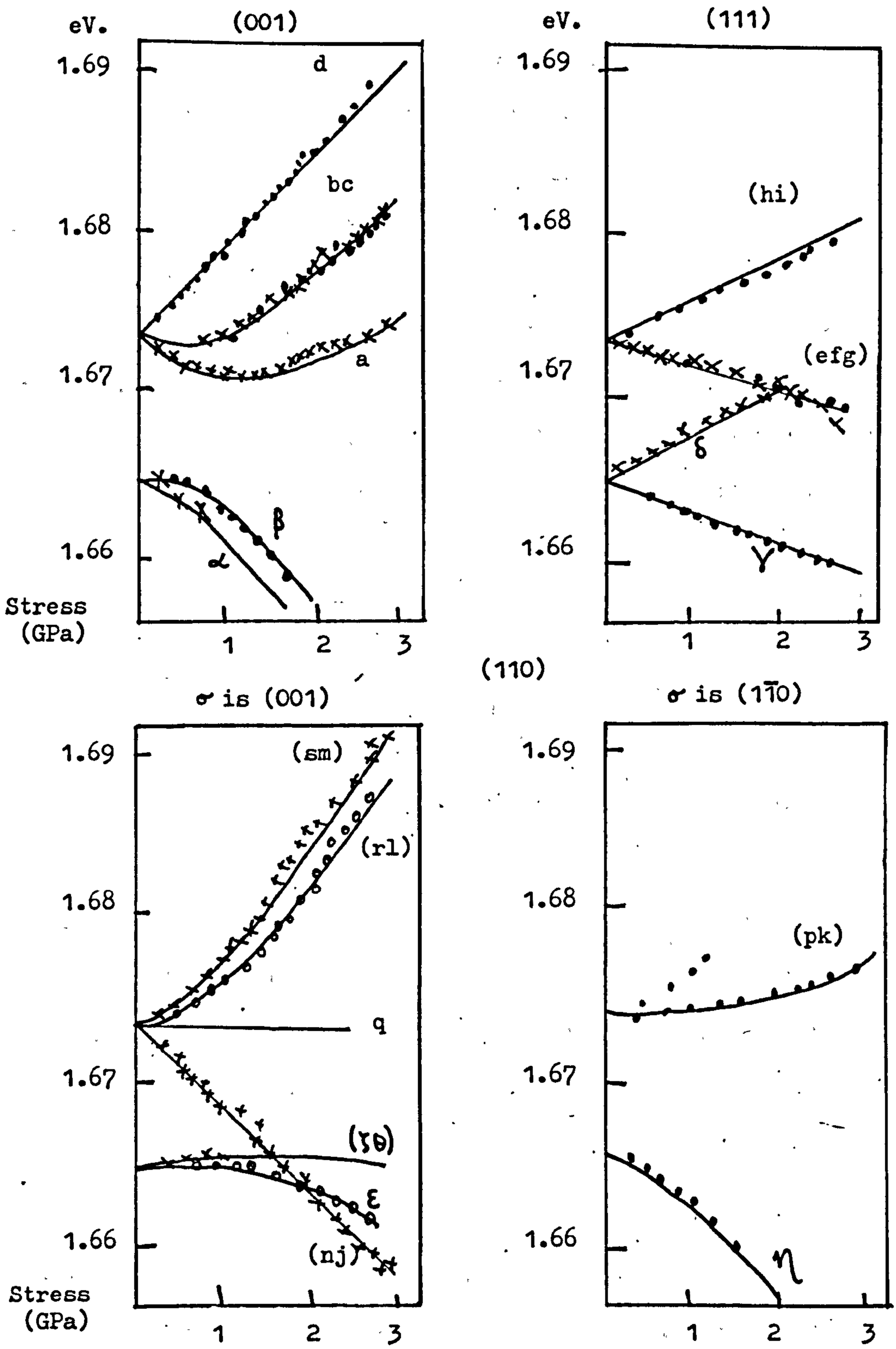

Figure 3.5

transitions involving the A_1 state would be forbidden.

The Hamiltonian for the GR centre can be written as

$$H = H_0 + c_{A_1}s_{A_1} + c_{E\theta}s_{E\theta} + c_{E\varepsilon}s_{E\varepsilon} + c_{yz}s_{yz} + c_{zx}s_{zx} + c_{xy}s_{xy} \qquad 3.2$$

in accordance with the analysis given in section 2.3. H_0 is the Hamiltonian at zero stress and the stresses are denoted by s, with $s_{E\theta} = 2s_{zz} - s_{xx} - s_{yy}$, $s_{E\varepsilon} = \sqrt{3}(s_{xx} - s_{yy})$ being the linear combinations of the stress components which transform as the E irreducible representation of T_d, and $s_{A_1} = s_{xx} + s_{yy} + s_{zz}$ being the totally symmetric combination. The s_{ij} (i, j, = x,y,z) are defined with respect to the cubic axes of diamond. The electronic operators, c, also transform as shown by their subscripts. From this Hamiltonian the secular matrix of H in the E, A_1, A_2 ground states can be constructed (see equation 2.23)

H	$E\theta$	$E\varepsilon$	A_1	A_2
$E\theta$	$W_E - Ds_{E\theta} + A_E s_{A_1}$	$Ds_{E\varepsilon}$	$E_{A_1}s_{E\theta}$	$E_{A_2}s_{E\varepsilon}$
$E\varepsilon$	$Ds_{E\varepsilon}$	$W_E + Ds_{E\theta} + A_E s_{A_1}$	$E_{A_1}s_{E\varepsilon}$	$E_{A_2}s_{E\theta}$
A_1	$E_{A_1}s_{E\theta}$	$E_{A_1}s_{E\theta}$	$W_{A_1} + A_{A_1}s_{A_1}$	0
A_2	$E_{A_2}s_{E\varepsilon}$	$E_{A_2}s_{E\varepsilon}$	0	$W_{A_2} + A_{A_2}s_{A_2}$

3.3

where $A_E = (E\theta|c_{A_1}|E\theta)$, $A_{A_1} = (A_1|c_{A_1}|A_1)$, $A_{A_2} = (A_2|c_{A_1}|A_2)$

$D = (E\theta|c_{E\varepsilon}|E\varepsilon)$, $E_{A_1} = (A_1|c_{E\varepsilon}|E\varepsilon)$, $E_{A_2} = (A_2|c_{E\varepsilon}|E\theta)$

and W_E, W_{A_1} and W_{A_2} are the energies of the E, A_1 and A_2 vibronic levels at zero stress.

$W_{A_1} - W_E = 8meV.$

$W_{A_2} - W_E = 17meV.$

The secular matrix for H in the zero-phonon level of the T_2 excited state is given on the following page (see also equation 2.22)

H	Tx	Ty	Tz
Tx	$W_T+A_T s_{A_1}+\frac{1}{2}B(\sqrt{3}s_{E\varepsilon}-s_{E\theta})$	Cs_{xy}	Cs_{xz}
Ty	Cs_{xy}	$W_T+A_T s_{A_1}-\frac{1}{2}B(\sqrt{3}s_{E\varepsilon}+s_{E\theta})$	Cs_{yz}
Tz	Cs_{xz}	Cs_{yz}	$W_T+A_T s_{A_1}+Bs_{E\theta}$

3.4

Here $A_T = (Tx|C_{A_1}|Tx)$, $B = \frac{1}{\sqrt{3}}(Tx|C_{E\varepsilon}|Tx)$, $C = (Tx|C_{xy}|Ty)$ and W_T = 1673meV. is the energy of the T_2 state at zerostress.Figure 3.6 shows the point group to which the GR centre is reduced for each direction of stress.

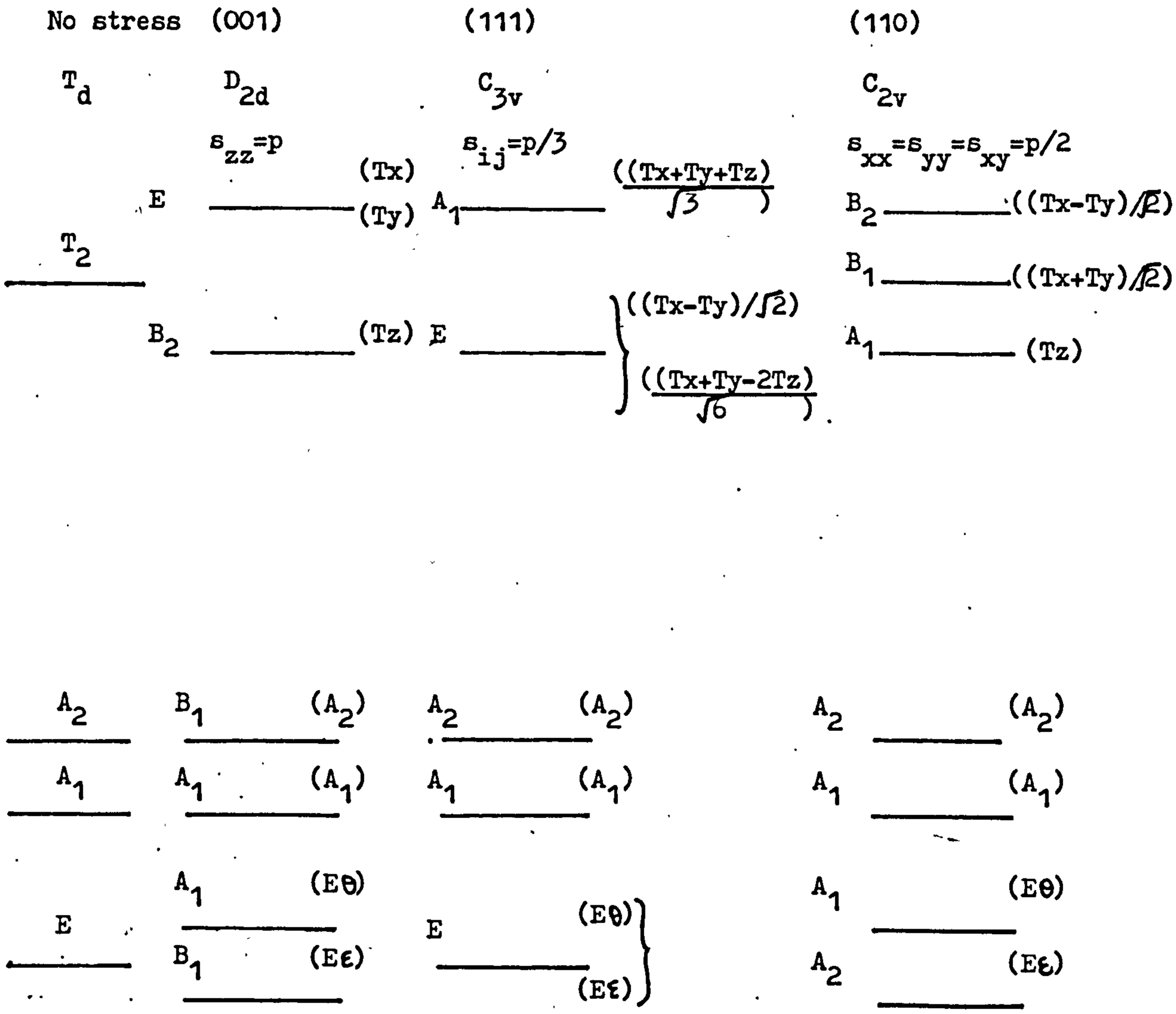

Figure 3.6

Eigenvalues and eigenvectors of the matrices 3.3 and 3.4 were found for trial values of the matrix elements.The selection rules for optical transitions are given by Kaplyanskii (1964b) and Griffiths (1964) so knowing these it was possible to relate the observed energies of the GR1 transition to differences in the eigenvalues of the T_2 and (E, A_1, A_2) states.In order to optimise the matrix elements a numerical least squares fit was applied to the equations obtained by diagonalisation of the two secular matrices.The results, shown in Table I, confirm and extend the earlier work of Davies and Penchina (1974) and Walker et al (1973); the lines of figure 3.5 have been calculated using this theory.

TABLE I

Stress matrix elements for the GR1 line.

The symbols are defined in equations 3.3 and 3.4 and the units are meV.$(GPa.)^{-1}$

	This work	Davies and Penchina
A_T-A_A	-0.22±0.3	-0.25±0.3
A_T-A_E	-0.15±0.3	-0.01±0.3
B	-0.85±0.3	-0.73±0.3
C	4.25±0.3	4.37±0.3
D	-2.18±0.3	-2.38±0.3
E_{A_1}	-2.40±0.3	-2.77±0.3
$\lvert E_{A_2} \rvert$	<1.07	-

As mentioned earlier, transitions between the A_2 ground state level are electric dipole forbidden so no line originating from this transition would be expected.Considering figure 3.6, however, it could be expected that the E⊗ vibronic ground state would interact with

the A_2 vibronic level.The non-linear variation with stress of the energies of lines such as a,b, in figure 3.5 arises through the stress induced interaction of the Eθ vibronic ground state and the A_1 first excited vibronic level (Davies and Penchina, 1974).If the Eε level did interact with the A_2 level, the line d for example, seen under (001) stress would be expected to show some curvature with stress (line d originates from the Eε level of the ground state and any curvature of this level caused by a stress interaction with the A_2 level would show in the line d).There is no detectable curvature of the line d so this enables an upper limit to be placed on the Eε-A_2 coupling. Considering only the (001) direction of stress, the value of E_{A_2} was increased from zero in the ground state secular matrix; for each value of E_{A_2} the theoretical variation of the line d with stress was plotted and the value at which curvature of d first lay outside the experimental uncertainties was taken as the upper limit.As E_{A_2} was increased above this value the curvature became more pronounced. This lack of interaction between the E state and the A_2 state is partly due to the energy separation of the two states being too large and partly due to the coupling term being small

4.The GR1 Luminescence Band.

The GR absorption band has many interesting and puzzling features but previously no good luminescence spectrum had been obtained.To increase the available information on the GR centre a high resolution luminescence spectrum for the GR1 band was obtained. Luminescence was excited in a diamond held at liquid nitrogen temperature using a Spectra-Physics 165 krypton laser.The luminescence was detected at right angles to the exciting beam using a Northcoast EO-817 intrinsic germanium diode, cooled to liquid nitrogen temperature.The spectra were recorded using a Spex 1400 monochromator fitted with

a 600 grooves $mm.^{-1}$ grating blazed at 1.6μm.The signal was d.c. amplified for presentation on a chart recorder.To obtain the true luminescence spectrum the chart recorder spectrum had to be corrected for the optical transfer function of the system.In order to do this the emission spectrum of a tungsten strip lamp was recorded over the range covered by the GR1 luminescence spectrum.The brightness temperature of the lamp was measured at 650nm. using an optical pyrometer and from the charts given by Rutgers and de Vos (1954) the true temperature of the lamp was found.From Planck's formula the number of photons per unit energy range emitted from unit surface area of a perfect black body is

$$n\,(f,T) = \frac{8\pi}{c^3} \cdot \frac{1}{(e^{hf/kT} - 1)} \cdot f^2 \qquad 3.5$$

where f is the photon frequency and c, h, and k have their usual meanings.To find this quantity for the tungsten strip lamp equation 3.5 had to be multiplied by the emissivity of tungsten, $\varepsilon(f,T)$, found from the graphs given by de Vos (1954).Thus, for the lamp

$$N\,(f,T) = \varepsilon(f,T) \cdot n\,(f,T) \qquad 3.6$$

Hence, knowing T and $\varepsilon(f,T)$ the theoretical spectrum from the tungsten lamp (i.e. that obtained by observing the lamp directly without the light having passed through the system) was calculated using equations 3.5 and 3.6.This was compared with the spectrum obtained from the lamp after passage through the spectrometer.For all values of f the ratio B/B' was found where B = the actual (theoretical) value for N(f) and B' = the experimental value, i.e. the value after passage through the optical system.In order, then, to obtain the true GR1 luminescence spectrum, each point on the experimental curve was multiplied by the value of B/B' at that frequency.

To obtain a true comparison of emission and absorption spectra

it is necessary to compare transition probabilities.This is done in figure 3.7 where the luminescence spectrum is shown on the left and the absorption spectrum is shown on the right.(In order to obtain the spectra in terms of transition probabilities, each point on the corrected emission spectrum was divided by f^3, where f is the frequency at that point, and each point on the absorption spectrum was divided by f).As can be seen from figure 3.7 the GR1 luminescence band has quite a different structure from the absorption band.The optic mode replicas are far less distinct in luminescence than in absorption; also the 40 meV. sideband is weak in luminescence.In section 3.5 the Jahn-Teller effects at the GR centre are discussed; there it will be seen that the T_2 state undergoes a weak coupling to e modes.This type of weak coupling results in a strong modulation of the strengths of successive sidebands in the E to T transitions, such that the first phonon sideband is enhanced, the second weakened and so on, relative to their strength with no e-mode coupling.(Lowther, 1979)Coupling to t modes was omitted in the calculations and it has been shown (see section 3.5) that there is weak t-mode coupling in the T_2 state; nevertheless, these results suggest that the lack of mirror symmetry in the GR1 absorption and luminescence bands probably originates solely in the Jahn-Teller effect.

The ratio of the intensities of the 1.665eV. line and the 1.673 eV. line can be measured from the luminescence spectrum.This ratio is dependent on the Jahn-Teller parameters for the E ground state and the excited T_2 state.In order to obtain an accurate measurement of this ratio, the observed intensities of the two lines must be corrected for self-absorption by the diamond.Considering a cube with sides of length l the intensity of light emitted a distance x from one face of the diamond, in the direction of that face, is i_o.After

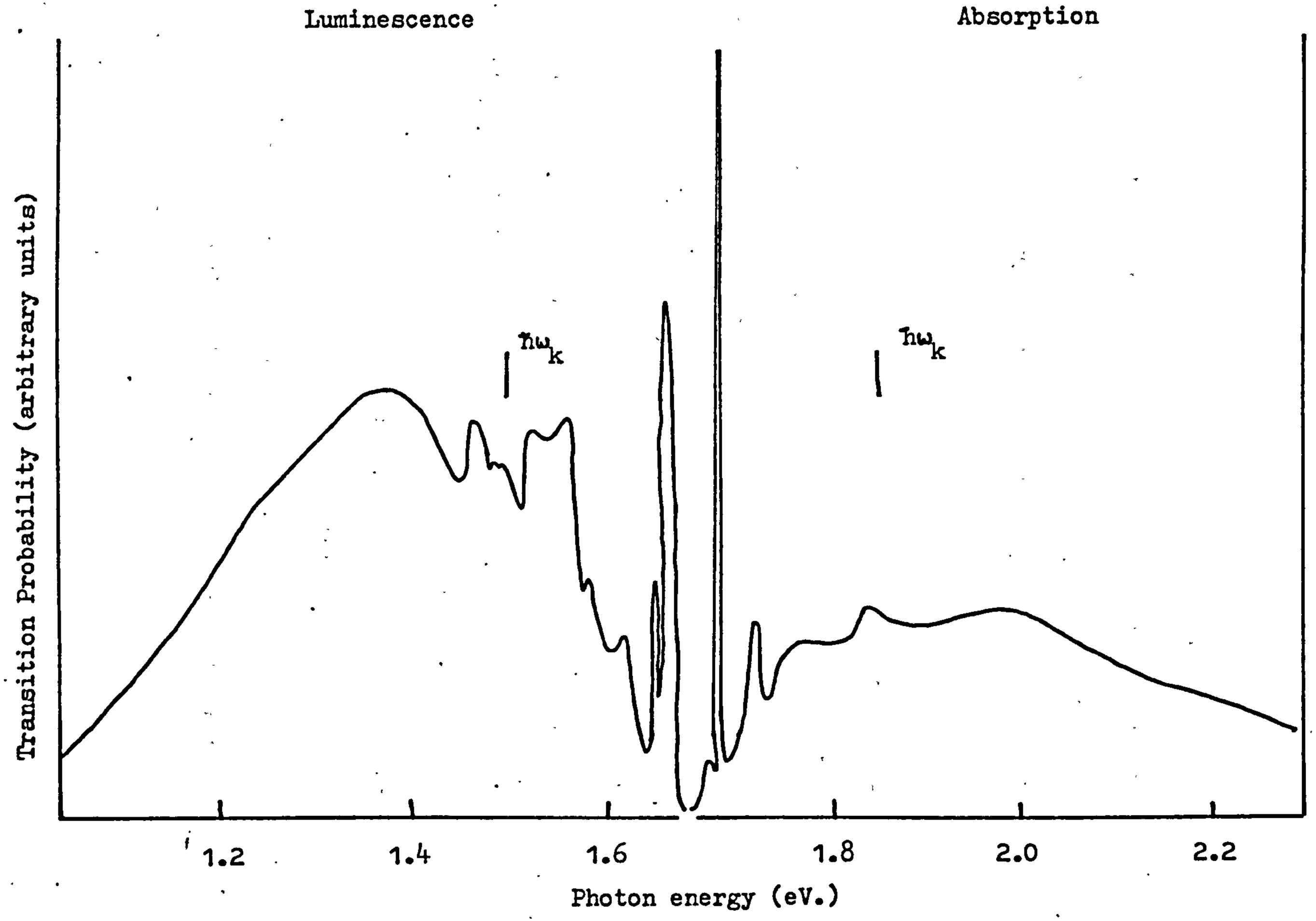
Luminescence
Absorption
$\hbar\omega_k$
$\hbar\omega_k$
Transition Probability (arbitrary units)
1.2
1.4
1.6
1.8
2.0
2.2
Photon energy (eV.)

Figure 3.7

passage through the diamond this intensity has been reduced to $i_o e^{-\mu x}$ where μ is the absorption coefficient for light of that frequency. Thus the total intensity of light emerging from that face of the crystal is

$$I = \int_0^l i_o\, e^{-\mu x}\, dx = \frac{i_o}{\mu}\left(1 - e^{-\mu l} \right) \qquad 3.7$$

In the experiments performed here l = 1mm.The absorption coefficient, μ, was found as a function of f from the absorption curve;the true intensity of luminescence could then be found at each value of f in the emission spectrum using the relationship

$$\text{experimental intensity} = \frac{i_o(f)}{\mu(f)} \cdot \left(1 - e^{-\mu(f).l} \right) \qquad 3.8$$

where $i_o(f)$ is the true intensity at frequency f corrected for self-absorption.The relative intensities thus obtained were

$$\frac{I_{1665}}{I_{1673}} = 0.163 \pm 0.03 \qquad 3.9$$

This value agrees with 0.155 ± 0.03 estimated from absorption measurements (Davies, 1974) and is consistent with the spectra of other workers. (Collins, 1978b, Nedvetskii and Gaisin, 1973)As will be seen in section 3.5, this experimental valueagrees with Davies (1979) calculations for the Jahn-Teller parameters of the GR centre.

5.Jahn-Teller Effects at the GR1 Centre.

In the discussion of the Jahn-Teller effect in section 2.2 it was shown that linear coupling of an E electronic state to e modes of vibration resulted in a "mexican hat" shape for the potential energy surface.A full treatment of the vibronic Hamiltonian for the E electronic state (equation 2.11) shows that for linear Jahn-Teller coupling of an E state to e-modes the ground state is a vibronic

doublet E state while the first excited state is another doublet belonging to A_1 and A_2.If quadratic Jahn-Teller coupling is included in the Hamiltonian then the accidental degeneracy in the excited doublet A_1, A_2 is lifted whilst E is unaffected (Ham, 1972)The extra terms in the Hamiltonian are called the "warping" terms since their effect is to "warp" the bottom of the trough in the potential energy surface of figure 2.2, giving three identical configurations of stable equilibrium. If the barriers between these new potential wells are sufficiently high the centre will show the static Jahn-Teller effect, where the initial double degeneracy of the E ground state is increased to three. The full effects of the warping terms are dealt with by O'Brien (1964) but, to clarify the situation for the GR centre, the lowest vibronic levels for E x e coupling are shown as a function of distortion in figure 3.8.As can be seen from this figure the increase in degeneracy of the E ground statecomes about through the A_1 state joining the E state in the highly distorted environment.

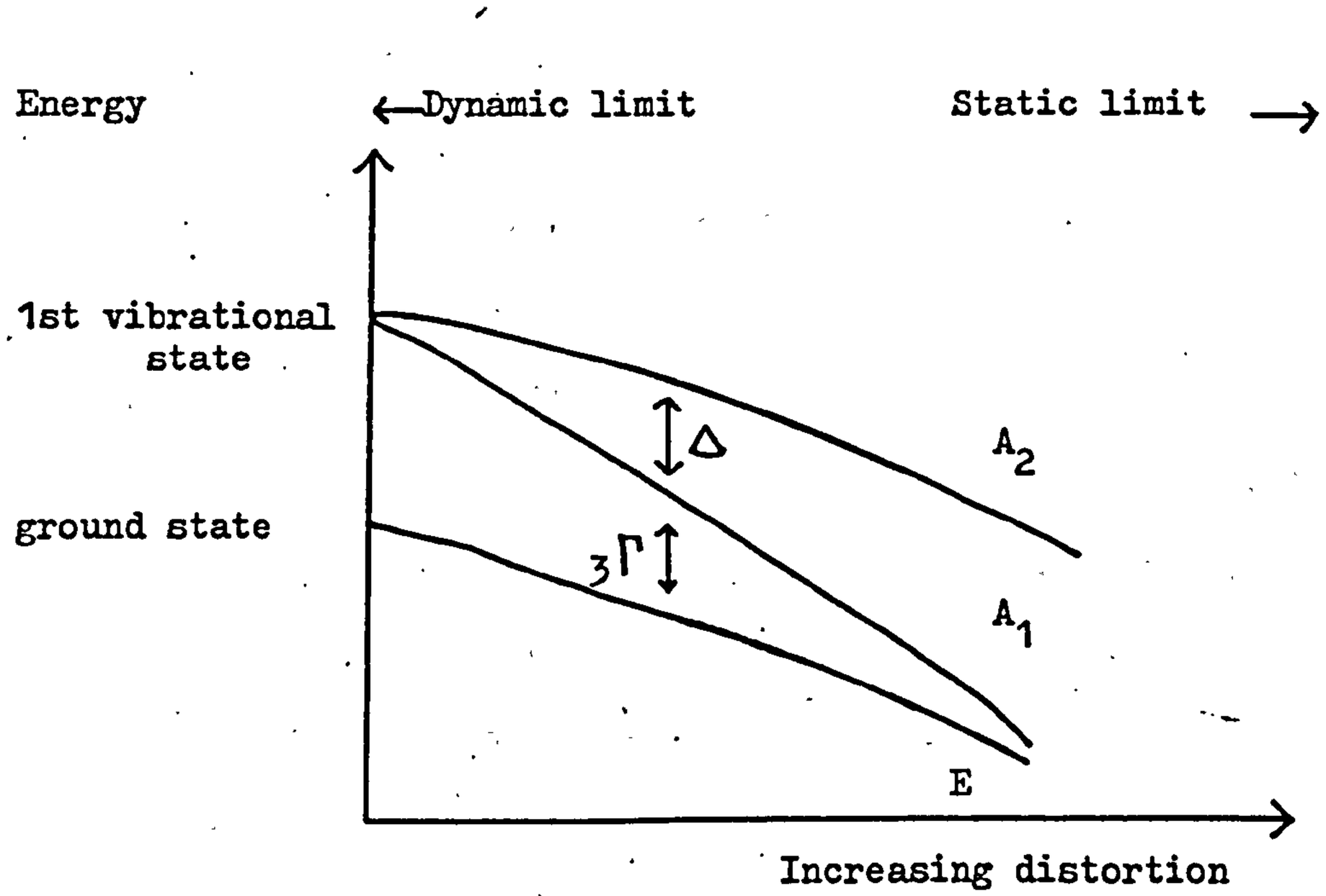

Figure 3.8

From this figure it can also be seen that the ratio $\Delta/3\Gamma$ gives an accurate measure of the extent of the distortions at the GR1 centre, since it varies from zero in the truly dynamic Jahn-Teller case to infinity in the static limit.The results of paragraph 3.2 give the ratio $\Delta/3\Gamma$ for the GR1 centre as

$$\Delta/3\Gamma = 1.1 \pm 0.1 \qquad 3.10$$

This is the first time that $\Delta/3\Gamma$ has been measured for any centre and it will be used later to give the warping terms in the Hamiltonian for the GR1 centre.

Another effect of the distortion is to change the ground state wave functions from their form in the truly tetrahedral environment (see also section 2.1).This changes the magnitude of the matrix elements of the stress operators of equation 3.3.In particular, E_{A_1} and D vary so that

$$|E_{A_1}| = D$$

in the truly tetrahedral site to

$$|E_{A_1}| = \sqrt{2}\,|D|$$

in the three distorted sites (Ham, 1972).From the present work (Table I) it is found that

$$\left|E_{A_1}/D\right| = 1.16 \pm 0.13 \qquad 3.11$$

The theory of Jahn-Teller effects becomes very involved very quickly; it is therefore customary to treat the vibrations of the atoms around the vacancy as if they all occurred at a single "effective" frequency, ω.Analysis is further simplified if, instead of working with the energy reduction E_{JT} when the vacancy distorts through the Jahn-Teller effect, the dimensionless ratio

$$S_E = E_{JT} / \hbar\omega \qquad 3.12$$

is used.Stoneham (1977) has estimated that in the E ground state of the vacancy, S_E=4.8, but this figure is subject to a large uncertainty (e.g. 50%).Previous work on Exe coupling has assumed S_E to be very large (O'Brien, 1964) which is the case in the strong coupling limit. Since it was by no means certain that the E ground state was in this limit, Davies (see Foy and Davies, 1979) calculated the ratios $\Delta/3\Gamma$, $|E_{A_1}/D|$ and $|E_{A_2}/D|$ for finite values of S_E by direct numerical diagonalisation of the E x e secular matrix.He used equation 2.11 rewritten in the standard form (Ham, 1972)

$$H = E_E I_E + \frac{1}{2\mu}(P_\theta^2 + P_\varepsilon^2) I_E + \tfrac{1}{2}\mu\omega^2 (Q_\theta^2 + Q_\varepsilon^2) I_E +$$
$$V_E(Q_\theta M_\theta + Q_\varepsilon M_\varepsilon) + V_q ((Q_\varepsilon^2 - Q_\theta^2) U_\theta + 2 Q_\theta Q_\varepsilon U_\varepsilon) \qquad 3.12$$

As in equation 2.11 these terms represent the electronic energy, E_E, at the origin of mode displacement ($Q_\theta = Q_\varepsilon = 0$) and the nuclear kinetic and potential energy terms; V_E is the linear coupling coefficient and the additional quadratic coupling term in V_q gives the warping terms.The matrices ordered in the θ , ε basis vectors are

$$I_E = \begin{pmatrix} 1 & 0 \\ 0 & 1 \end{pmatrix} \qquad U_\theta = \begin{pmatrix} -1 & 0 \\ 0 & 1 \end{pmatrix} \qquad U_\varepsilon = \begin{pmatrix} 0 & 1 \\ 1 & 0 \end{pmatrix} \qquad 3.13$$

This gives (Ham, 1968)

$$S_E = V_E^2 / 2\mu\hbar\omega^3 \qquad 3.14$$

Defining $\alpha = \frac{\hbar\omega}{4S_E}$, $\quad |\beta| = \frac{V_q \cdot \hbar^2}{2\mu\alpha}$ 3.15

provides a dimensionless constant (β/α), known as the warping parameter.The results of Davies' calculations show that

$$|\beta/\alpha| = 1.4 \pm 0.1$$

assuming $S_E \geqslant 3$.This value of $|\beta/\alpha|$ is in agreement with both the energy spacing ratio $\Delta/3\Gamma$ and the stress matrix element ratio

obtained experimentally (Stoneham (1977) has estimated $|\beta/\alpha|$ as 1.9 but the new experimental data should make the above value more reliable) Davies calculations also predict $|E_{A_1}/D| = 1.125 \pm 0.015$ which lies in the experimental range (equation 3.11) and $|E_{A_2}/D| \sim 0.85$ which is not as small as the experimental value.Unfortunately the reason for this discrepancy is not obvious but the energy of the A_2 state is 17 meV. above the zero phonon level, comparable with phonons of 40 meV. which occur at the GR1 centre so, perhaps, in this case the model breaks down.

As mentioned earlier, Lowther (1976) showed that the existence of the 1.665eV. line is evidence for a weak Jahn-Teller coupling to e- modes in the T_2 electronic state of the GR1 line.Davies (1979b) has recalculated the effects of this Jahn-Teller energy on the relative transition probabilities of the 1.665 and 1.673eV. lines; his results show that the experimental ratio (equation 3.9) is obtained when the Jahn-Teller relaxation of the e-modes coupling in the T_2 state is

$$S_T^E = 0.135 \pm 0.015$$

This is about seven times larger than Lowther's value but it can be seen that the Jahn-Teller energy in the T_2 state is small, being only about 4% of that in the ground state.Davies has also shown that the relaxation of the T_2 state in the t-modes of vibration is

$$S_T^T \sim 0.15$$

which means that the coupling of the T_2 electronic state is weak to both e and t modes.This fits in with the general conclusion (Davies, 1979a) that Jahn-Teller effects in theexcited states of optical centres in diamond tend to be negligable, in contrast to the strong effects in the ground state.

To summarize this section, the experimental determination of the energy of the A_2 vibronic level led to a more accurate determination

of the warping terms in the Jahn-Teller effect in the GR1 ground state and the experimental determination of the ratio of the intensities of the 1.665 and 1.673eV. lines gave a revised valuefor the e-mode coupling in the T_2 state and led to an estimate of the t-mode coupling in this state.But although the Jahn-Teller properties of the GR centre have now been fixed with more precision than hitherto, there are still many unanswered problems, particularly concerning the shapes of the GR1 absorption and luminescence bands.

CHAPTER IV

The GR Centre, II

Introduction:

Thr GR band has many other interesting and puzzling features as well as the zero-phonon line doublet; principal among these are the prominent 40 meV. 1 phonon sideband and the very sharp GR 2-8 lines seen in absorption.In this chapter we identify the symmetry of the 1-phonon sideband from its response to uniaxial stress and report the analysis of stress effects on the GR 2-8 lines.

1.The 40 meV. Sideband.

The GR1 zero-phonon line is replicated by a strong phonon sideband involving phonons of all the allowed energies in the host diamond lattice (see figure 3.1).In particular there is a prominent 40 meV. sideband, this energy lying in the low energy acoustic modes of diamond.The shape of the GR1 absorption curve is by no means understood so, as a first stage in this study, the response of the 40 meV. sideband to uniaxial stress was studied.The stress was applied as described in section 1.5; the effects of this stress are shown in figure 4.1 where a reasonable background has been assumed to represent the underlying phonon structure.

The full width at half height of this phonon sideband is $\sim$20 meV. and as the stress is increased it broadens considerably.No splitting was observed as the applied stress was increased so in order to compare the behaviour of this sideband with its parent zero-phonon line as a function of stress, the change in the centroids of the GR1 lines and the sideband was found.Two methods were used to find these centroids: the first, simple method used equal areas taken from the transmission spectrum, the second was far more rigorous.

In general the absorption coefficient, μ at a specific frequency

Absorption spectra, measured at liquid nitrogen temperature, showing the effect of 3GPa compressive stress on the GR1 zero-phonon line and the 40 meV one-phonon sideband

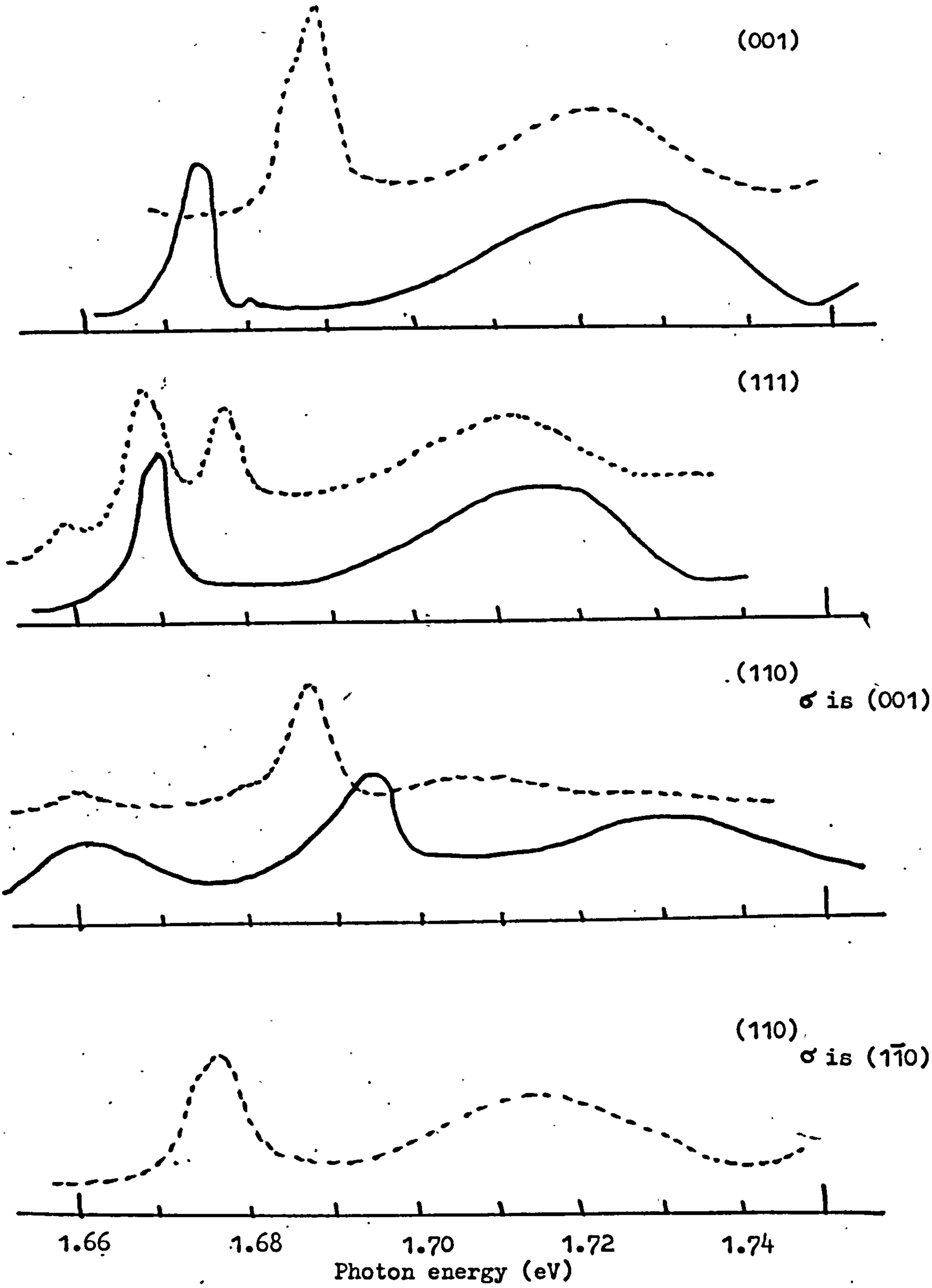

Figure 4.1

may be written as

$$\mu = \ln\left(I_o/I_T\right) \qquad 4.1$$

where the symbols I_o and I_T are explained in figure 4.2a and unit thickness of specimen is considered. Equation 4.1 may be rewritten as

$$\mu = \ln\left(\frac{I_T + \Delta}{I_T}\right) = \ln\left(1 + \frac{\Delta}{I_T}\right) \qquad 4.2$$

If $\Delta/I_T \ll 1$, i.e. the absorption is small, then

$$\ln\left(1 + \frac{\Delta}{I_T}\right) \sim \left(\frac{\Delta}{I_T}\right)$$

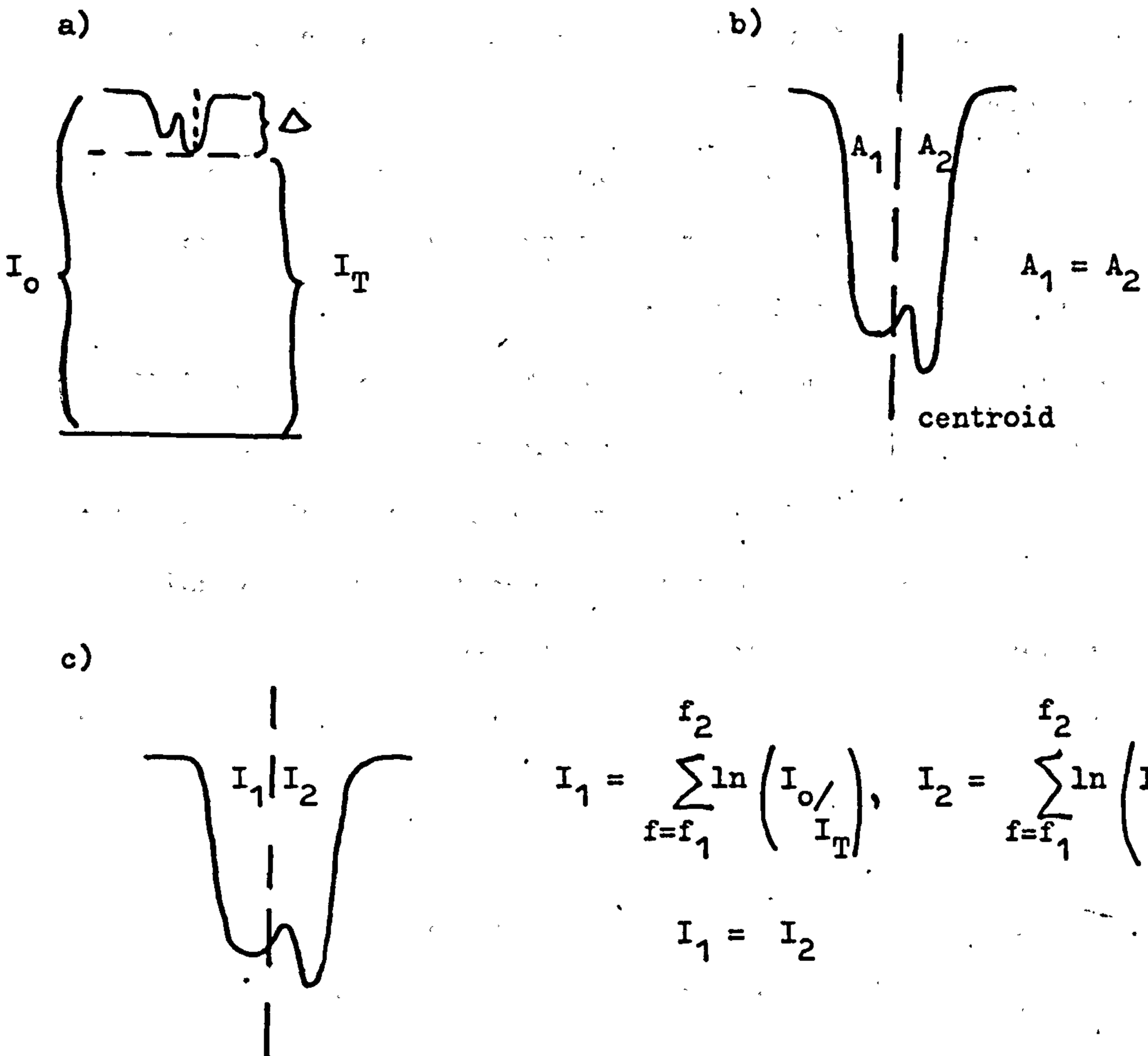

$$I_1 = \sum_{f=f_1}^{f_2} \ln\left(I_o/I_T\right), \quad I_2 = \sum_{f=f_1}^{f_2} \ln\left(I_o/I_T\right)$$

$$I_1 = I_2$$

Figure 4.2

In this case the total absorption in a spectral line is

$$\sum_{f=f_1}^{f_2} \mu_f = \sum_{f=f_1}^{f_2} \left(\frac{\Delta}{I_T} \right) \qquad 4.3$$

where the sum is taken over the total extent of the spectral line.If, however, $(\Delta / I_T) \sim 1$ then the total absorption is

$$\sum_{f=f_1}^{f_2} \mu_f = \sum_{f=f_1}^{f_2} \ln \left(I_o / I_T \right) \qquad 4.4$$

From equation 4.3 the total intensity may be found simply by taking the total area of the spectral line and dividing it by an average value for I_T.In this case the centroid of the line is that point which divides it into equal areas (see figure 4.2b).From equation 4.4 the total intensity may be found by taking the value of $\ln(I_o/I_T)$ at each point on the spectral line and then finding the sum; the centroid is then the point.which divides the line into equal intensities (figure 4.2c) It was thought that the equal areas method would be sufficient for this analysis but the second method was used to check the accuracy of the first.Both methods gave the same values for the changes of the centroids with stress; these are plotted in figure 4.3.

Under (001) stress the π component of the 40 meV. sideband has a linear shift rate, in contrast to the curved shift of the π zero-phonon line.This would indicate that the π sideband component originates in the E_ε component of the E ground state and not in its $E\theta$ component (figure 4.4a)This change in selection rule implies that the 40meV. sideband is an E to T_1 transition, in contrast to the E to T_2 electric dipole transition for the zero-phonon line. This is clarified by figure 4.4b which shows the allowed electric dipole transitions, together with their relative intensities, from

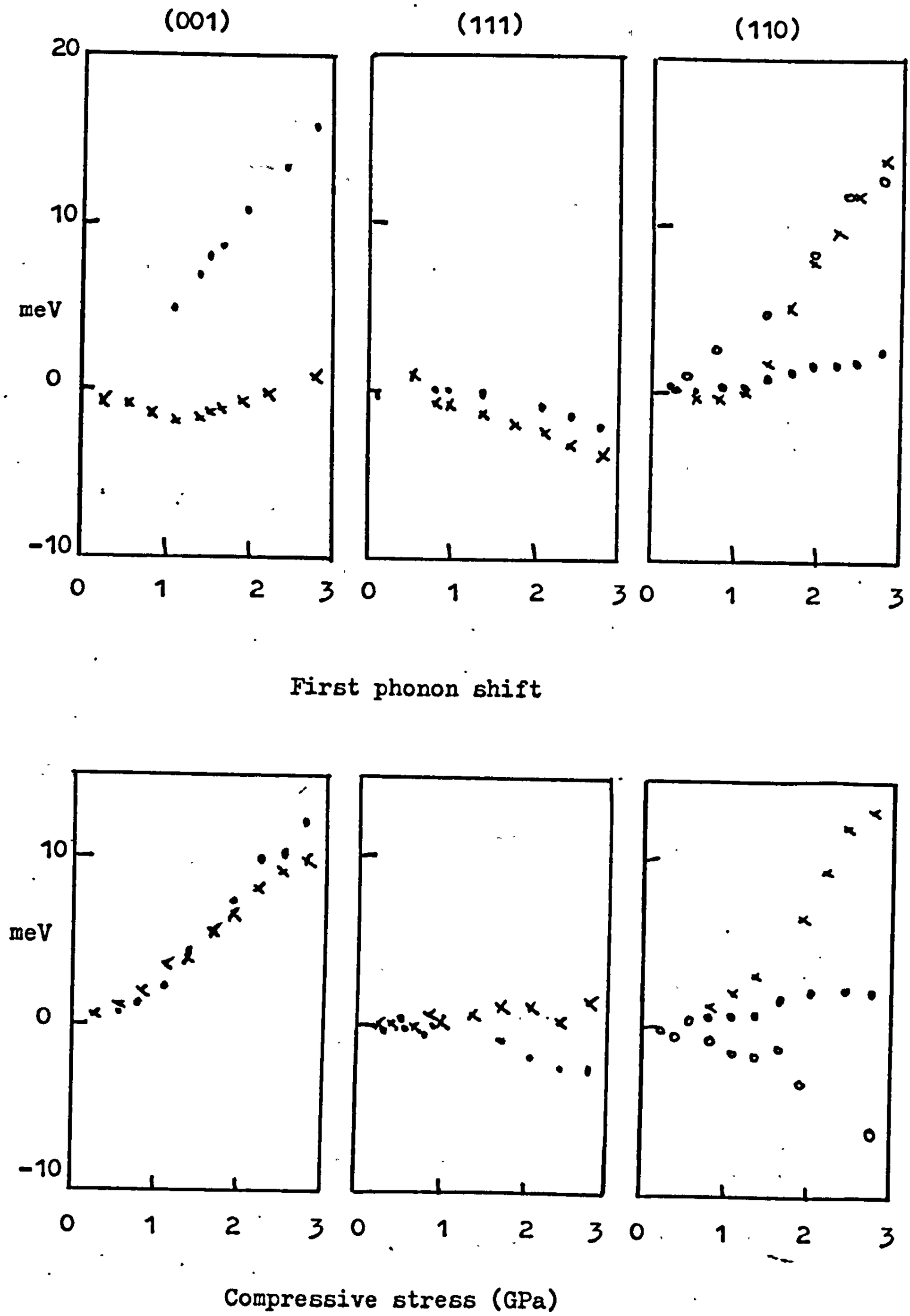
Zero phonon shift
(001)
(111)
(110)
20
10
meV
0
-10
0
1
2
3
First phonon shift
10
meV
0
-10
Compressive stress (GPa)

Figure 4.3

a)

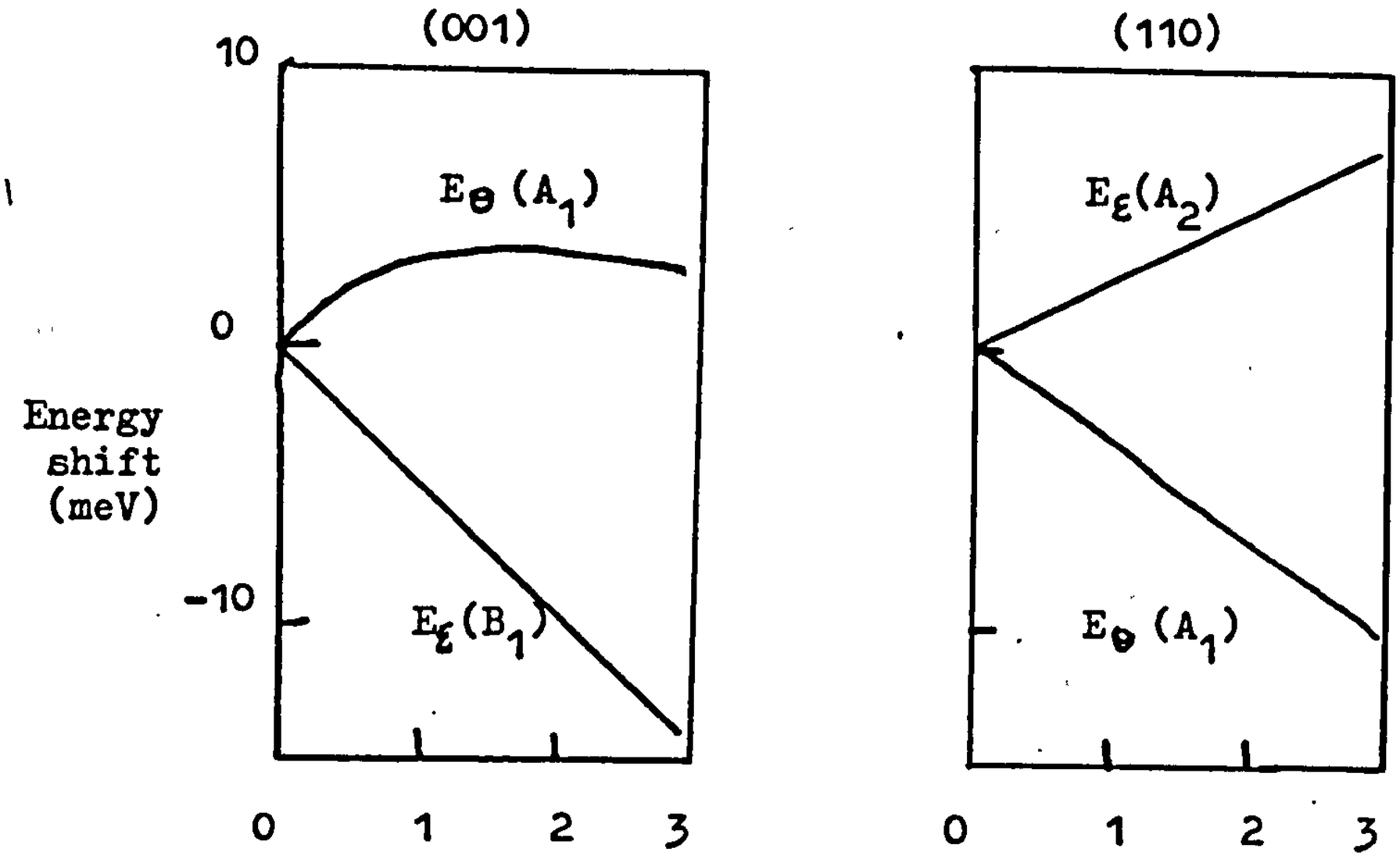
(001)
(110)
10
0
-10
Energy shift (meV)
$E_\theta (A_1)$
$E_\varepsilon (B_1)$
$E_\varepsilon (A_2)$
$E_\theta (A_1)$
0 1 2 3
0 1 2 3
Compressive stress (GPa)

b)

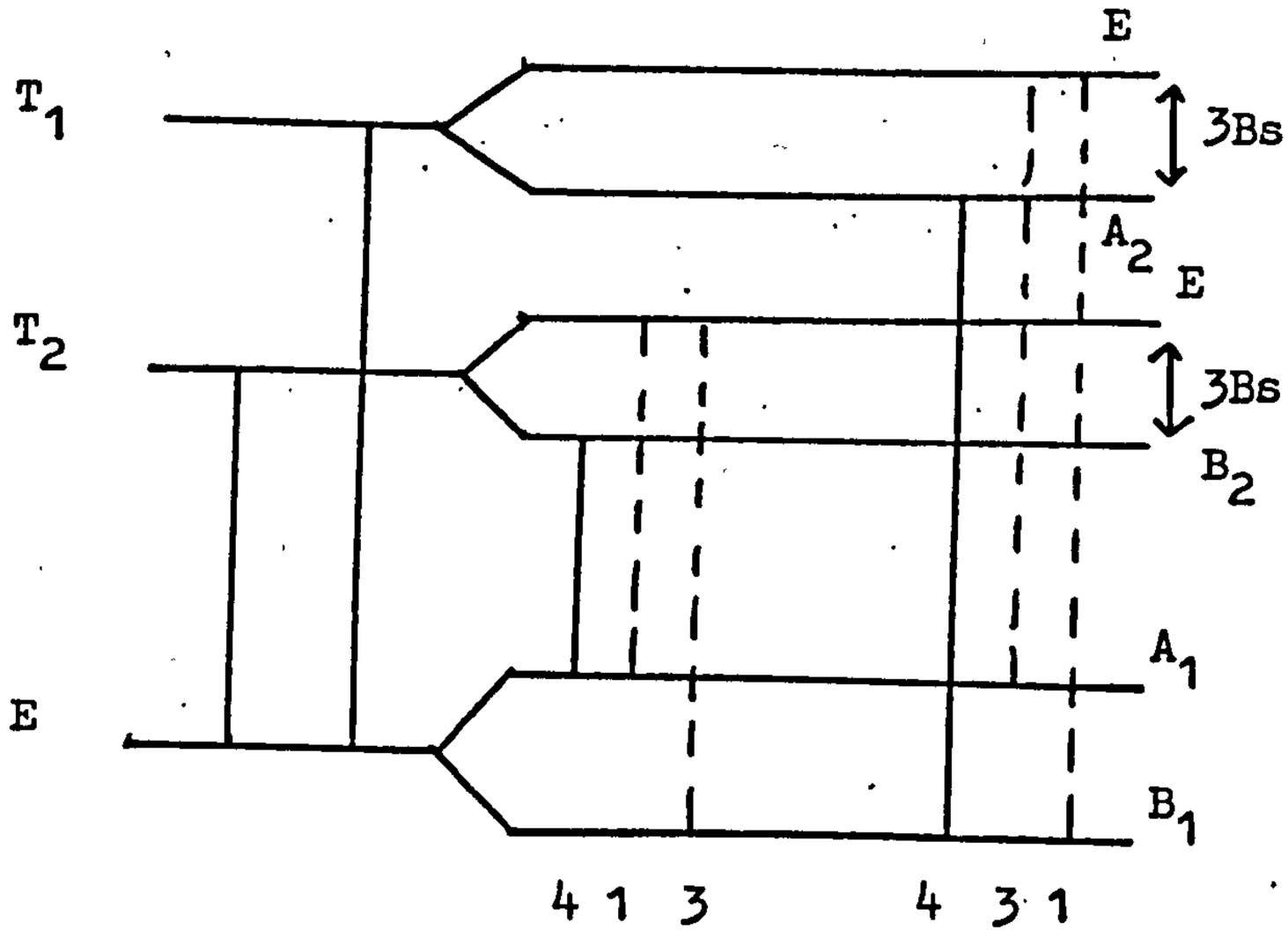
E
T_1
3Bs
A_2
E
T_2
3Bs
B_2
A_1
E
B_1
4 1 3
4 3 1
T_d
D_{2d}

Figure 4.4

an E state to T_2 and T_1 states under (001) stress.

Under (110) stress the only difference between the change of centroid for the 40meV. sideband and the zero-phonon line is in the σ(001) component.For an E to T_1 transition this component originates in the E_ξ level of the E ground state whereas for E to T_2 it originates in the E_θ component (figure 4.4b).If the 40 meV. sideband π component originates from the E_ξ component of the ground state under (001) stress, and the π component of the zero-phonon line originates from the E_θ component, then its intensity could be expected to increase with stress relative to that of the zero-phonon line.Similarly, the intensity of the σ(001) component of the 40 meV. sideband should decrease relative to that of the zero-phonon line under (110) stress; from figure 4.4 it can be seen that this is the case.

The splitting of the T_1 vibronic level under stress may be equated to the splitting of the parent electronic state if the dependence of phonon energy on stress (Parsons, 1977; Grimsditch et al, 1978) and the complications that may arise through the Ham effect being different in different vibronic levels are ignored.Under (001) stress the T_1 vibronic level splits into E and A_2 states separated by 3Bs, where s is the applied stress and B is defined in equation 3.4, with the value given in Table I.At 3 GPa, then, the π component of the one phonon sideband should shift by 9B less than the σ component of the zero-phonon line; this is observed experimentally (figure 4.3). The σ one phonon component should have a smaller shift at low stresses than the σ zerophonon component but at high stress they shoul adopt similar shift rates as the E ground state becomes depopulated; again this is observed experimentally.The data for the (110) and (111) stress directions may be understood using the same approach.It is therefore concluded that the 40 meV. sideband in the GR1 absorption

spectrum is a transition to an excited state which transforms as T_1.

In section 3.5 it was stated that the GR1 T_2 electronic state coupled weakly to e and t modes of vibration.From the character table for the T_d point group (Tinkham, 1964) the direct products give $T_2 \times E = T_1 + T_2$ and $T_2 \times T_2 = T_1 + T_2 + E + A_2$.Thus, from group theory, it is possible for a T_2 electronic state to couple to e modes and t modes of vibration to give a T_1 vibronic state.Sakamoto and Muramatsu (1978) have shown that T x e and T x t coupling is complicated, the exact order of energy levels depending on the admixture of the two components, but one of the possibilities is a T_1 first excited vibronic state.The behaviour, then, of the 40 meV. sideband under stress is further evidence for the Jahn-Teller coupling in the T_2 excited state since a sideband produced by a totally symmetric phonon would have the same selection rules in its stress spectra as its parent zero-phonon line.

2.The GR 2-8 Lines.

The GR 2-8 lines shown in figure 4.5 (see also figure 3.1) lie to much higher energy than the GR1 lines; They are superimposed on the "ultra-violet" continuum at energies between 2.88 and 3.01 eV. and are very sharp and closely spaced.Work on the temperature dependence of the intensity of the GR1 and the GR 2-8 lines by Walker et al (1974) indicated that these lines all originate at the same defect.These workers also concluded from their uniaxial stress data that the GR 2 and 3 lines were transitions from the E ground state of the GR centre to excited levels transforming as T_1.The present work has confirmed this analysis and has extended it to cover the GR 4-8 lines which have also been found to be transitions to T_1 excited states.As has already been noted, the detailed correlations by Walker et al (1974) and the quantitative analysis in the present work (section 4.3) imply that the GR lines

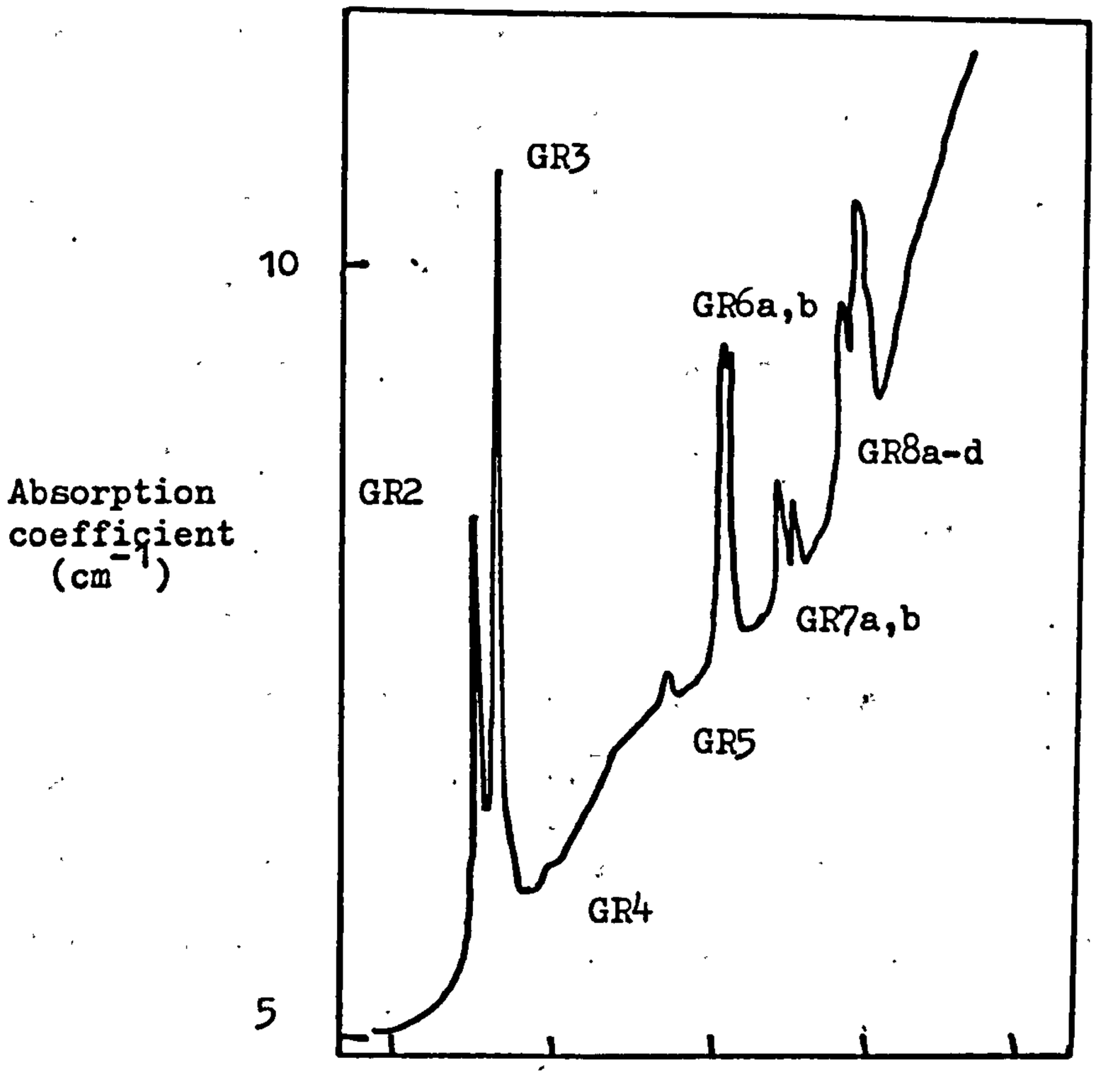

Figure 4.5

all occur at the same centre; this contrasts with the Stark effect measurements reported by Kaplyanskii et al (1971).These indicated a linear effect for GR1, 6, and 8 and a quadratic effect for GR2 and 3. A linear Stark effect suggests that the lines occur at optical centres without inversion symmetry whereas a quadratic effect indicates optical centres with inversion symmetry.However, recent remeasurements of the Stark effect on the GR lines cast strong doubts on the accuracy of the existing data (Davies and Manson, unpublished).

Dyer and du Preez (1965) observed reversible bleaching behaviour between the GR1 and ND1 bands; this was attributed to charge

exchange effects between the two centres.As the GR1 band changed in intensity during thermal bleaching and optical illumination treatments, the corresponding variations of intensity of the ultra-violet absorption band were also observed and this led to the suggestion that the threshold of the ultra-violet continuum corresponded to the ionisation of the GR defect.This led Farrer and Vermeulen (1972) to investigate the photoconductivity of the GR centre.They showed that there is a sequence of photoconduction minima which correspond exactly to the optical absorption maxima of GR1.It therefore appears that the optical excitation of GR1 does not give rise to free charge carriers. However, their high resolution study of the photoconductivity of GR 2-8 showed that sharp photoconduction maxima are developed at the same positions as the optical absorption maxima; this indicates that absorption by the GR 2-8 lines creates free charge carriers.Clark et al (1979) have shown that photoexcitation of the GR 2 and 3 lines produces free positive holes.

The occurence of sharp peaks in the photoconduction spectra of solids is unexpected, although some cases are known; sharp peaks are normall associated with transitionsbetween bound states whereas transitions involving the valence or conduction bands are characterised by broad absorption features.One of the main problems, then, in explaining the origin of the GR 2-8 lines is to account for their sharpness and their low temperature photoconductivity.Some theories of their origin will be outlined in section 4.4, although currently their is no really satisfactory explanation for them.

3. Uniaxial Stress Measurements on the GR 2-8 Lines.

Uniaxial stress measurements were made on the GR 2-8 lines as described in section 1.5.Stresses up to 3 GPa. were applied to the samples held at liquid nitrogen temperature.A confirmatory set of

results was also obtained with the samples held at about 10K in a helium flow cryostat.At zer stress GR 2 and 3 are clear sharp lines; GR4 and GR5 are very weak whilst GR6 and GR7 both consist of two nearly degenerate lines.Collins (1978) has shown that GR8 consists of five very sharp, close lines of different intensities; however, it was not possible to resolve all five lines in this work so GR8 was parameterised assuming only four lines, which could be clearly resolved.If the very weak fifth line has the same transformation properties as the other four then this omission is qualitatively unimportant.

Since the lines are all very close together there was a great deal of mixing of the states under stress; there was, however, no detectable interaction between the GR2, 3, and 4 lines and the higher GR5-8 lines so the lines were analysed as two groups.The GR2-4 group is considered first.

At very low stress, before any appreciable mixing of states occurs, the GR2,3, and 4 lines behave as predicted for E to T_1 transitions at a T_d centre (Kaplyanskii, 1964b); see figure 4.6, where the stress split components of the GR2-4 lines at 0.5GPa. are compared with the theoretical stress splitting patterns for an E to T transition in T_d symmetry at infinite temperature (i.e. population of ground state levels equal).As the stress is increased, however, considerable mixing of states occurs and it becomes necessary to take account of this.The secular matrix for stress perturbations within each T_1 state has the same form as equation 3.4.The secular matrix for three interacting T_1 states has the form shown in figure 4.7.

Thus, the GR 2-4 states can be described by a 9 x 9 secular matrix.The energy of each optical transition is then the difference between the appropriate eigenvalues of the 9 x 9 matrix for the T_1 levels and the 4 x 4 matrix for the E, A_1, A_2 ground state levels

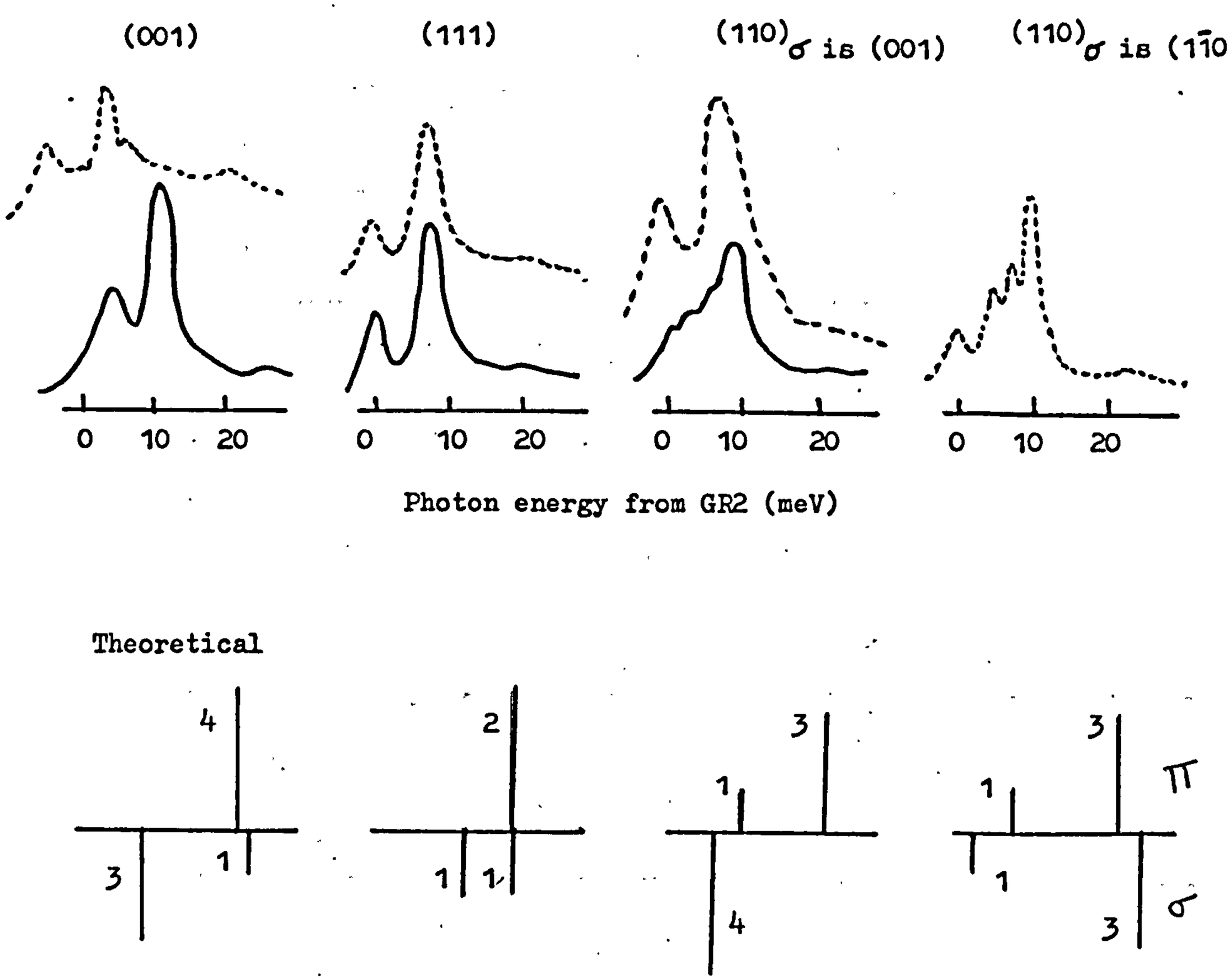

Figure 4.6

(see equation 3.3).The stress parameters were estimated from the behaviour of the lines at low stress and were optimised by varying them about these estimated values until a best fit to experiment was obtained.The lines in figure 4.8 were calculated using this theory and the stress matrix elements used are listed in Table II.The notation used in Table II is similar to that of equation 3.4; for example, B_2 describes coupling to $s_{E\theta}$ and $s_{E\varepsilon}$ within the excited state of the GR2 line while B_{23} describes the coupling of the excited states of GR2 and GR3

a) The GR 2-4 block matrix.

	2	3	4
2	M_{22}	M_{23}	M_{24}
3	M_{23}	M_{33}	M_{34}
4	M_{24}	M_{34}	M_{44}

b) with i,j, = 2,3,4

$$M_{ij} = M_{ji} =$$

	x_i	y_i	z_i
x_j	$W_n + A_{ij}s_A + \frac{1}{2}B_{ij}(\sqrt{3}\, s_{E\varepsilon} - s_{E\theta})$	$C_{ij}s_{xy}$	$C_{ij}s_{xz}$
y_j	$C_{ij}s_{xy}$	$W_n + A_{ij}s_A - \frac{1}{2}B_{ij}(\sqrt{3}\, s_{E\varepsilon} + s_{E\theta})$	$C_{ij}s_{yz}$
z_j	$C_{ij}s_{xz}$	$C_{ij}s_{yz}$	$W_n + A_{ij}s_A + B_{ij}s_{E\theta}$

n = 2,3 or 4, $W_n = 0$ for $i \neq j$

c) $A_{ij} = (\, x_i | c_A | x_j \,)$, $B_{ij} = (\, x_i | c_{E\theta} | x_j \,)(-2)$, $C_{ij} = (\, x_i | c_{xy} | y_j \,)$

Figure 4.7

by $s_{E\theta}$ and $s_{E\xi}$.The agreement between experiment and calculation is reasonable except for the lines (a) and (b) seen under (001) stress. The fit for these lines may be improved (at the expense of fits in other stress directions) by changing only the interaction parameters A_{23} and B_{23}.This suggests that there may be another excited state very close to GR2 and GR3 which has not been observed in absorption experiments. This possibility will be discussed later in section 4.4.

The overall validity of the theory can be checked by calculating the intensity of the stress split components of the lines and comparing it with experiment.The total intensity, I, of a transition from the j^{th} level of the ground state to the k^{th} level of an excited state is

$$I \propto |\langle\psi_j| \underline{x} |\psi_k\rangle|^2 P_j \qquad 4.1$$

where ψ_j, ψ_k are the wave functions for the two levels, $\underline{x}$ is the

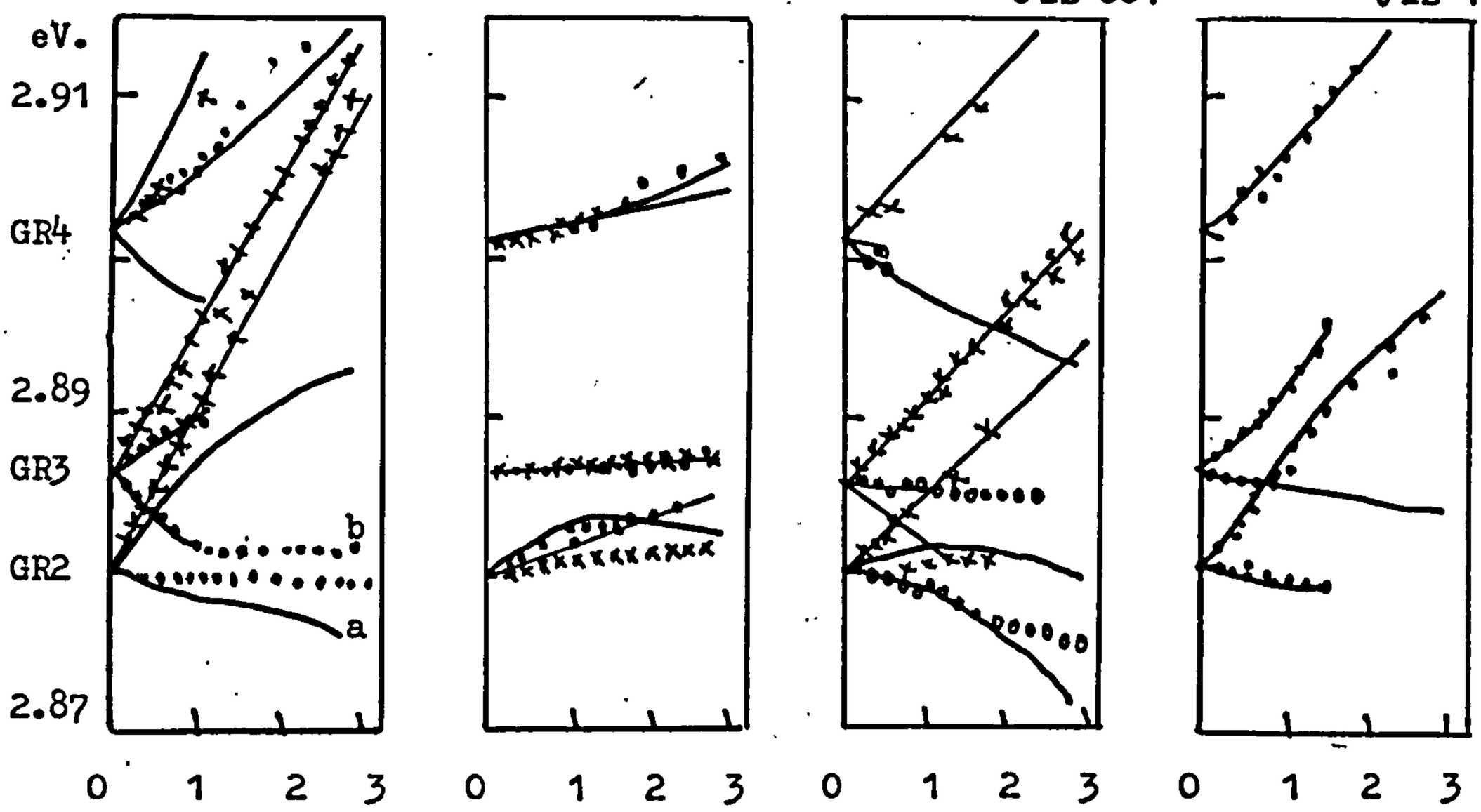

Figure 4.8

TABLE II

The stress matrix elements for the T_1 states of GR 2-8. Units are meV$(GPa)^{-1}$ with an uncertainty of approximately $\pm$ 0.5meV$(GPa)^{-1}$. Those terms equal to zero in the theory of section 4.2 are not listed.

$A_2 - A_E$	3.0	$A_{8a} - A_E$	-3.3	A_{6a6b}	0.5
B_2	0.94	B_{8a}	2.0	B_{6a6b}	-0.25
C_2	3.0	C_{8a}	0	C_{6a6b}	0
$A_3 - A_E$	0.25	$A_{8b} - A_E$	-0.3	A_{6a7a}	0.6
B_3	1.9	B_{8b}	-2.2	B_{6a7a}	-0.3
C_3	0.2	C_{8b}	2.55	C_{6a7a}	1.8
$A_4 - A_E$	1.0	$A_{8c} - A_E$	0.8	A_{6b7a}	1.0
B_4	2.0	B_{8c}	-0.7	B_{6b7a}	1.0
C_4	0	C_{8c}	2.3	C_{6b7a}	0
$A_5 - A_E$	1.34	$A_{8d} - A_E$	0	A_{7a7b}	-2.0
B_5	-2.0	B_{8d}	-1.0	B_{7a7b}	3.0
C_5	-2.0	C_{8d}	-2.0	C_{7a7b}	-5.0
$A_{6a} - A_E$	0.8	A_{23}	-0.5	A_{7b8a}	-1.0
B_{6a}	0.8	B_{23}	0.5	B_{7b8a}	-1.0
C_{6a}	-0.1	C_{23}	-2.5	C_{7b8a}	0
$A_{6b} - A_E$	0.03	A_{34}	1.0	A_{8a8b}	0.5
B_{6b}	-1.5	B_{34}	-1.0	B_{8a8b}	0.5
C_{6b}	-0.5	C_{34}	1.0	C_{8a8b}	0
$A_{7a} - A_E$	0.2	A_{56a}	1.0	A_{8b8c}	0.6
B_{7a}	2.0	B_{56a}	1.0	B_{8b8c}	0.6
C_{7a}	0.14	C_{56a}	0	C_{8b8c}	0
$A_{7b} - A_E$	0.1	A_{56b}	0.2		
B_{7b}	0.1	B_{56b}	0.2		
C_{7b}	0.06	C_{56b}	0		

electric dipole operator for the transition and P_j is a weighting factor for the population of the j^{th} level of the ground state.At zero stress the unperturbed wave functions ψ, for the ground state levels would be of the form

$$\psi_\theta\ ,\ \psi_\varepsilon, \psi_{A_1}, \psi_{A_2}$$

and for the excited T_1 states of the GR2, 3, and 4 lines

$$\psi_{x2},\ \psi_{y2}, \psi_{z2}, \psi_{x3},\ \text{-------}\ \psi_{z4}$$

where the subscript x2 refers to the Tx level of the GR2 state etc.

At stress, however, where mixing of levels occurs, typical wave functions for the j^{th} ground state level and the k^{th} excited state level would be

$$\psi_j = a_{1j}\psi_\theta + a_{2j}\psi_\varepsilon + a_{3j}\psi_{A_1} + a_{4j}\psi_{A_2}$$

$$\psi_k = b_{1k}\psi_{x2} + b_{2k}\psi_{y2} + b_{3k}\psi_{z2} + b_{4k}\psi_{x3} + \text{-------} b_{9k}\psi_{z4}$$

4.2

where the a are the eigenvectors for the j^{th} level and the b are the eigenvectors for the k^{th} level (as explained above, the GR2-4 lines can be treated independently of the GR5-8 lines)The eigenvectors were calculated for each eigenvalue at all stresses using the NAG library of the University of London on a CDC 6600 computer and the value of P_j for each level could be calculated at all stresses.Knowing the coupling coefficients of E and T_1 under the electric dipole operator (Griffiths, 1964) and the intensity of each transition at zero stress, the total intensity of each transition at every stress could be found from equation 4.1.In order to make a meaningful comparison between calculation and experiment the actual shapes of the stress split spectra were calculated.A Lorentzian line-shape of the form

$$I(f) = \frac{a}{(f - f_o)^2 + b} \qquad 4.3$$

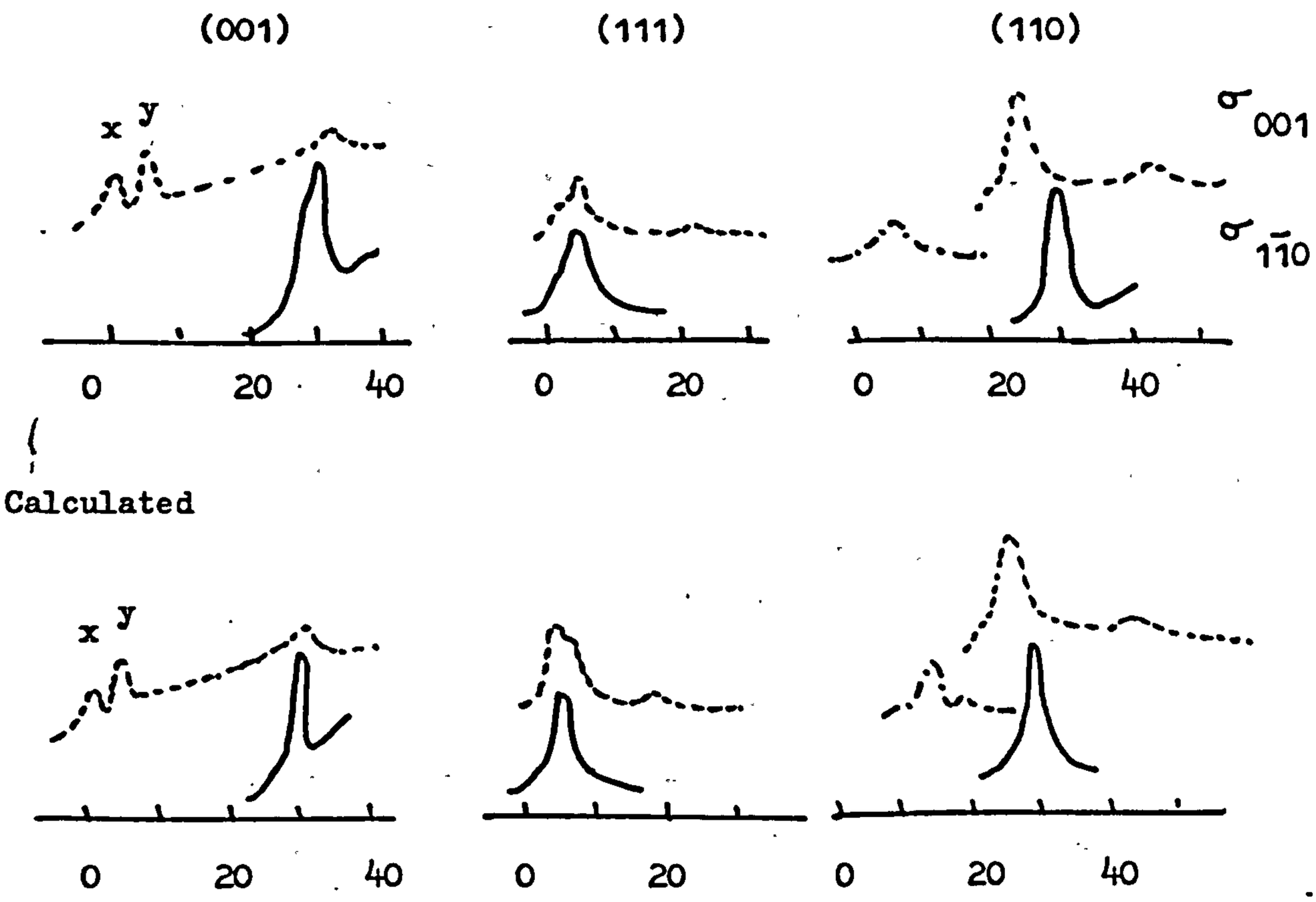

Figure 4.9

was assumed, where a/b = the height, h, of the spectral line when $f=f_o$ and the width, w, at half height = $2\sqrt{b}$. The calculations on equation 4.1 give the total intensity I at a particular stress fo a particular component of the absorption spectrum.This is related to the parameters of equation 4.3 by

$$I = \frac{\pi . a}{\sqrt{b}} \qquad 4.4$$

b is found from the width of each component.This width was set equal to the width of the parent state at zero stress, whereas in practice the lines tend to broaden with increasing stress due to inhomogeneities in the stress field; the calculate spectra should therefore be imagined

to be spread out somewhat.The calculated and experimental spectra for the GR 2-4 lines at a stress of 3 GPa. are shown in figure 4.9 where the overall agreement is quite good.

The GR 5-8 lines were analysed in the same way as the GR 2-4 lines.The problem was slightly more complicated since a 27 x 27 matrix was required for the analysis of the 9 T_1 states of the GR5, 6a, 6b, 7a, 7b, and 8 a-d lines.The parameters used to calculate the shifts and intensities of the lines are given in Table II; in general it was found that only interactions between neighbouring zero stress states need to be taken into account so that parameters such as $A_{57a} \sim 0$.The shifts with stress of the GR 5-8 lines are shown in figure 4.10 and a comparison of the experimental and calculated spectra is shown in figure 4.11. Again the agreement between experiment and theory is good.

The stress experiments performed at a sample temperature of 10K confirmed that the GR 2-8 lines were all T_1 states since the transitions predicted to occur from the higher level of the E ground state for each stress direction froze out as the stress was increased.The low temperature experiments also confirmed the predicted temperature dependence of the lines; for example, as a result of stress induced mixing of the GR 2 and 3 levels the lines x and y of figure 4.9 are not simply related to the GR 2 and 3 lines at zero stress, despite their similar appearance. The line x is frozen out at 10K as predicted by the theory.The full energy level diagram for the GR 1-8 lines is given in figure 4.12

The E ground state of the GR system has a large Jahn-Teller relaxation estimated at 0.63eV. by Stoneham (1977).In view of the small size of the stress parameters of the GR 2-8 excited states it could be expected that each of the GR 2-8 lines has a vibronic sideband of similar shape to the GR1 band.To test this theory, the GR1 absorption spectrum was scaled down for each of the GR 2-8 lines;

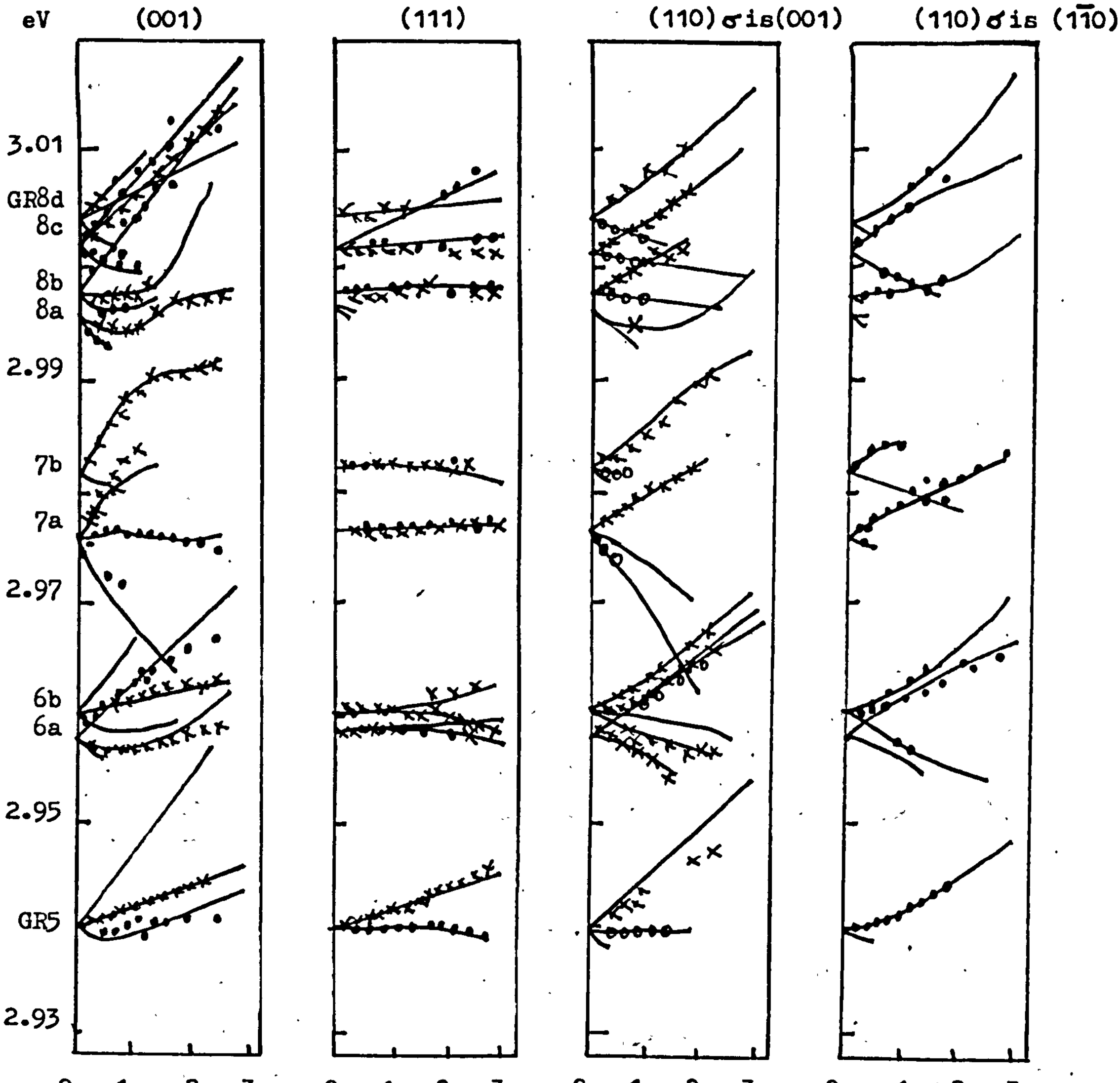
eV
(001)
(111)
(110) σ is (001)
(110) σ is (1$\bar{1}$0)
3.01
GR8d
8c
8b
8a
2.99
7b
7a
2.97
6b
6a
2.95
GR5
2.93
0 1 2 3 0 1 2 3 0 1 2 3 0 1 2 3
Compressive stress (GPa)

Figure 4.10

a)The GR 2-8 lines at zero stress.

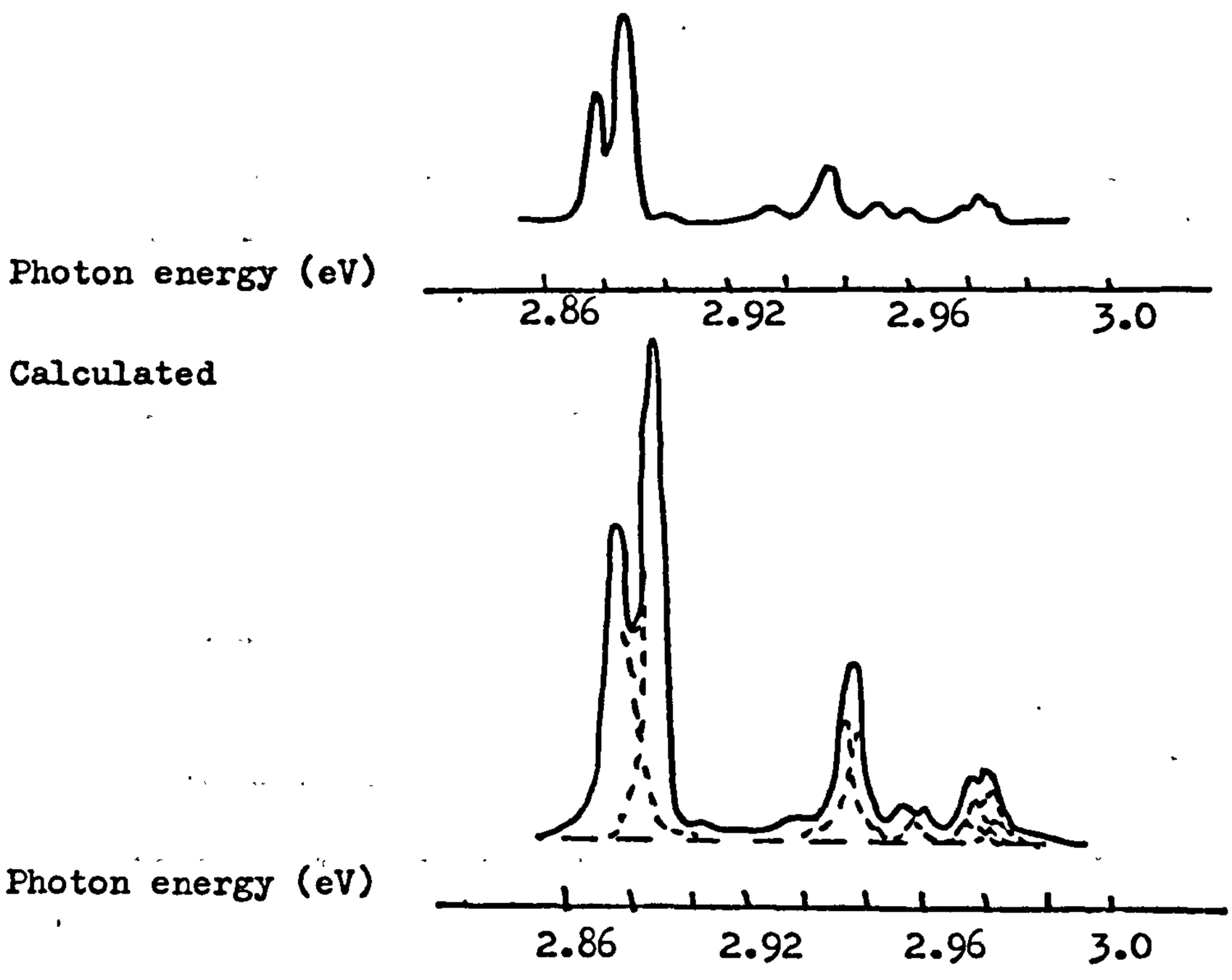

b)The GR5-8 lines at 3GPa.

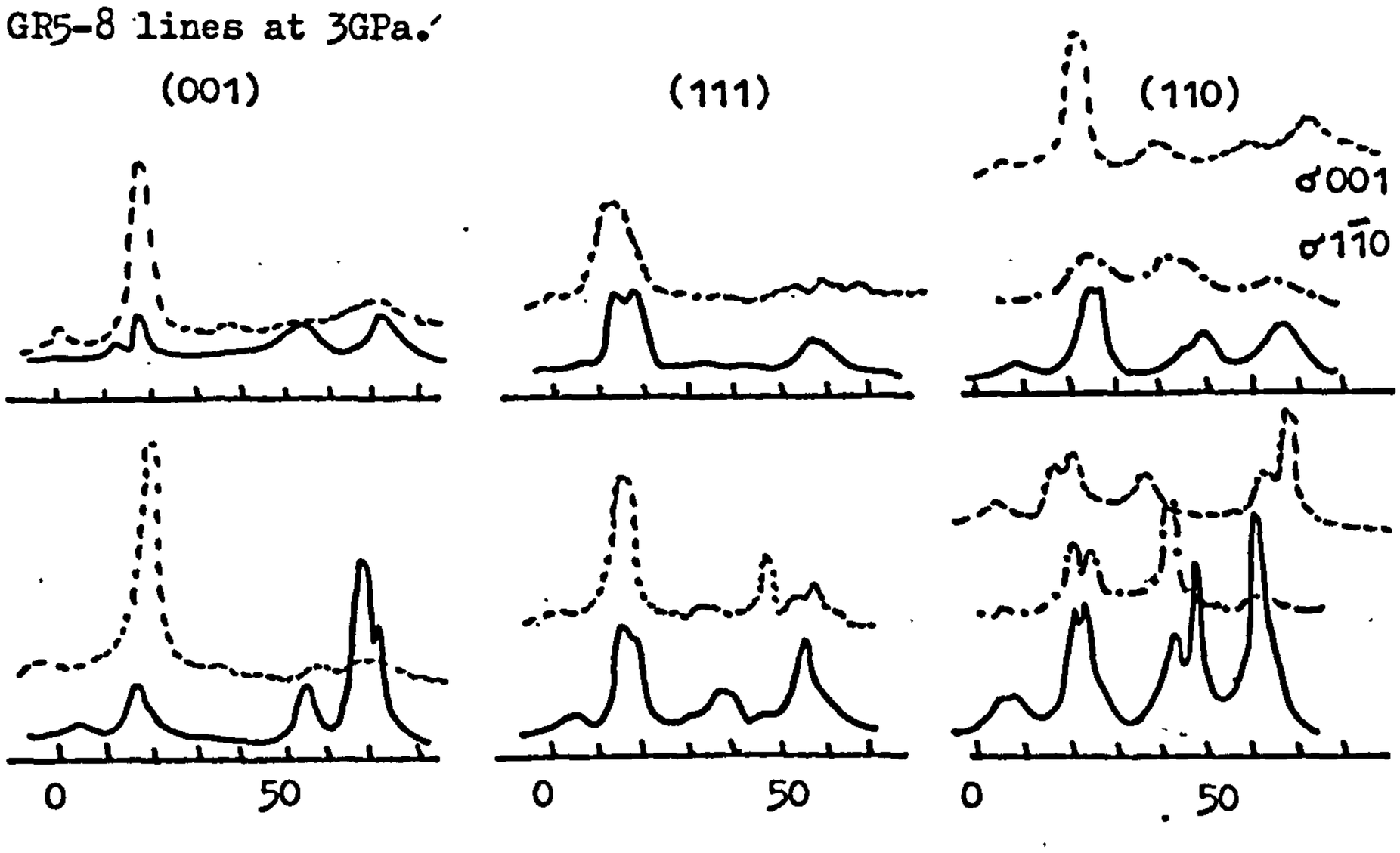

Figure 4.11

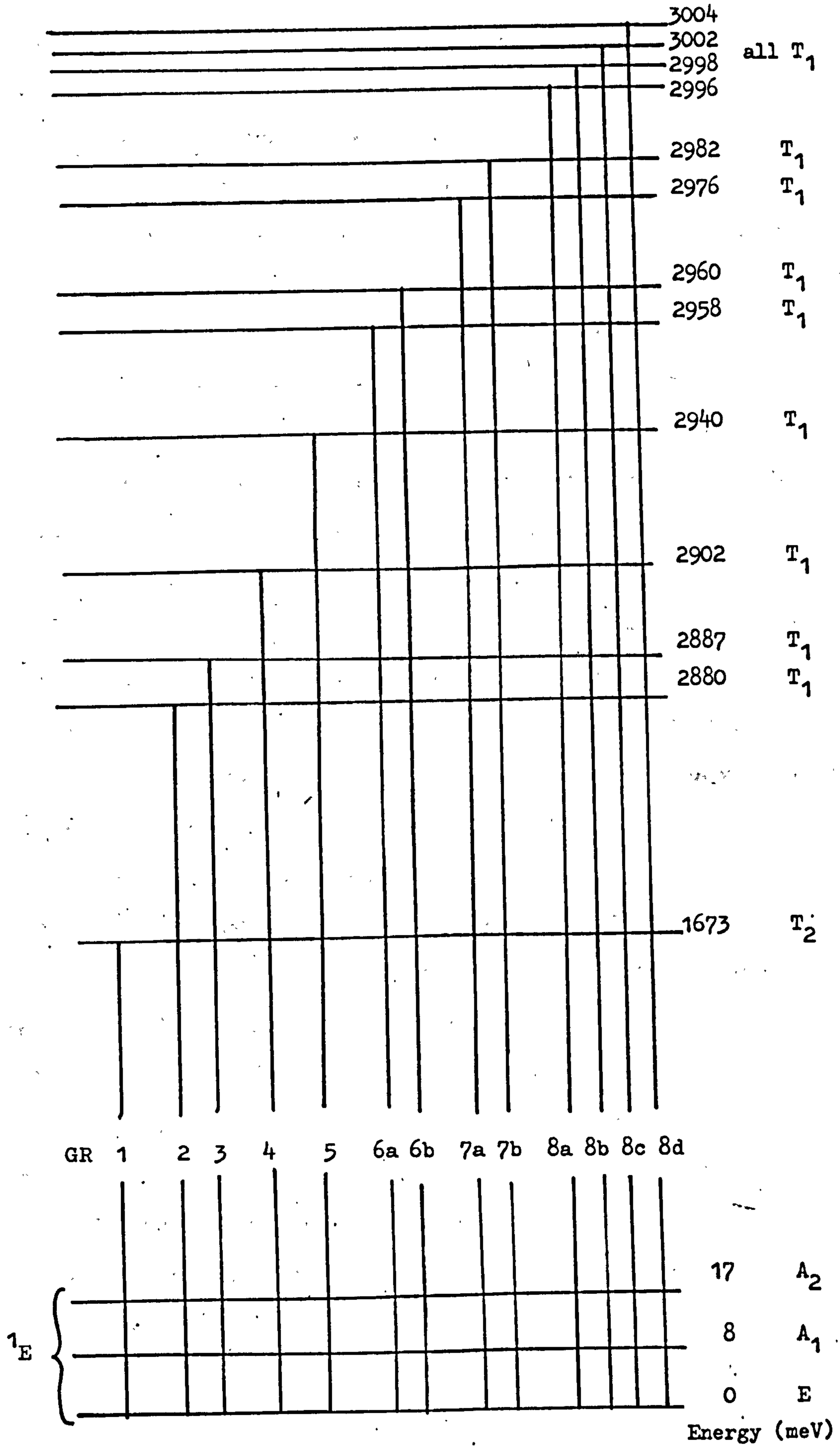
3004
3002
2998
2996
all T1
2982 T1
2976 T1
2960 T1
2958 T1
2940 T1
2902 T1
2887 T1
2880 T1
1673 T2
GR 1 2 3 4 5 6a 6b 7a 7b 8a 8b 8c 8d
17 A2
8 A1
0 E
1E
Energy (meV)

Figure 4.12

for example, to obtain a vibronic bandshape for the GR2 line, all the points on the GR1 absorption curve were multiplied by the factor

$$\frac{\text{Intensity of GR2 at zero stress}}{\text{Intensity of GR1 at zero stress}}$$

A similar scaling factor was applied for all the GR 2-8 lines.The picture obtained by adding all these vibronic sidebands is shown in figure 4.13. This simple picture will be modified by the interactions between the GR 2-8 excited states, which may account for the 1 phonon sidebands of GR 2 and 3 being too intense on this simple picture.However, it can be seen that this approach produces a substantial continuum above 2.9 eV and so the observed continuum can be considered to originate simply in the phonon sidebands of the GR 2-8 lines.

The extraordinary situation, then, is that the GR 2-8 lines are 13 closely spaced sharp lines whose excited states belong to the same irreducible representation.The theory outlined above fits the observed shifts and intensities of the lines under stress, but, as will be seen in section 4.5, no really satisfactory theoretical model has been advanced to explain these lines.

4.A Possible Explanation for Discrepencies in the GR 2 and 3 Data.

As shown in the previous section, the fit of theory to experiment for the GR 2-8 lines is very good except for the lines (a) and (b) of GR 2-3 seen under (001) stress (figure 4.8).A possible explanation for this discrepency could be that there is another, undetected state near the GR2 and GR3 levels; if this state were close to the GR2 and GR3 excited levels it could interact with these without seriously interacting with the other states and so it need not produce a worse fit for the other lines.As noted in the previous section, changing the interaction parameters A_{23} and B_{23} does produce a worse fit to the other components of GR 2-3 so an undetected excited

The GR 2-8 Band

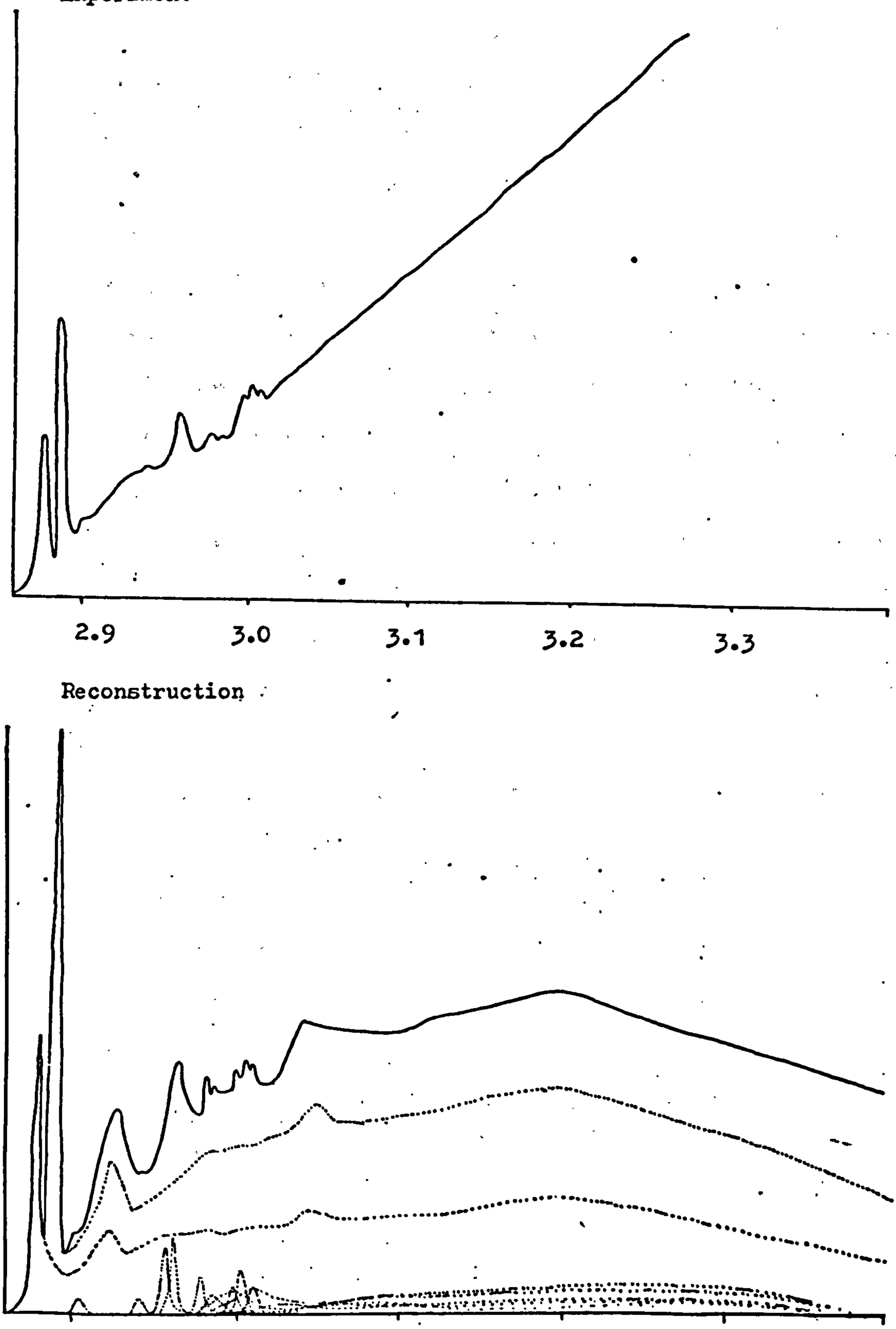

Figure 4.13

state seems to be the most likely cause of the discrepency.

The nature of this hypothetical undetected state must be such that under (001) stress it will interact with the states giving rise to the σ transitions of GR2 but not with those giving rise to the π transitions since the theory and experiment agree well for the π line. From figure 4.4b it can be seen that the allowed electric dipole transitions from the E ground state of the GR centre to an excited T_1 state are from B_1 to A_2 for π polarisation and from A_1 and B_1 to E for σ polarisation. The transformation properties of this state must therefore be such that it woll interact with the E component of T_1 but not the A_2 component under (001) stress.In the reduced point group D_{2d} of T_d, E is equivalent to Tx, Ty and A_2 is equivalent to Tz of T_d.

The only possible states allowed for a centre of T_d symmetry are A_1, A_2, E, T_1, and T_2 and if the stress axis is along (001) then the stress transforms as the E_θ component of the E irreducible representation.If this hypothetical state is to couple with the T_1 level of GR2 under stress the direct product of its irreducible representation with E must contain T_1.From the character table for T_d it is found that

$$T_1 \times E = T_1 + T_2, \qquad \text{and} \qquad T_2 \times E = T_1 + T_2$$

the other direct products of A_1, A_2 and E with E yielding combinations of A_1, A_2 and E only.This state must therefore transform either as T_1 or T_2.The effect of an operator transforming as E_θ on the coupling of T_1, T_1 and T_1, T_2 states can be found from Griffiths (1964)

coupling of T_1 to T_1:

T_1	x	y	z
x	$-\frac{1}{2}$	.	.
y	.	$-\frac{1}{2}$	.
z	.	.	1

T_1

coupling of T_1 to T_2:

T_1	x	y	z
x	$-\frac{1}{2}\sqrt{3}$	.	.
y	.	$\frac{1}{2}\sqrt{3}$	.
z	.	.	.

T_2 (4.5

From equation 4.5 it can be seen that coupling of the T_1 state to another T_1 state will affect both the E (Tx, Ty) and the A_2 (Tz) levels of T_1 whereas coupling to T_2 will affect only the E level.Thus, if a state does exist close to the GR2 and GR3 states it must be a T_2 state since this is the only state which will interact with the levels giving rise to lines (a) and (b) of figure 4.8 whilst leaving the others relatively unaffected.

The problem, however, is why this state remains undetected, since E to T_2 electric dipole transitions are allowed.Collins (1978a) has obtained very high resolution optical spectra of the GR 2-8 lines and there was no evidence of the transition that would result from the presence of this T_2 state in his work.If, however, this transition was very weak (as, for example, GR4 is very weak) and was within about 2meV. of the GR2 transition, then it is possible that it would remain undetected since it would be completely masked by the GR2 transition.

Thus the discrepency in the GR 2-3 data can be explained if an excited state transforming as T_2 and lying very close to the T_1 state of GR2 is postulated.

5.Theories of the Origin of the GR 2-8 Lines.

Many theoretical treatments have been proposed for the neutral vacancy in diamond; Clark and Mitchell (1977) have suggested that, for the GR centre, the ground state is $\sim$ 2.4eV. above the top of the valence band and the GR 1-8 transitions correspond to the excitation of holes.The GR 2-8 levels then lie inside the valence band.Lowther (1977) has suggested that GR1 is a transition between molecular orbitals localised on the dangling bonds about the vacancy while the GR2-8 lines arise from molecular orbitals localised on other sp^3 hybrids of the first neighbours to the vacancy.These orbitals would

be in the valence band, within about 0.55eV. of its edge.However, the spread of the GR 2-8 lines is ~ 125meV. which is not consistent with all of them arising from separate molecular orbitals localised within the valence band.Also, there has been some caution about suggesting that sharp optical transitions such as GR 2-8 could result from discrete energy levels within a band because they would be expected to decay into band states with a short lifetime, thus making the linewidths large.Mainwood (1978) has shown that transitions out of localised states within the valence band can only have narrow enough linewidths to fit the GR 2-8 lines if they are localised quite closely on the nearest neighbours to the vacancy and their energies are very close to the valence band edge; in this case, however,they would be too close to the edge for them all to originate in this way.

Dunn (1976) has proposed the following model for the GR lines: The GR centre is a vacancy V^{o} which can compensate the boron acceptor levels in type IIb diamond; this makes V^{o} positively charged (Coulson and Larkins, 1971).V^{+} has a lowest spin allowed transition at ~ 6eV. which is therefore not observed in the absorption spectrum.The GR1 band is identified as the excitation of the neutral vacancy to a state described by a positive hole bound to a negatively charged vacancy.

$$V_o^o \rightarrow (V_o^- + h)_o \qquad 4.6$$

The transitions GR 2-8 are supposed to arise from the excitation of the neutral vacancy in its ground state to a state of a hole bound to the n^{th} excited state of the negative vacancy.

$$V_o^o \rightarrow (V_n^- + h)_o \qquad 4.7$$

The ultra-violet continuous absorption and its associated photocarriers

(observed to be positive holes) are then identified with the excitation of the neutral vacancy to form a negatively charged vacancy and a free positive hole.

$$V_o^o \rightarrow \quad V_o^- \; + \; h \qquad 4.8$$

These transitions appear to be allowed at the site of a neutral vacancy so that an energy overlap between the processes of equations 4.7 and 4.8 provides an explanation of the sharp line photoconductivity and autoionisation behaviour of GR 2-8.

Of the theories so far put forward to explain the GR 2-8 lines, Dunn's seems to be the best.However, more theoretical analysis of this centre, which has already been the subject of a great deal of experimental and theoretical treatment is needed in order to give a full description of the puzzling behaviour of these lines.

To summarize this chapter, then, the 40meV. 1 phonon sideband of the GR1 line has been shown to have a T_1 excited state, in contrast to the T_2 excited state of its parent zero-phonon line; this gives more evidence for the Jahn-Teller coupling in the T_1 excited state. The GR 2-8 lines have all been shown to have T_1 excited states, giving 13 sharp, closely spaced lines of the same irreducible representation, a situation not found at any other defect centre in diamond.

CHAPTER V

The TR12 Centre

Introduction:

Electron irradiation of type II diamonds produces two sharp lines at 2.639eV. and 2.672eV. known as TR12 and TR13 respectively, together with accompanying phonon structure.In this chapter we analyse the uniaxial stress measurements on the TR12 and TR13 lines and obtain their stress parameters.We also report the stress effects on a sharp line seen at 2.437eV. in the TR12 luminescence spectrum.

1.Previous Work on TR12 and TR13.

The TR12 and TR13 zero-phonon lines were first observed by Clark et al (1956a,b).They, and Walker (1975), showed that these lines were usually present in type II diamonds that had been electron or neutron irradiated.O'Donnell (1979) has obtained a full luminescence and excitation spectrum of the TR12 centre; this is shown in figure 5.1 where it can be seen that,there is a gross breakdown in mirror symmetry between the relative intensities of the band features observed in excitation and luminescence.It had previously been thought that the TR13 line was a phonon replica of TR12 but from the luminescence spectrum it can be seen that TR13 is itself a zero-phonon like line. From the temperature dependence of the two lines O'Donnell (1979) has shown that the TR12 and TR13 transitions originate from a common ground state and have excited states of equal degeneracy.He has also used the high resolution excitation of the total luminescence to identify the absorption features labelled TR14-17 by Clark et al (1956b)In figure 5.1 TR14a is the acoustic phonon replica of TR12; TR14 and TR16 are the optic phonon replicas of TR12 and TR13 respectively, and TR17 is a transition equivalent to the sharp line at 2.437eV. seen in luminescence.The line at 2.437eV., labelled s in figure 5.1,

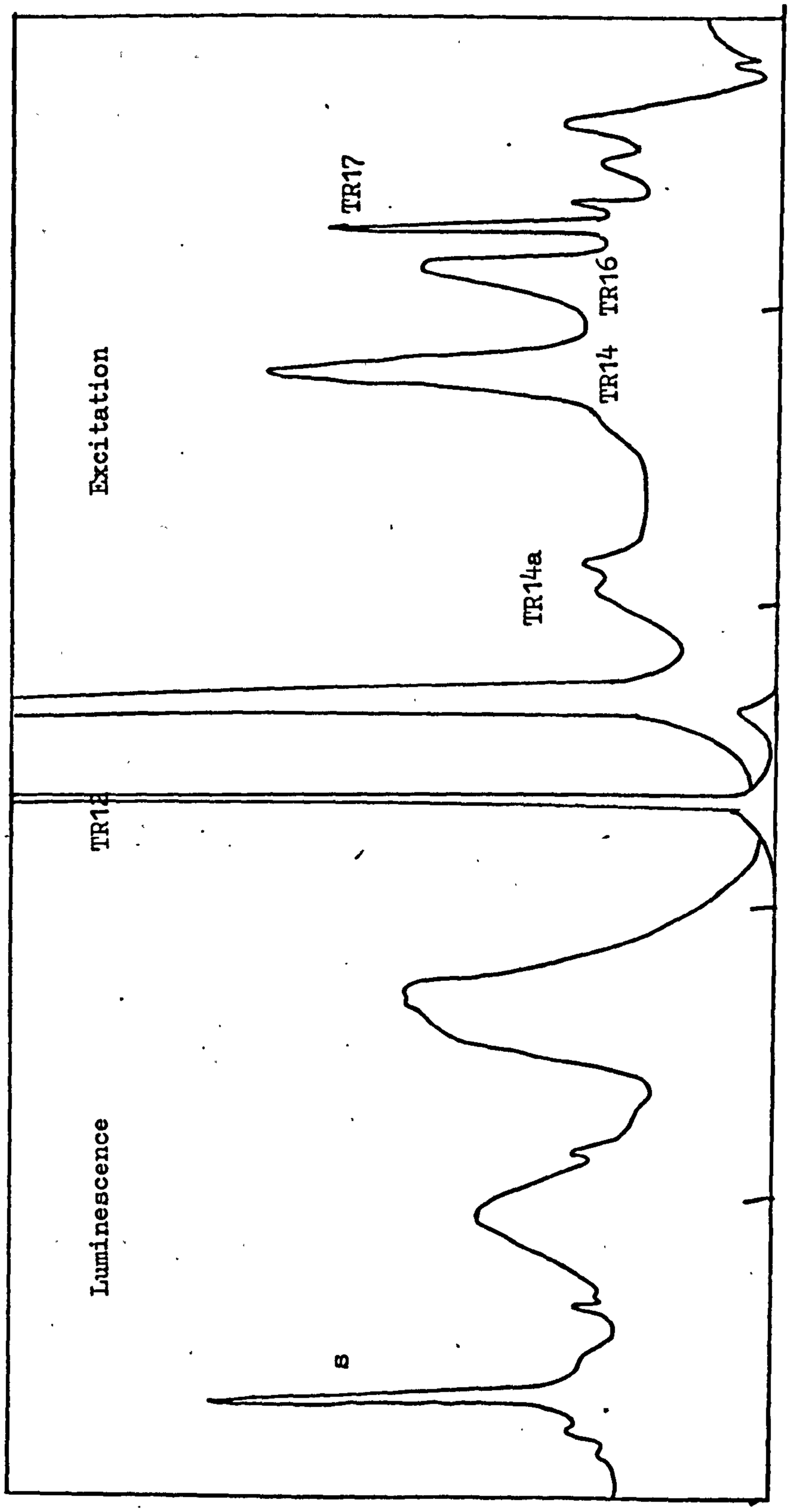
TR17
TR16
TR14
TR14a
TR12
TR8
Excitation
Luminescence
2.8
2.7
2.6
2.5
Photon energy (eV)

Figure 5.1

will be discussed in section 5.3.

Walker (1975) performed uniaxial stress experiments on the TR12 line and from his measurements concluded that the centre involved was probably of monoclinic I symmetry.Unfortunately the stresses applied by Walker were too low and he was unable to resolve all the splittings fully; also, no stress work was done on the broader TR13 line which, as will be shown in section 5.2, interacts with TR12 under stress.

Although the TR12 system is weak usually it is worth studying since it has several interesting properties, namely, the doublet nature of the TR12 and TR13 lines, the lack of mirror symmetry in the absorption and luminescence spectrum, and the sharp luminescence line at 2.437eV.In the present work very high stresses up to 3GPa were applied to TR12 and TR13 in order to investigate their interaction and the luminescence line at 2.437eV. was investigated in order to confirm that it was most probably a local phonon.

2.Uniaxial Stress Analysis of the TR12 and TR13 Lines.

The specimens used in this analysis were irradiated as described in section 1.3 and the uniaxial stress experiments were performed as described in section 1.5, with the specimens held at liquid nitrogen temperature.The results of these experiments are shown in figure 5.2 where the lines have been calculated as described lates in this section. TR13 has a line width of 4.8meV at zero stress and is therefore much broader than TR12 which has a width of 1.4meV; this made it difficult to observe any real splitting of TR13.The number of stress split components of TR12 indicated that the transition occurred from a σ oscillator at a monoclinic I centre (Kaplyanskii, 1964a) in agreement with Walker's analysis, but the intensities of the stress split components were very different from those predicted by Kaplyanskii. It was also impossible to obtain a good theoretical fit to the shifts

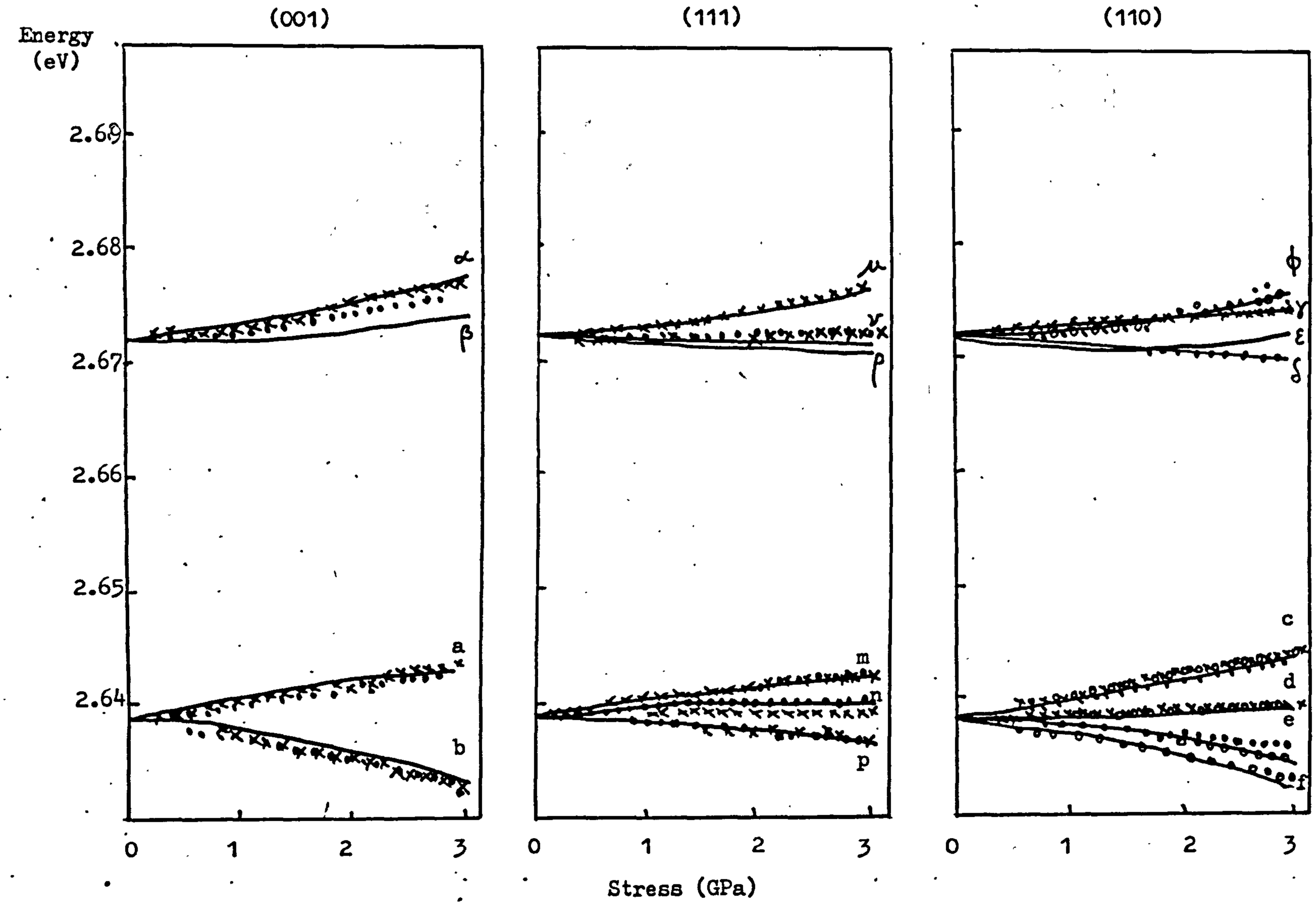
(001)
(111)
(110)
Energy (eV)
2.69
2.68
2.67
2.66
2.65
2.64
α
β
a
b
μ
ν
ρ
m
n
p
φ
γ
ε
δ
c
d
e
f
0
1
2
3
Stress (GPa)

Figure 5.2

of the lines under stress using the simple equation (equation 2.17) derived by Kaplyanskii for centres of monoclinic I symmetry.It was therefore concluded that the TR12 and TR13 transitions occurred at a σ oscillator at a monoclinic I centre but that there was stress induced mixing of the two excited states.

A monoclinic I centre has point groups C_{2h}, C_2, C_{1h}.The centre is shown diagramatically in figure 5.3a; here the C_2 axis is the Z axis and, as can be seen from figure 5.3b, the electric vector is described by the X and Y coordinates for a σ oscillator.In the C_{2h} point group X and Y transform as B_u and from the character table for C_{2h} (Tinkham, 1964) it is found that the only states between which transitions can occur are A_g and B_u, and A_u and B_g.The ground state

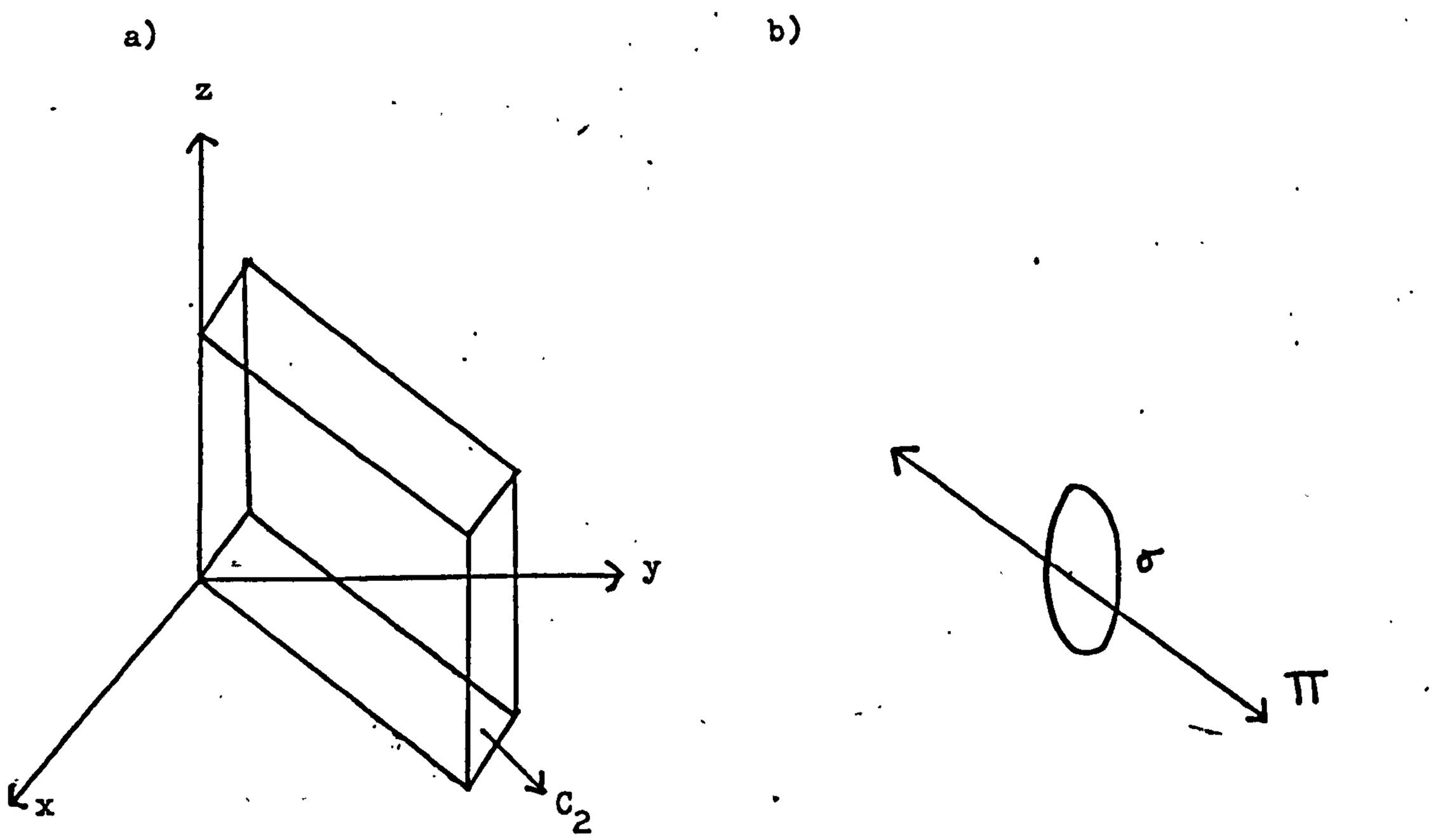

Figure 5.3

of the TR12 centre has therefore been taken as an A_g state and the two excited states to which the TR12 and TR13 transitions occur have been taken as B_u states.The analysis which follows would have been identical if the states had been taken as B_g and A_u.

There are 12 inequivalent orientations of the C_{2h} centrewith respect to a definite axis such as the stress axis.For convenience a set of local coordinates, X, Y, Z, are defined for each of the 12 inequivalent orientations; these are shown in Table III.

TABLE III

Centre	X	Y	Z
1	001	$1\bar{1}0$	110
2	$00\bar{1}$	110	$1\bar{1}0$
3	001	$\bar{1}10$	$\bar{1}\bar{1}0$
4	$00\bar{1}$	$\bar{1}\bar{1}0$	$\bar{1}10$
5	010	$\bar{1}01$	101
6	$0\bar{1}0$	101	$\bar{1}01$
7	010	$10\bar{1}$	$\bar{1}0\bar{1}$
8	$0\bar{1}0$	$\bar{1}0\bar{1}$	$10\bar{1}$
9	100	$0\bar{1}1$	$0\bar{1}\bar{1}$
10	$\bar{1}00$	011	$01\bar{1}$
11	100	$01\bar{1}$	011
12	$\bar{1}00$	$0\bar{1}\bar{1}$	$0\bar{1}1$

Since the crystal strains are small ($\leq 10^{-3}$) the dominant stress perturbation is given by terms linear in the stress tensor components, s_{LJ}, at each centre.The Hamiltonian at any centre is then

$$H = H_o + a_{Ag}s_{xx} + b_{Ag}s_{yy} + c_{Ag}s_{zz} + d_{Ag}s_{xy} + e_{Bg}s_{yz} + f_{Bg}s_{zx} \qquad 5.1$$

where the electronic operators a, b etc. transform as indicated by their subscripts and H_o is the Hamiltonian at zero stress.The $\varepsilon_{LJ} = p\, n_I n_K$ where p is the magnitude of the applied stress and n_I, n_K are the direction cosines of p with the I and K axes of the centre.Only electronic operators transforming as the totally symmetric representation can have non-zero matrix elements within the non-degenerate B_u states.The secular matrix for the two interacting B_u states is then

H	B_u^1	B_u^2
B_u^1	$A_1^1\varepsilon_{xx} + (A_2^1 - A_3^1)\varepsilon_{yy} + (A_2^1 + A_3^1)\varepsilon_{zz} + 2\sqrt{2}A_4^1\varepsilon_{xy} + W_1$	$A_1^{12}\varepsilon_{xx} + (A_2^{12} - A_3^{12})\varepsilon_{yy} + (A_2^{12} + A_3^{12})\varepsilon_{zz} + 2\sqrt{2}A_4^{12}\varepsilon_{xy}$
B_u^2	$A_1^{12}\varepsilon_{xx} + (A_2^{12} - A_3^{12})\varepsilon_{yy} + (A_2^{12} + A_3^{12})\varepsilon_{zz} + 2\sqrt{2}A_4^{12}\varepsilon_{xy}$	$A_1^2\varepsilon_{xx} + (A_2^2 - A_3^2)\varepsilon_{yy} + (A_2^2 + A_3^2)\varepsilon_{zz} + 2\sqrt{2}A_4^2\varepsilon_{xy} + W_2$

5.2

where the superscripts 1,2, and 12 refer to the TR12 state, the TR13 state and the mixture of the two respectively.

W_1 = 2639meV. and W_2 = 2672meV.

are the unperturbed energies of the B_u excited states.The matrix elements between these states are

$$A_1^1 = \langle B_u^1 | a_{Ag} | B_u^1 \rangle, \qquad A_2^1 - A_3^1 = \langle B_u^1 | b_{Ag} | B_u^1 \rangle$$

$$A_2^1 + A_3^1 = \langle B_u^1 | c_{Ag} | B_u^1 \rangle, \qquad 2\sqrt{2}\, A_4^1 = \langle B_u^1 | d_{Ag} | B_u^1 \rangle$$

with similar definitions for the A^2, A^{12}.

These definitions are consistent with Kaplyanskii's (1964a) notation for non-interacting states (see also equation 2.17).

The ground A_g state of the centre is perturbed only by the totally symmetric stresses and since the energy of a transition is

TABLE IV

The equations used for the least squares fit programme for the TR12 and TR13 lines. (at P = 1 a Pa)

Stress axis	Line	Centres giving transition	Equation
001	$\alpha+$ } $A-$ }	1,2,3,4	$\frac{1}{2}(W_1+W_2+A_1^1+A_{1-}^{2+}((W_1-W_2-A_1^1+A_1^2)^2 +4(A_1^{12})^2)^{\frac{1}{2}})$
	B	5,6,7,8, 9,10,11,12	$\frac{1}{2}(W_1+W_2+A_2^1+A_2^2-((W_1-W_2-A_2^1+A_2^2)^2 +4(A_2^{12})^2)^{\frac{1}{2}})$
111	$\mu+$ } $M-$ }	4,8,12	$\frac{1}{2}(W_1+W_2+X+Y^+_- ((W_1-W_2-X+Y)^2 +0.44Z^2)^{\frac{1}{2}})$
	$\nu+$ } $N-$ }	1,3,5,7, 9,11	$\frac{1}{2}(W_1+W_2+X^+ +Y^+ \pm ((W_1-W_2-X^+ +Y^+)^2 +0.44(Z^+)^2)^{\frac{1}{2}})$
	P	2,6,10	$\frac{1}{2}(W_1+W_2+X^- +Y^- -((W_1-W_2-X^- +Y^-)^2 +0.44(Z^-)^2)^{\frac{1}{2}})$
110	$\gamma+$ } $C-$ }	7,8,11,12	$\frac{1}{2}(W_1+W_2+Q^++R^{++}_- ((W_1-W_2-Q^++R^+)^2 +0.44(S^+)^2)^{\frac{1}{2}})$
	D	5,6,9,10	$\frac{1}{2}(W_1+W_2+Q^-+R^--((W_1-W_2-Q^-+R^-)^2 +0.44(S^-)^2)^{\frac{1}{2}})$
	$\varepsilon+$ } $E-$ }	1,3	$\frac{1}{2}(W_1+W_2+T^{+}+U^+ \pm((W_1-W_2-T^++U^+)^2 +0.44(V^+)^2)^{\frac{1}{2}})$
	F	2,4	$\frac{1}{2}(W_1+W_2+T^-+U^--((W_1-W_2-T^-+U^-)^2 +0.44(V^-)^2)^{\frac{1}{2}})$

For (111)stress

$X=(A_1^1+2A_2^1+2A_3^1)/3$, $Y=(A_1^2+2A_2^2+2A_3^2)/3$, $Z=(A_1^{12}+2A_2^{12}+2A_3^{12})/3$

$X^{\pm}=(A_1^1+2A_2^1-2A_3^1 \pm 4A_4^1)/3$, $Y^{\pm}=(A_1^2+2A_2^2-2A_3^2 \pm 4A_4^2)/3$

$Z^{\pm}=(A_1^{12}+2A_2^{12}-2A_3^{12}\pm 4A_4^{12})/3$

For (110)stress

$Q^{\pm}=(A_1^1+A_2^1 \pm 2A_4^1)/2$, $R^{\pm}=(A_1^2+A_2^2 \pm 2A_4^2)/2$, $S^{\pm}=(A_1^{12}+A_2^{12}\pm 2A_4^{12})/2$

$T^{\pm}=(A_2^1 \pm A_3^1)$, $U^{\pm}=(A_2^2 \pm A_3^2)$, $V^{\pm}=(A_2^{12}\pm A_3^{12})$

the difference in energy between the final and the initial states, the ground state can be treated as unperturbed so that the coefficients A_1^1 etc. in the secular matrix give the difference in response of the B_u excited and A_g ground states to the applied stress.

The energy of each transition can be calculated for any applied stress by diagonalising the secular matrix; the equations obtained, and the lines to which they relate, are shown in Table IV.The values of the parameters A_1^1 etc. were found by taking a least squares fit to these equations; the values thus obtained are listed in Table V.

TABLE V

Units are meV.$(GPa.)^{-1}$ with an uncertainty of $\pm$0.5meV.$(GPa.)^{-1}$

A_1^1	A_2^1	A_3^1	A_4^1
2.38	-0.3	0.12	-0.74
A_1^2	A_2^2	A_3^2	A_4^2
0.98	-0.64	-0.14	0.6
A_1^{12}	A_2^{12}	A_3^{12}	A_4^{12}
-3.16	4.1	-0.52	0.24

The bold lines in figure 5.2 have been calculated by inserting these values into the secular matrix for each stress direction and then finding the eigenvalues at all stresses.In this way the behaviour with stress of all the stress split components of the TR13 state could be predicted even though only some of them could be resolved experimentally.Thus, considering the lines γ and ϵ of TR13 seen under (110) stress, for example, the hteory indicates that there are two overlapping components for each of the lines, giving 4 stress split components, in agreement with the 4 resolved components, c, d, e, and f, of TR12.

If there had been no mixing under stress between the two excited B_u states then the relative intensity of each transition would be simply given by the square of the projection of the electric vector of the light on the X and Y coordinates of each centre.However, the mixing that occurs under stress makes the calculations more complicated. At zero stress the intensities of the TR12 and TR13 lines are given by

$$I_{12} \propto \left| \left(A_g \middle| X \middle| B_u^1 \right)\alpha + \left(A_g \middle| Y \middle| B_u^1 \right)\beta \right|^2$$

$$I_{13} \propto \left| \left(A_g \middle| X \middle| B_u^2 \right)\alpha + \left(A_g \middle| Y \middle| B_u^2 \right)\beta \right|^2$$

5.3

where α and β are projection factors projecting the electric vector on the X and Y coordinates of each centre respectively.As stress is applied the eigenstates $|+)$, $|-)$, whose eigenvalues are W_+ and W_- are, from equation 5.2

$$|+) = a^+ \left| B_u^1 \right) + b^+ \left| B_u^2 \right)$$

$$|-) = a^- \left| B_u^1 \right) + b^- \left| B_u^2 \right)$$

5.4

where, at zero stress, $a^+ = 0$, $b^- = 0$.The values of $a^{\pm}$, $b^{\pm}$ can be found at each stress and for each direction of stress using the University of London NAG library on a CDC 6600 computer.The intensities of the TR12 and TR13 lines at any stress become

$$I_{12} \propto \left| \left(A_g \middle| X \middle| - \right)\alpha + \left(A_g \middle| Y \middle| - \right)\beta \right|^2 . N$$

$$I_{13} \propto \left| \left(A_g \middle| X \middle| + \right)\alpha + \left(A_g \middle| Y \middle| + \right)\beta \right|^2 . N$$

5.5

where N gives the number of centres participating in each transition. Thus, knowing the relative intensities of the lines at zero stress, the intensities at any other stress may be calculated.The spectra shown in figure 5.4a have been calculated using this theory and

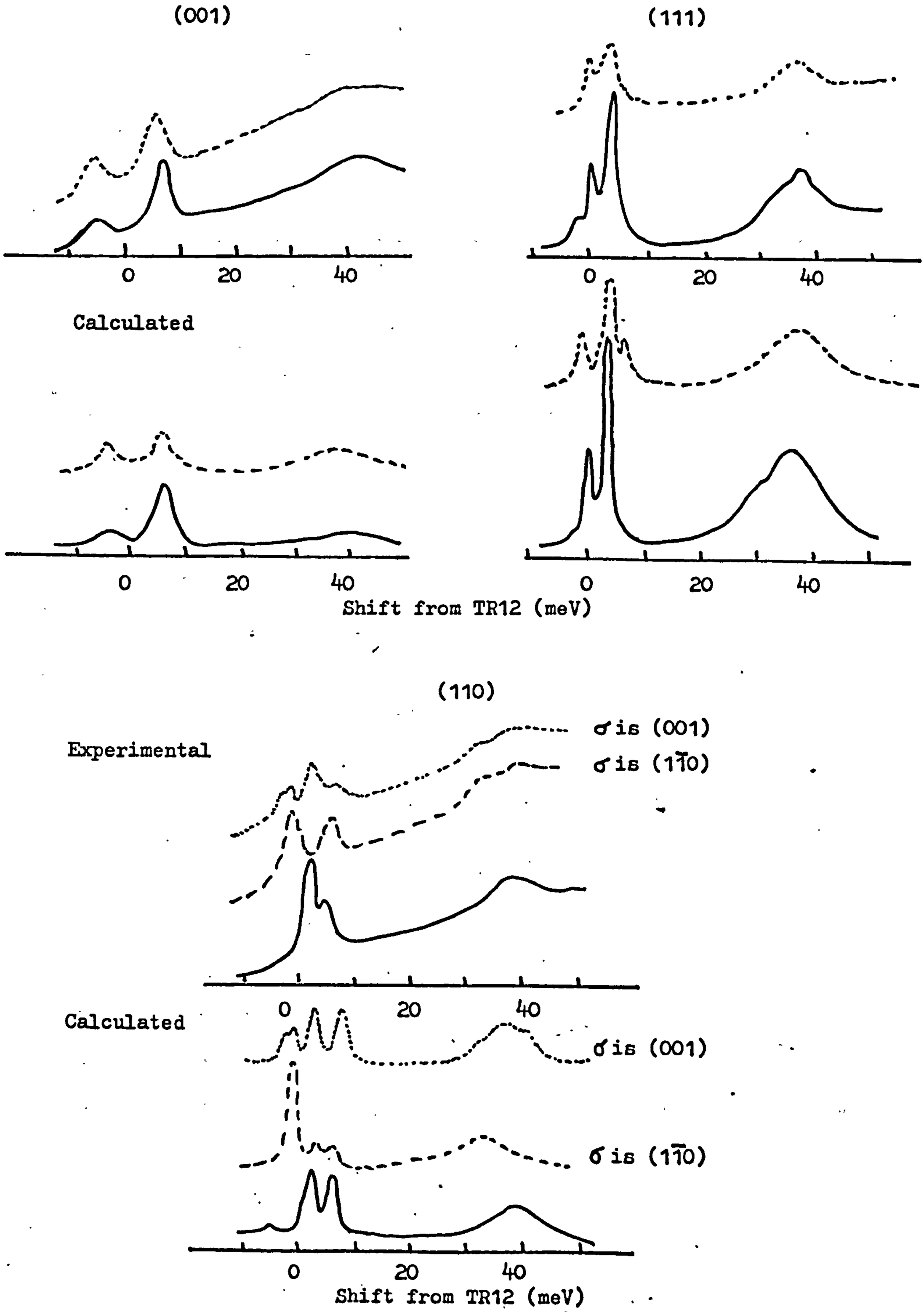
(001)
(111)
Experimental
Calculated
0
20
40
Shift from TR12 (meV)
(110)
Experimental
σ is (001)
σ is (1$\bar{1}$0)
Calculated
σ is (001)
σ is (1$\bar{1}$0)
0
20
40
Shift from TR12 (meV)

Figure 5.4a

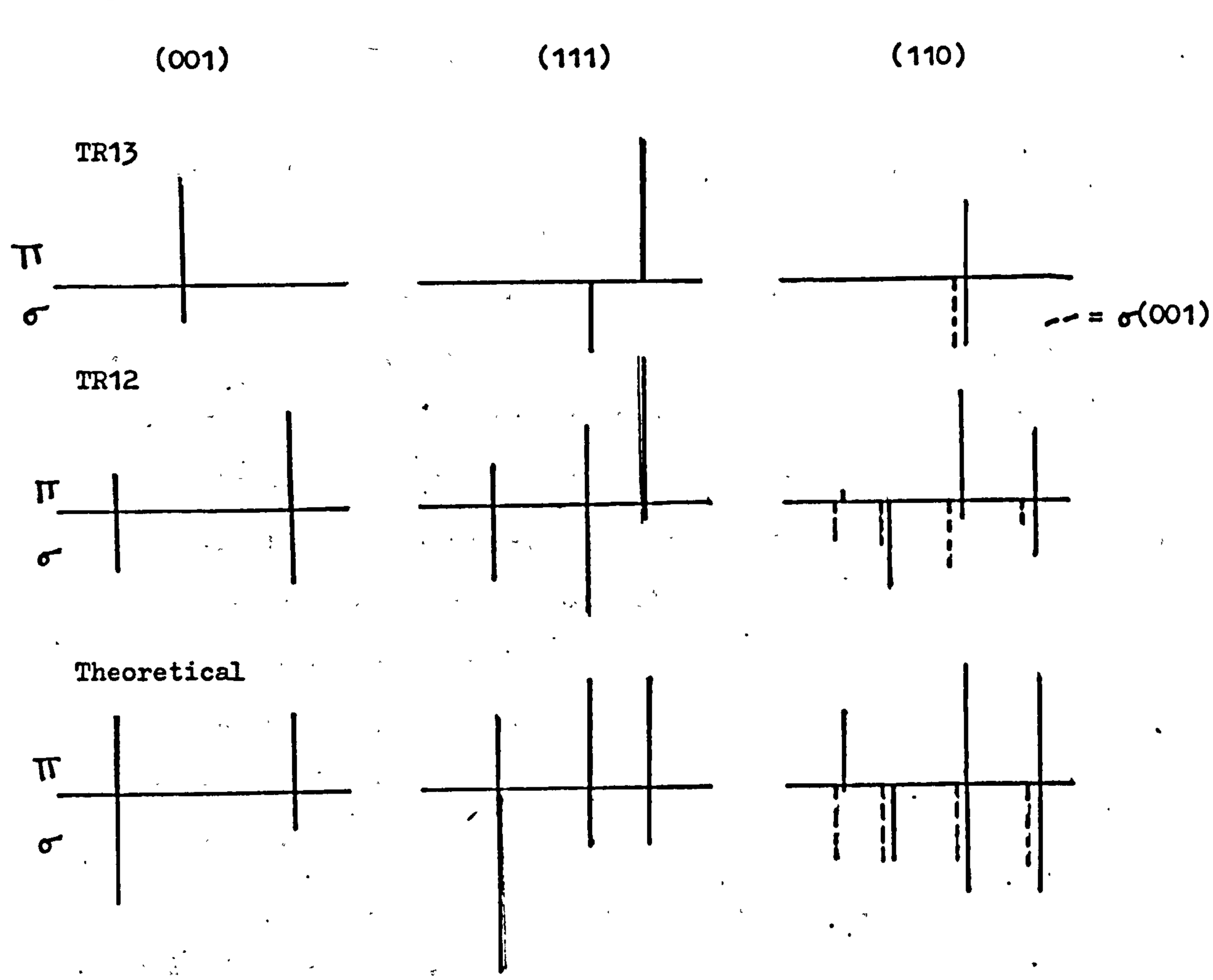

Figure 5.4b

assuming a Lorentzian line shape, as described in section 4.3; the spectra are given at a stress of 3GPa.Figure 5.4b shows a comparison between the spike spectra for TR12 and TR13 at 3GPa. and the spike spectra predicted by Kaplyanskii (1964a) for non-interacting states of a σ oscillator at a monoclinic I centre.The good agreement between experiment and theory for both the energies and intensities of the TR12 and TR13 lines confirms Walker's (1975) initial assignment of a σ oscillator at a monoclinic I centre; it also confirms that mixing between the two excited TR12 and TR13 levels occurs under stress.

3.Luminescence Measurements on the TR12 Centre.

As mentioned in section 5.1 the luminescence spectrum of the TR12 centre and the temperature dependence of the TR12 and TR13 lines show that TR13 is a zero-phonon transition and not a phonon replica of TR12.It also shows a sharp line at 2.437eV., labelled s in figure 5.1. O'Donnell (1979, private communication) has used a method due to Davies to deconvolute the observed luminescence spectrum and obtain the one phonon profile of the centre; subtraction of this synthesised spectrum shows an overlapping emission system with a prominent line at 2.437eV. and vibronic structure similar to that of TR12 (figure 5.5a,b).This line therefore seems to originate at the same centre as TR12 and TR13 and is probably a local phonon.In order to investigate this, the stress behaviour of the TR12 line and the 2.437eV. line in luminescence were compared.

The diamond was held at liquid nitrogen temperature in the stress cell described in section 1.5.Luminescence was excited by a mercury lamp fitted with a 435.8nm. Ealing TFP interference filter. The luminescence was detected at right angles to the exciting light and the direction of the applied stress was perpendicular to both of these.The incident light was unpolarised but the luminescence was recorded both with and without a polaroid filter.The aim of these measurements was simply to compare the behaviour of the TR12 line and the 2.437eV. line, since the previous absorption work had already confirmed the symmetry of the centre.

The experimental results are shown in figure 5.6 where the left-hand scale refers to the TR12 line and the right-hand scale to the 2.437eV. line; results are given for both polarised and unpolarised luminescence for comparison.The TR12 line was quite weak in luminescence and it was not possible to resolve all the lines

a) The experimental TR12 luminescence spectrum.

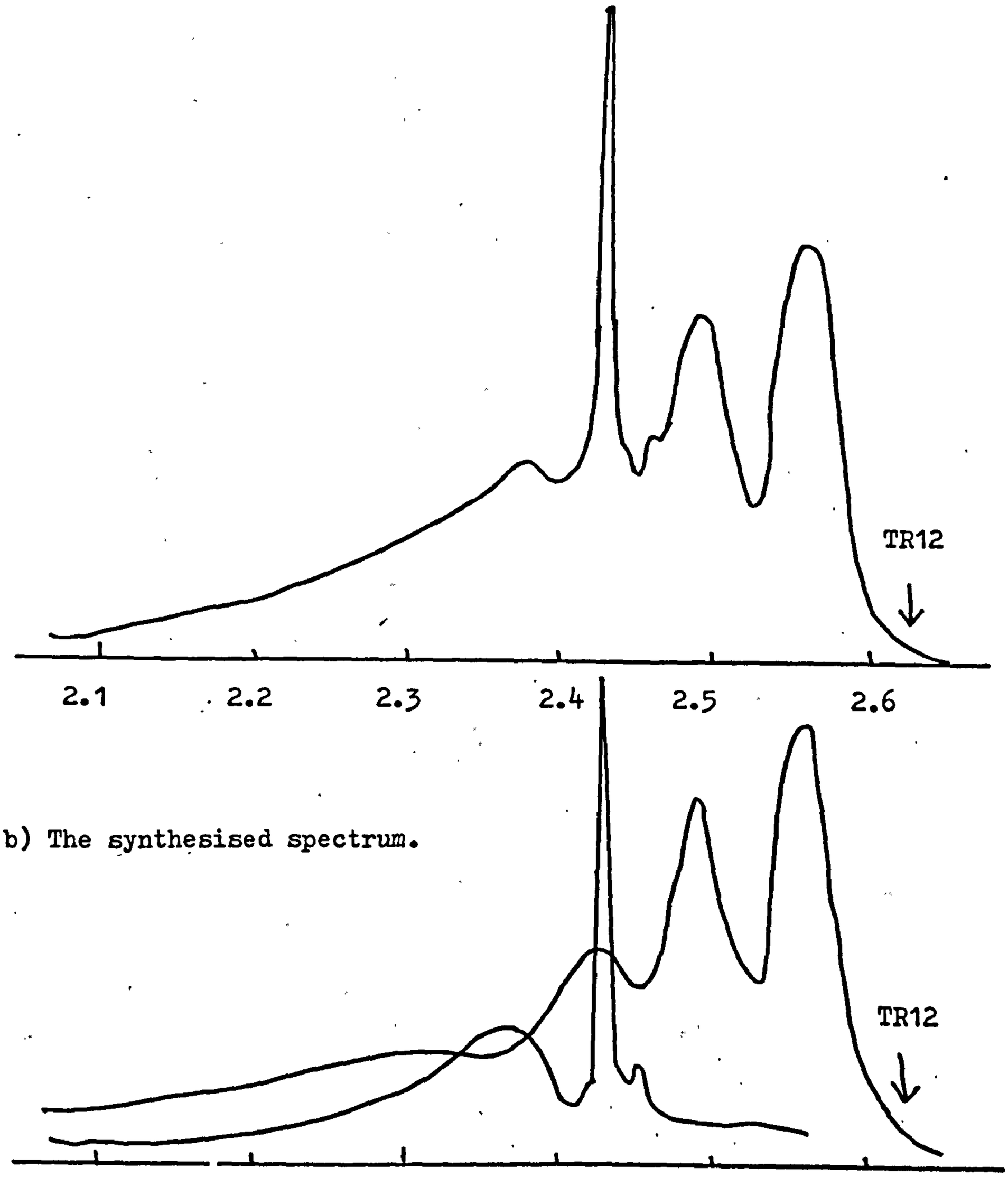

Figure 5.5

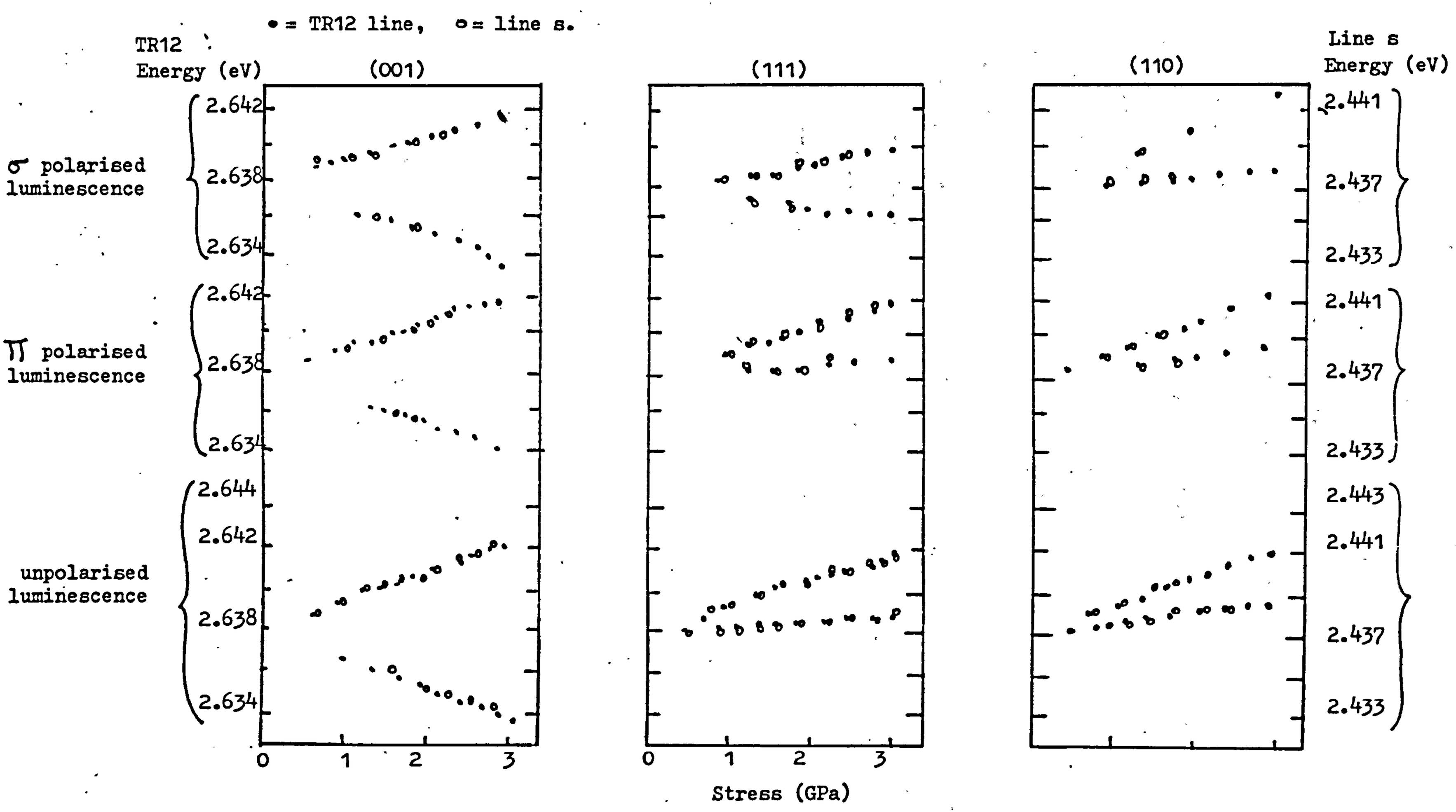
● = TR12 line, ○ = line s.
TR12 Energy (eV)
(001)
(111)
(110)
Line s Energy (eV)
σ polarised luminescence
Π polarised luminescence
unpolarised luminescence
2.642
2.638
2.634
2.644
2.441
2.437
2.433
2.443
0
1
2
3
Stress (GPa)

Figure 5.6

seen in absorption; however those that were resolved had the same stress behaviour in both luminescence and absorption.The 2.437eV. line was very weak and the use of the polaroid filter reduced the recorded luminescen intensity even more, so as the stress was increased the splittings of this line became more difficult to observe.In spite of this, though, it can be seen from figure 5.6 that the shifts and splittings under stress of this line are the same as those for TR12.This indicates that the luminescence line is a transition from the TR12 excited state down to a level which, from the character table of C_{2h} must transform as A_g. It also indicates that the 2.437eV. line is indeed a local phonon of the TR12 centre.The line TR17 seen in absorption, corresponds with the 2.437eV. line both in shift from TR12 and in magnitude; it would seem then, that there is a vibronic origin for both these lines.In view of this, the energy level diagram shown in figure 5.7 is proposed for the observed transitions at this centre.

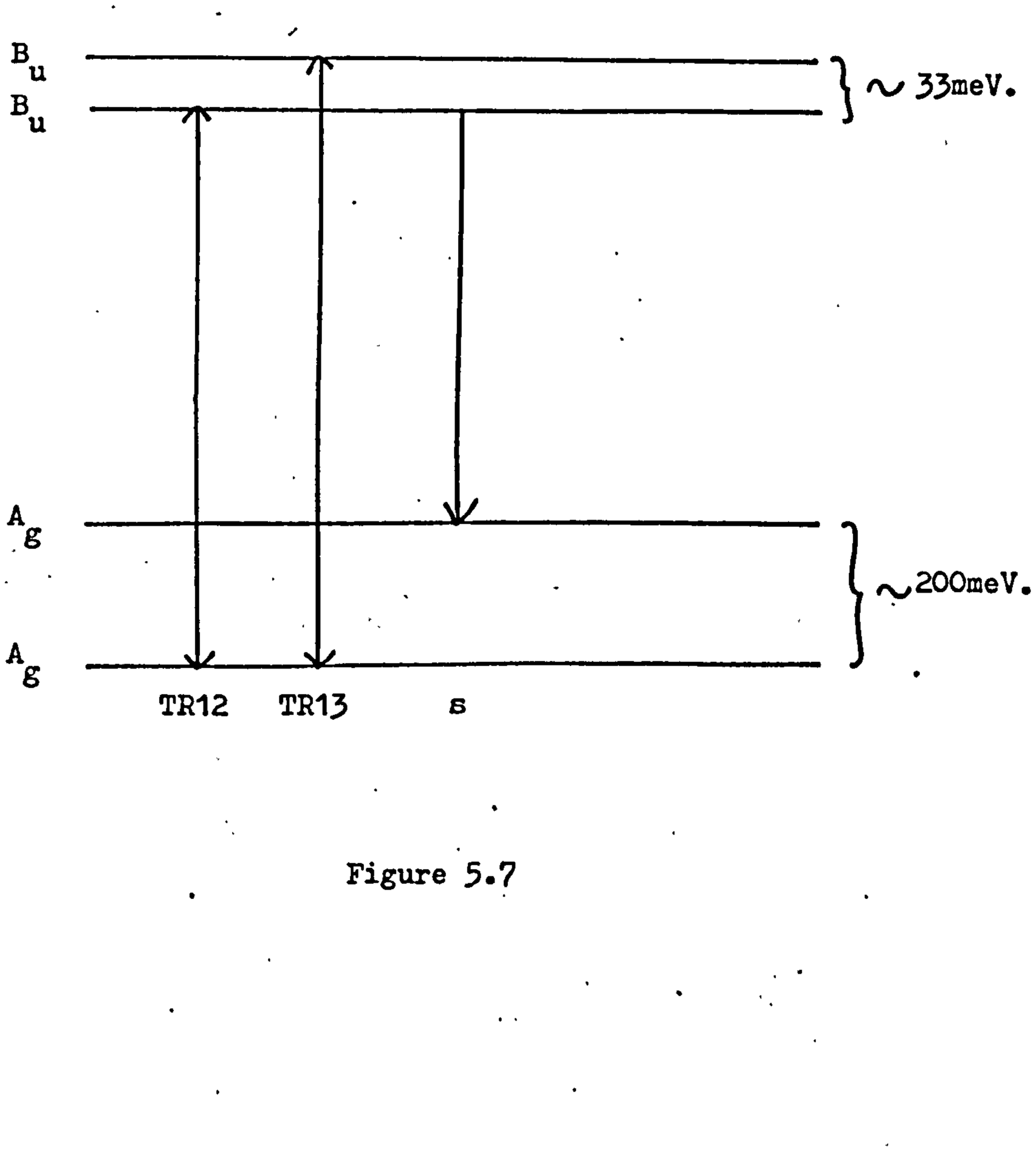

Figure 5.7

4.The Nature of the TR12 Centre.

The TR12 and TR13 lines have been detected in type II diamonds but not in type I (Clark et al, 1956a,b).Type II diamonds contain considerably less nitrogen impurity than type I (see section 1.1). As mentioned in section 1.3 the primary effect of radiation damage is to create a vacancy, there is no evidence for the formation of a stable interstitial.It can therefore be suggested that the TR12 centre involves a vacancy.Walker (1977) has shown that annealing for 3 hours at 770K increases the TR12 intensity five-fold over its post irradiation value but after longer times, or at higher temperatures, the system disappears. The vacancy is immobile below about 1 000K (Clark and Walker, 1973) whereas interstitials are mobile at much lower temperatures; the increase in intensity of the TR12 system with annealing thus indicates that an interstitial could also be involved with the centre.This conclusion is supported by the non-appearance of TR12 in type I diamonds where the nitrogen impurity is quite efficient at trapping interstitial carbon.However, caution is needed when suggesting the involvement of an interstitial since very little is known about the interstitial carbon atom, which might well be mobile at temperatures below liquid nitrogen temperature.

There is, at present, no model for the TR12 centre.O'Donnell is currently working on a vibronic model for the centre in which he is endeavouring to account for the quenching of the 70meV. phonon sideband in absorption (figure 5.1) in terms of the interactions which couple TR12 and TR13.He is using the stress parameters given in Table V in his work but as yet no satisfactory conclusion has been reached.

A detailed theoretical study of the TR12 band is therefore needed both to determine the nature of the centre and to explain the differences in the luminescence and excitation spectra.

CHAPTER VI

The 1.795eV and 2.358eV Lines.

Introduction:

In this chapter we report the discovery of two zero-phonon like lines in type Ib diamond.The lines have not previously been documented and have only been observed in two type Ib diamonds which had been electron irradiated and then annealed for a very short time.Uniaxial stress experiments indicate that the two centres giving rise to the lines are both trigonal but the non-appearance of the lines in other type Ib diamonds investigated makes them very puzzling.

1.The Occurrence of the Lines.

As noted in section 1.1 the nitrogen in type Ib diamond is present on isolated substitutional lattice sites.Before irradiation the visible spectrum of type Ib diamond is characterised by a continuous absorption whose strength is proportional to the concentration of these isolated nitrogen atoms (Dyer and du Preez, 1965).Room temperature electron irradiation of type Ib diamonds produces many zero-phonon lines, most of which anneal out at temperatures above about 700^{o}C.Most of the features of the optical absorption spectrum of a type Ib diamondwhich has been irradiated and annealed have been well described (see for e.g. Collins 1979, for a review of these features). In the present work two sharp lines at 1.795eV and 2.358eV were observed in the absorption spectrum of two Ib diamonds which had been electron irradiated, as described in section 1.3, andannealed at approximately 1 000^{o}C for a nominal 30 seconds.No previously published information could be discovered for these two lines which are shown, together with the main lines of the optical absorption spectrum of type Ib diamond, in figure 6.1.The lines were only found in two of the eight type Ib diamonds examined.All the diamonds investigated had been electron

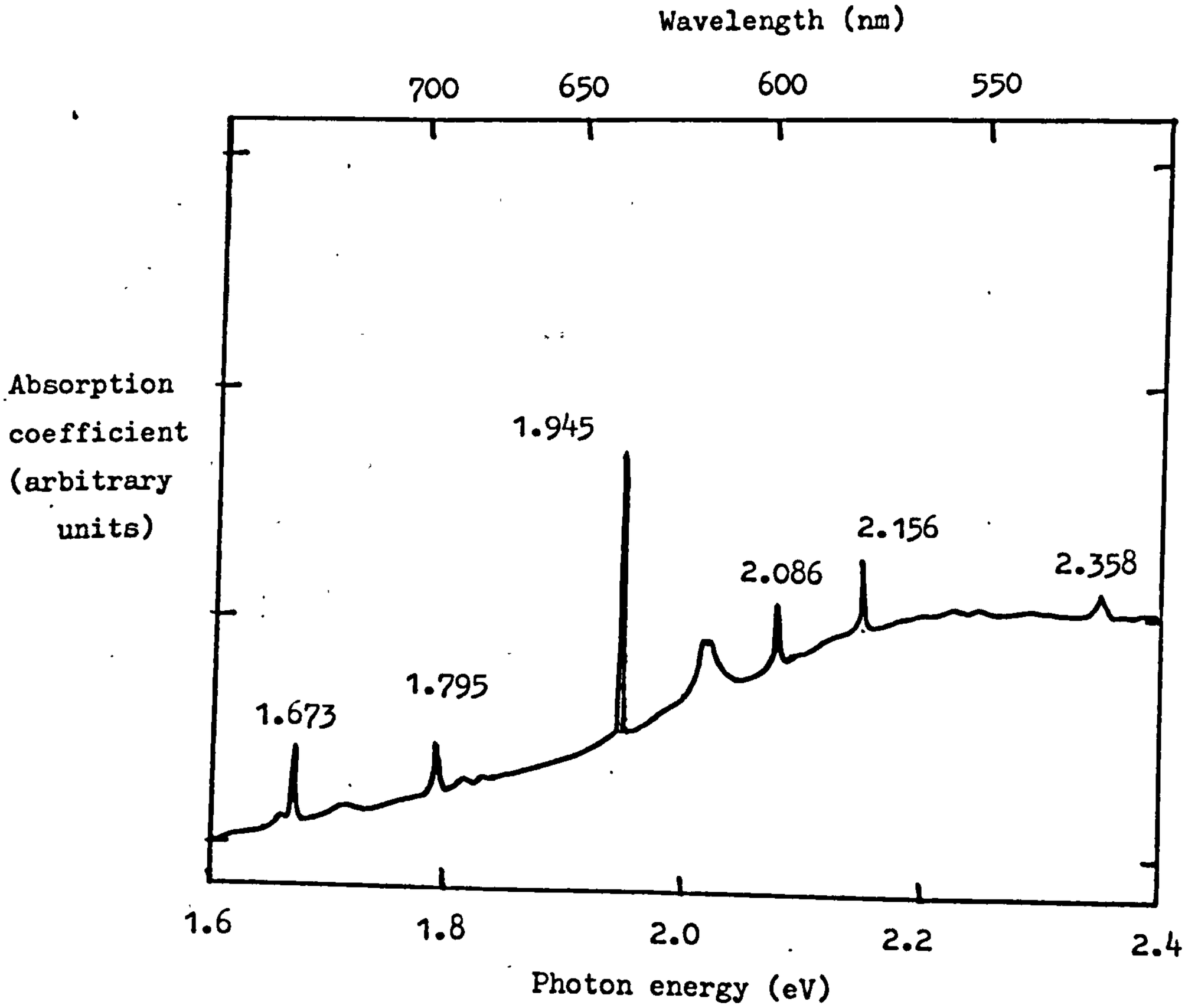

Figure 6.1

irradiated but had different annealing histories; all showed the prominent 2.085eV line, whose presence is use by gemmologists as an indicator of man-made radiation colouring of diamonds (Crowningshield, 1958; Collins, 1978b). and some, namely the mauve ones, showed the 1.945eV line which is believed to be a vacancy trapped at a substitutional nitrogen atom (Davies and Hamer, 1976).

The six type Ib diamonds which did not show the two lines in question were subjected to various annealing treatments with temperatures ranging between 800°C and 1 000°C and with annealing times of two minutes to three hours.The annealings were carried out with the sample

in a vacuum of appriximately 10^{-7} Torr.Some of the samples underwent colour changes but, at the end of each anneal, none showed the 1.795eV or the 2.358eV lines.Only the two diamonds which had been annealed at 1 000°C for 30 seconds showed the lines in absorption.No luminescence of the lines could be detected using a mercury lamp as the exciting source.

One of the first stages in the investigation of an optical centre in diamond should be the determination of its symmetry.Uniaxial stresses were applied to the diamond as described in section 1.5.Both the diamonds were light mauve in colour and were 1mm. cubes which had been cut to have (001), $(1\bar{1}0)$, (110) faces.The lines were slightly more intense and sharp in one diamond than in the other, so this sample was used for the stress experiments.

2.The 1.795eV. Lines.

The 1.795eV system consists of a sharp zero-phonon line at 1.795eV and two phonon replicas at 1.819eV and 1.832eV (figure 6.2)

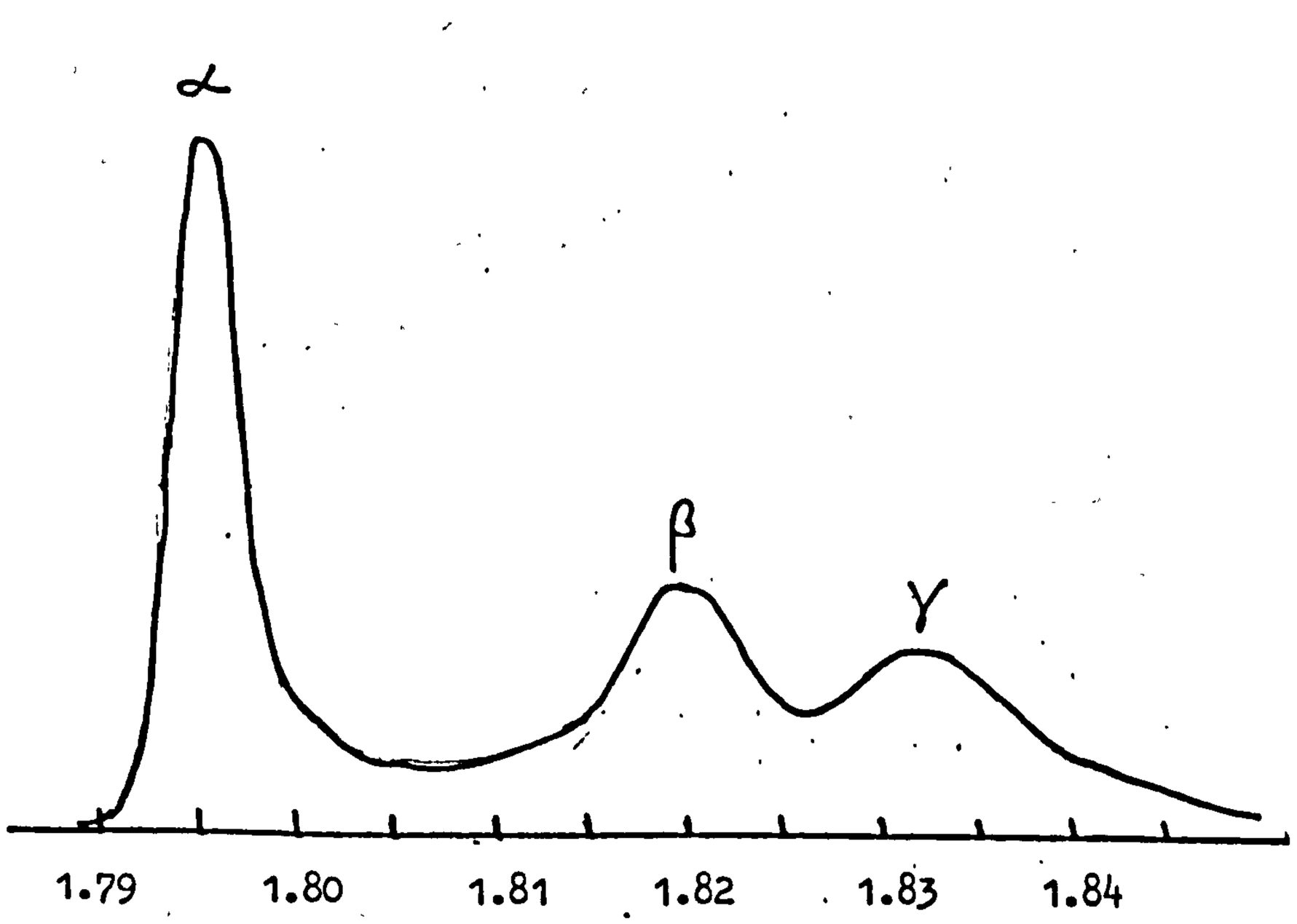

Figure 6.2

The results of the application of uniaxial stresses to the lines are shown in figure 6.3.Since the diamond which shows these lines was cut to (001), $(1\bar{1}0)$, (110) faces no data are available for the (111) direction of stress; however, the results obtained allow a fairly conclusive allocation of symmetry to this centre.

The number of stress split components for stress along (001) and (110) is consistent with a σ oscillator at a trigonal centre (kaplyanskii, 1964a).The intensities of the stress split components of the zero-phonon line also confirm this allocation, as can be seen from figure 6.4 where spike spectra for the lines, taken at 3GPa, are compared with the theoretical spike spectra for a σ oscillator at a trigonal centre.The zero stress line-width of the line α is 2.3meV, that of β is 5.8meV and that of γ is 6.8meV; therefore, since β and γ are much wider than α , no splitting was observed for them as stress was increased.The line γ broadened and flattened out considerably as the stress was increased so only the intensities of α and β are shown in figure 6.4.

The selection rules for σ oscillator electric dipole transitions at a trigonal centre show that the transition must be $A \leftrightarrow E$; no thermalisation effects on the intensities of the 1.795eV line components were observed so it was concluded that the transition was from an A (A_1 or A_2) ground electronic state to an E excited state. In this particular case only the orientational degeneracy of the centre is lifted by the stress, the electronic degeneracy in the E excited state remains.Thus the analysis given by Hughes and Runciman (1967) which deals with an A to E transition where the electronic degeneracy in the E state is lifted is not applicable here.The fact that the electronic degeneracy in the E state is not lifted by the stress is consistent with the observation that orbitally degenerate excited

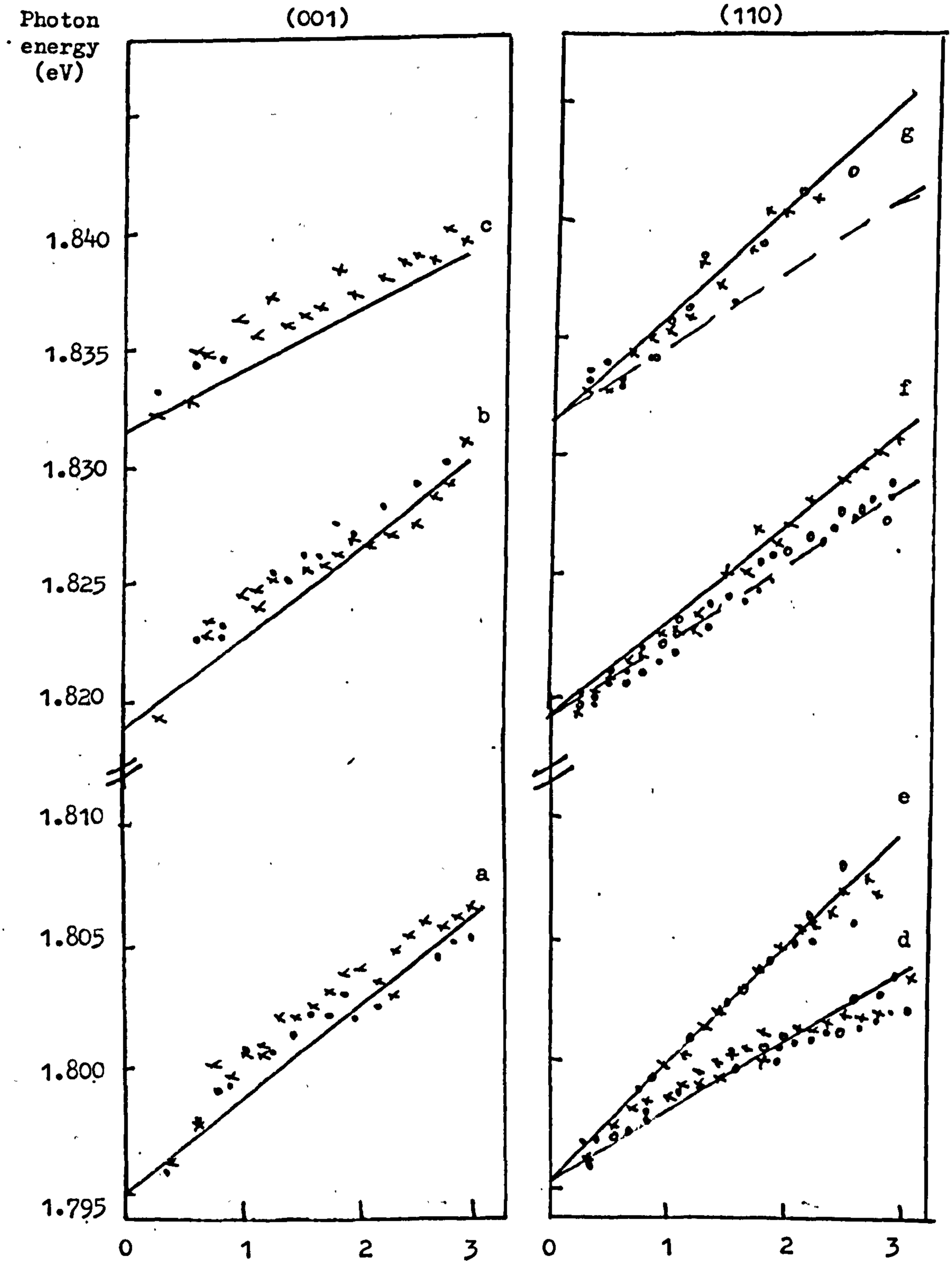
Photon energy (eV)
(001)
(110)
1.840
1.835
1.830
1.825
1.820
1.810
1.805
1.800
1.795
a
b
c
d
e
f
g
0
1
2
3
Stress (GPa)

Figure 6.3

states in diamond have small or negligable Jahn-Teller relaxations. (Davies, 1979a).

A trigonal centre, shown in figure 6.5a with the directions of the σ and Π oscillators shown in figure 6.5b, has one rotational C_3 axis which coincides with the (111) axis; let this be the Z axis of the centre, let the X axis be along $(11\bar{2})$ and the Y axis along $(1\bar{1}0)$.The multiplicity of orientational degeneracy for the centre is

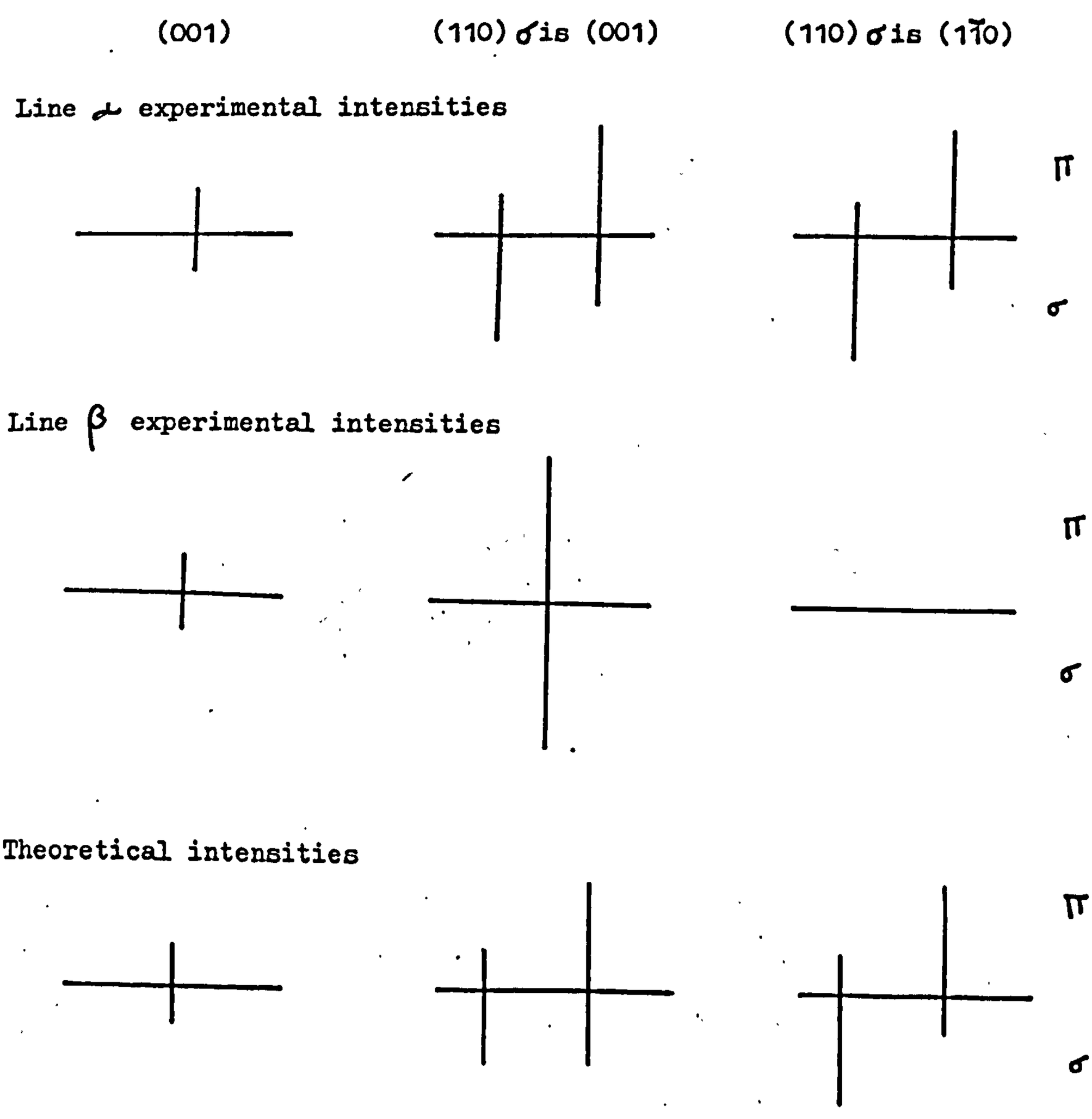

Figure 6.4

eight but it is taken to be four in stress work since stresses have even parity under inversion.The shifts under stress for an A to E transition at a trigonal centre can be found from equation 2.17

$$\Delta = A_{xx}s_{xx} + A_{yy}s_{yy} + A_{zz}s_{zz} + 2A_{xy}s_{xy} + 2A_{yz}s_{yz} + 2A_{zx}s_{zx} \qquad 6.1$$

and using the piezospectroscopic stress tensor given by Kaplyanskii (1964a) for a trigonal centre

$$\begin{matrix} A_1 & A_2 & A_2 \\ & A_1 & A_2 \\ & & A_1 \end{matrix} \qquad 6.2$$

For stress along (001) there is only one possible orientation of the centre with respect to the stress axis and the shift is given by

$$\Delta = A_1 s \qquad 6.3a$$

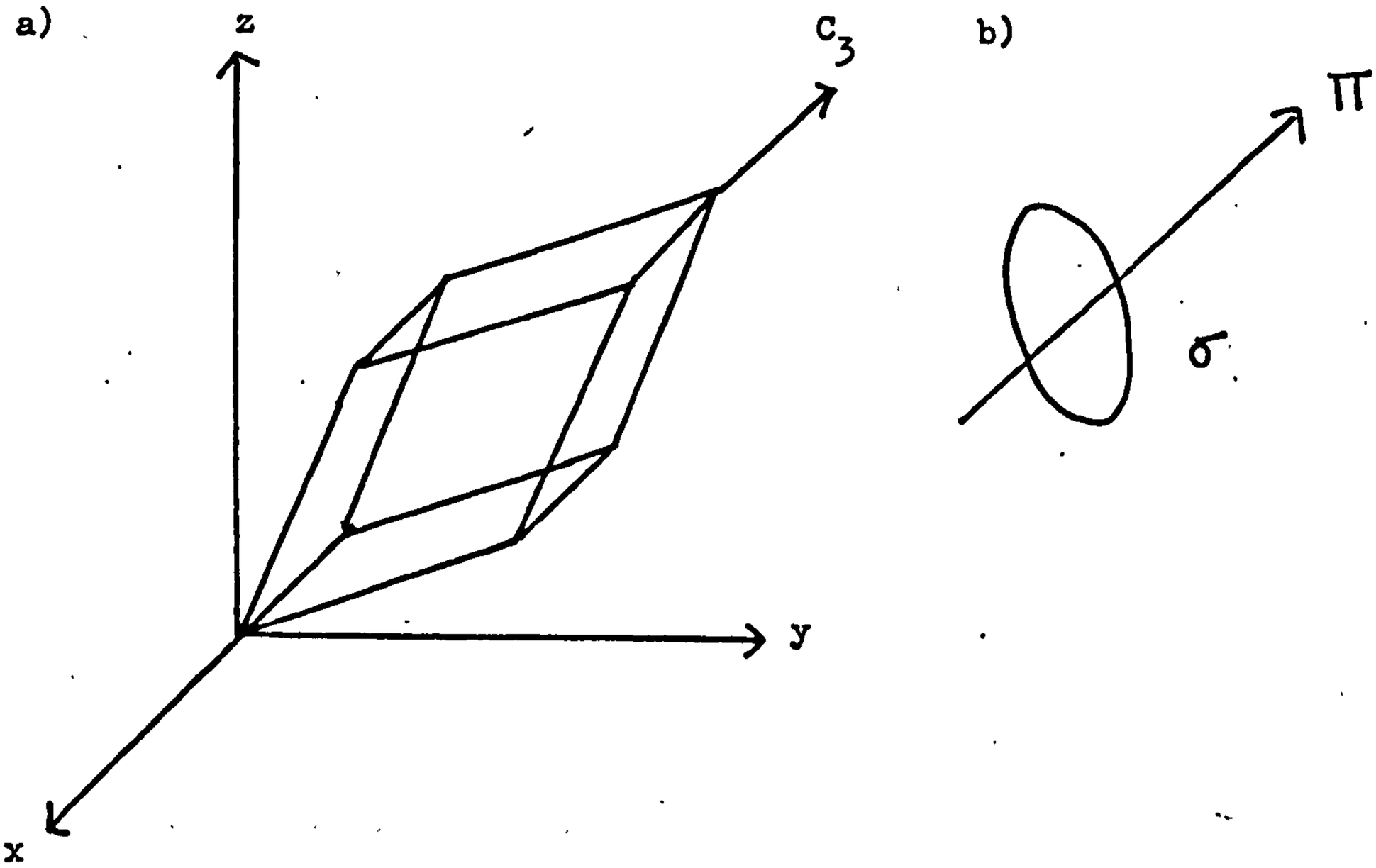

Figure 6.5

where s is the applied stress.For stress along (110) there are two inequivalent orientations of the centre and the two shifts are given by

$$\Delta_1 = (A_1 + A_2) s$$
$$\Delta_2 = (A_1 - A_2) s \qquad 6.3b$$

The shift of the stress split component d of α, seen under (110) stress was identified with $\Delta_1 = (A_1 + A_2)s$ and that of e with $\Delta_2 = (A_1 - A_2)s$ The shifts of the lines f and g of β and γ followed the more intense e component of the parent zero-phonon line so the following equations were used in the least squares fitting proceedure to the shifts of the observed lines:

(001) stress

Line	a	b	c
Equation	$A_1 s$	$B_1 s$	$C_1 s$

(110) stress

Line	d	e	f	g
Equation	$(A_1+A_2)s$	$(A_1-A_2)s$	$(B_1-B_2)s$	$(C_1-C_2)s$

6.4

The A are the stress parameters for the parent zero-phonon line and B and C are the parameters for β and γ respectively.The parameters obtained are given in Table VI.

Table VI

A_1	A_2	B_1	B_2	C_1	C_2
3.86	-1.0	3.76	-0.24	2.48	-2.2

The units are meV$(GPa)^{-1}$ and there is an uncertainty of $\pm$0.5meV$(GPa)^{-1}$

The lines of figure 6.3 have been calculated using these parameters. The shift with stress of the centroid of the lines d and e has been

plotted as the dotted line in figure 6.3 and it can be seen that the shifts of the lines f and g of β and γ follow it well.Since a totally symmetric phonon should have the same stress response as its parent zero-phonon line, this indicates that β and γ are indeed phonon replicas of α.

The theoretical stress split spectra were calculated as described previously in section 4.2; there was a very steep background to the experimental spectra so, for convenience of comparison, the calculated spectra are shown both with and without the estimated background in figure 6.6. for a stress of 3GPa.

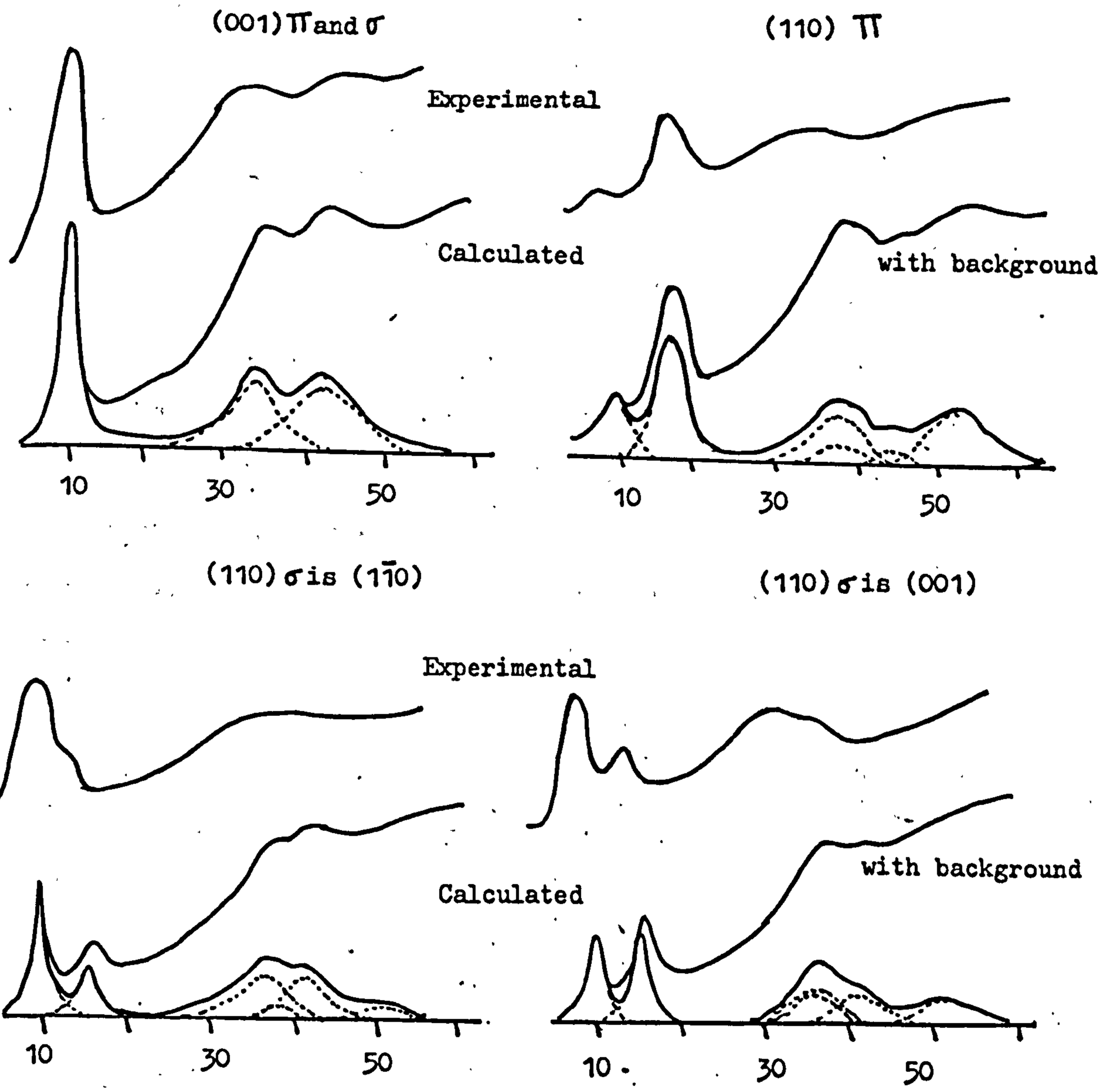

Figure 6.6

The dotted lines in figure 6.6 give the predicted positions and intensities of the components of lines β and γ and the bold line shows the resultant theoretical shape.

When the series of uniaxial stress experiments on these lines had been completed the diamond was annealed for 30 minutes at a temperature of 1 000°C.The intensities of both the 1,795eV line and the 1,945eV line were reduced by the anneal but their relative intensities remained approximately constant.A further anneal for 30 minutes at 1 100°C reduced the intensity of the 1.945eV line considerably and rendered the 1.795eV line undetectable.The 1.945eV line has been shown to arise from an A to E transition at a trigonal centre (Davies and Hamer, 1976).Davies and Hamer have also shown that the one-phonon sideband of the absorption spectrum of the 1.945eV line is split into a doublet and these authors propose the model of a substitutional nitrogen atom, N, plus a vacancy, V, for this centre.On this N-V model the N atom could tunnel into the vacancy giving an equivalent V-N centre; the tunnelling motion provides a mechanism for splitting the one-phonon sideband of the absorption spectrum into the observed doublet.The two phonon replicas of the 1.795eV line could be considered to be a phonon doublet similar to that of the 1.945eV line.This, together with the identical symmetry and similar annealing behaviour of the 1.795eV and 1.945eV lines could indicate that the 1.795eV line originates at the same centre as the 1.945eV line.If some more diamonds which show the 1.795eV line could be obtained then detailed correlation experiments would confirm or refute this postulate.

3.The 2.358eV Line.

The 2.358eV line is, like the 1,795eV line, very peculiar.It, too, was only observed in the two Ib diamonds which had been irradiated and annealed for 30 seconds at 1 000°C.Its response to uniaxial stress

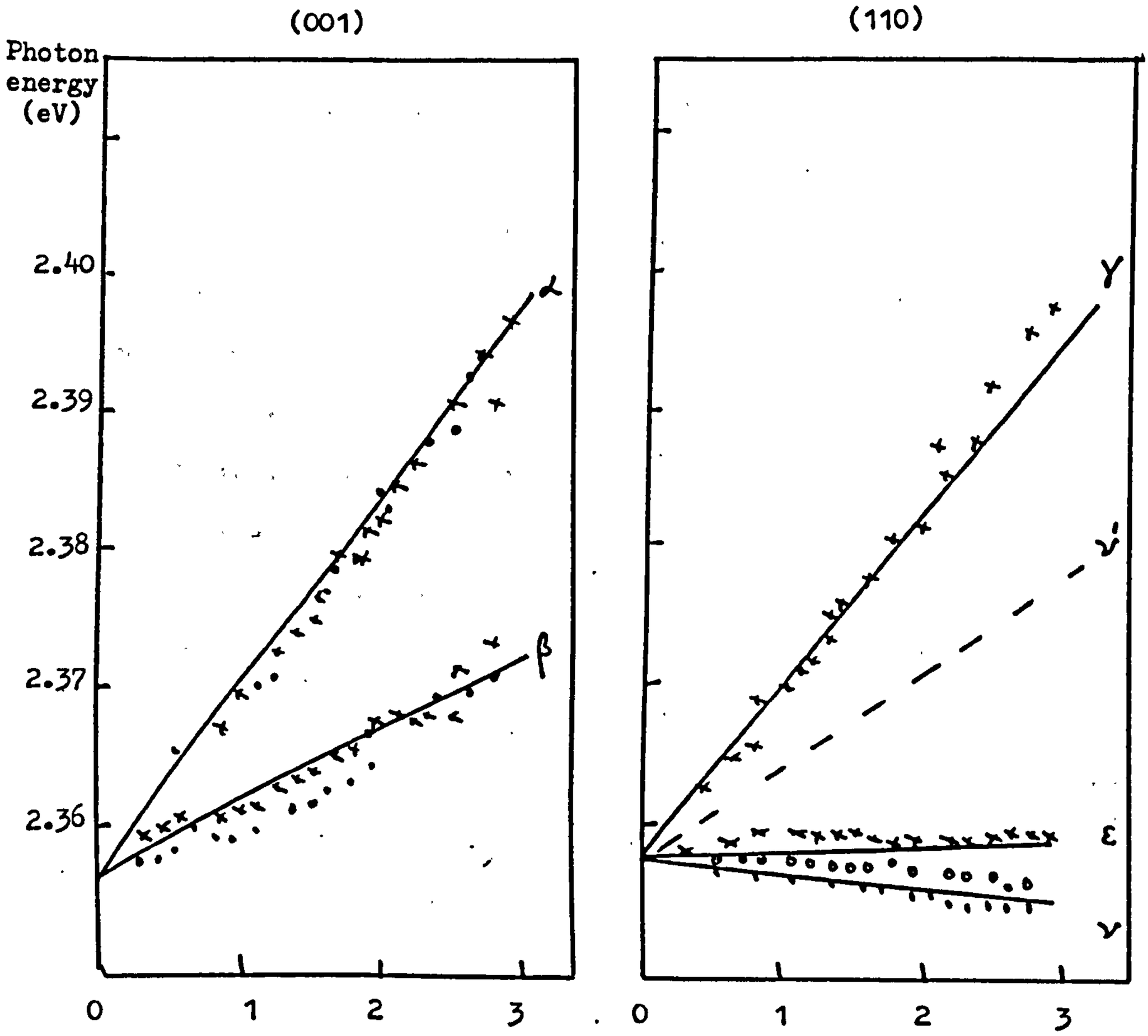

Figure 6.7

is shown in figure 6.7.This stress response was very odd and complied with none of the features listed by Kaplyanskii (1964a,b) in his two papers on the piezospectroscopic properties of cubic and non-cubic centres in crystals.Hughes and Runciman (1967) and Davies and Nazare (1980) have shown that electric dipole E to E transitions at a trigonal centre can have a variable number of stress-split components, up to a maximum of 17, with intensities that are not uniquely defined.

The reason for this is that the transitions may occur with the electric vector of the light parallel to or perpendicular to, the trigonal axis of the centre, the two polarisations coupling to different dipole oscillators.The relative intensity of each transition therefore depends on the ratio of these dipole oscillators.It seemed, therefore, that the only possibility for the 2.358eV line was an E to E transition at a trigonal centre, and the piezospectroscopic data were analysed accordingly.This analysis was hampered slightly by the absence of any data for the (111) direction of stress but nevertheless, fairly satisfactory results were obtained.

Trigonal centres have C_{3v}, D_3, and D_{3d} symmetry and for each orientation of the centre in a cubic lattice a set of local axes X,Y,Z can be defined.Z is the trigonal axis, X is invariant under the reflection (or C_2 rotation) operation of the C_{3v} (or D_3, D_{3d}) point group and Y is such as to complete the righthanded Cartesian coordinate system.The stress tensor components s_{xx} etc. are defined with respect to these local axes.The Hamiltonian for the system then takes the form

$$H = H_o + c_{A_1}(s_{xx} + s_{yy} + s_{zz}) + \tfrac{1}{2} c'_{A_1}(2s_{zz} - s_{xx} - s_{yy}) + c_{E\theta}(s_{yy} - s_{xx}) + 2c_{E\epsilon}s_{xy} + 2c'_{E\theta}s_{xz} + 2c'_{E\epsilon}s_{yz} \qquad 6.5$$

where H_o is the Hamiltonian at zero stress, the electronic operators transform as shown by their subscripts and each combination of stress tensors transforms in the same way as its associated operator.The matrix elements of $c_{E\theta}$, $c_{E\epsilon}$ are related in terms of the basis set $|\theta\rangle$, $|\epsilon\rangle$ of an E electronic state through

$$\langle\epsilon|c_{E\theta}|\epsilon\rangle = \langle\epsilon|c_{E\epsilon}|\theta\rangle = \langle\theta|c_{E\epsilon}|\epsilon\rangle = -\langle\theta|c_{E\theta}|\theta\rangle$$
$$\langle\theta|c_{E\theta}|\epsilon\rangle = \langle\epsilon|c_{E\theta}|\theta\rangle = \langle\theta|c_{E\theta}|\theta\rangle = \langle\epsilon|c_{E\theta}|\epsilon\rangle = 0 \qquad 6.6$$

with equivalent expressions for $c'_{E\theta}$ and $c'_{E\varepsilon}$.

The stress perturbations to the energies of the E states may then be obtained from equations 6.5 and 6.6.Davies and Nazare (1980) have listed these perturbations and those that are relevant to the present analysis are listed in Table VII, where, using the standard notation

$$A_1 = \langle\theta|\, c_{A_1}\,|\theta\rangle, \qquad A_2 = \tfrac{1}{2}\langle\theta|\, c'_{A_1}\,|\theta\rangle$$

$$B = \tfrac{1}{3}(\langle\varepsilon|\, c_{E\theta}\,|\varepsilon\rangle + \sqrt{2}\,\langle\varepsilon|\, c'_{E\theta}\,|\varepsilon\rangle)$$

$$C = \tfrac{1}{3}(2\langle\varepsilon|\, c_{E\theta}\,|\varepsilon\rangle - \sqrt{2}\,\langle\varepsilon|\, c'_{E\theta}\,|\varepsilon\rangle) \qquad 6.7$$

TABLE VII

Stress	Initial State	Final State	Π	σ	Line
001	$A_1^g+2B^g$	$A_1^e+2B^e$	$(2D+\sqrt{2}d)^2$	$(\sqrt{2}d-D)^2$	α
		$A_1^e-2B^e$	•	$3D^2$	
	$A_1^g-2B^g$	$A_1^e+2B^e$	•	$3D^2$	
		$A_1^e-2B^e$	$(\sqrt{2}d-2D)^2$	$(\sqrt{2}d+D)^2$	β
			Π	$\sigma_{1\bar{1}0}$ σ_{001}	
110	$A_1^g+A_2^g-B^g+C^g$	$A_1^e+A_2^e-B^e+C^e$	$(\sqrt{2}D-2d)^2$	• $(2D+\sqrt{2}d)^2$	ε
		$A_1^e+A_2^e+B^e-C^e$	•	$6D^2$ •	
	$A_1^g+A_2^g+B^g-C^g$	$A_1^e+A_2^e-B^e+C^e$	•	$6D^2$ •	
		$A_1^e+A_2^e+B^e-C^e$	$(\sqrt{2}D+2d)^2$	• $(2D-\sqrt{2}d)^2$	γ
	$A_1^g-A_2^g+B^g+C^g$	$A_1^e-A_2^e+B^e+C^e$	•	$(\sqrt{2}D+2d)^2$ $(2D-\sqrt{2}d)^2$	ν
		$A_1^e-A_2^e-B^e-C^e$	$6D^2$	• •	
	$A_1^g-A_2^g-B^g-C^g$	$A_1^e-A_2^e+B^e+C^e$	$6D^2$	• •	
		$A_1^e-A_2^e-B^e-C^e$	•	$(\sqrt{2}D-2d)^2$ $(2D+\sqrt{2}d)^2$	ν'

In Table VII the superscripts e and g refer to the excited and ground states respectively.The transition probabilities for the transitions are also listed in Table VII where the matrix elements for the dipole operators are related through

$$D \propto \langle \varepsilon_1 | X | \varepsilon_2 \rangle = \langle \varepsilon_1 | Y | \theta_2 \rangle = \langle \theta_1 | Y | \varepsilon_2 \rangle = - \langle \theta_1 | X | \theta_2 \rangle$$

and $$d \propto \langle \theta_1 | Z | \theta_2 \rangle = \langle \varepsilon_1 | Z | \varepsilon_2 \rangle \qquad 6.8$$

The subscripts (1,2) label the initial and final states of the transition.From Table VII it can be seen that the number of energetically different transitions is variable according as D = 0 or not.With this, and the inevitable thermalisation effects in the split ground state, it is likely that not all the stress split components will be observed and this has been assumed to be the case for the 2.358eV line.

The line to which each energy shift has been taken to refer is shown in Table VII.The small number of observable transitions made it possible to determine only the differences in ground state and excited state parameters.The values for these, obtained by a least squares fitting proceedure, are listed in Table VIII and the bold lines drawn in figure 6.7 have been calculated using these values.

TABLE VIII

$$(A_1^e - A_1^g) = 4.70$$
$$(A_2^e - A_2^g) = 1.80$$
$$(B^e - B^g) = 1.05$$
$$(C^e - C^g) = -4.90$$

The units are $meV(GPa)^{-1}$ with an uncertainty of $\pm 0.7 meV(GPa)^{-1}$

In the analysis of the 2.358eV line it was assumed that $D \sim 0$.The fit to those lines which can be observed experimentally is quite good but

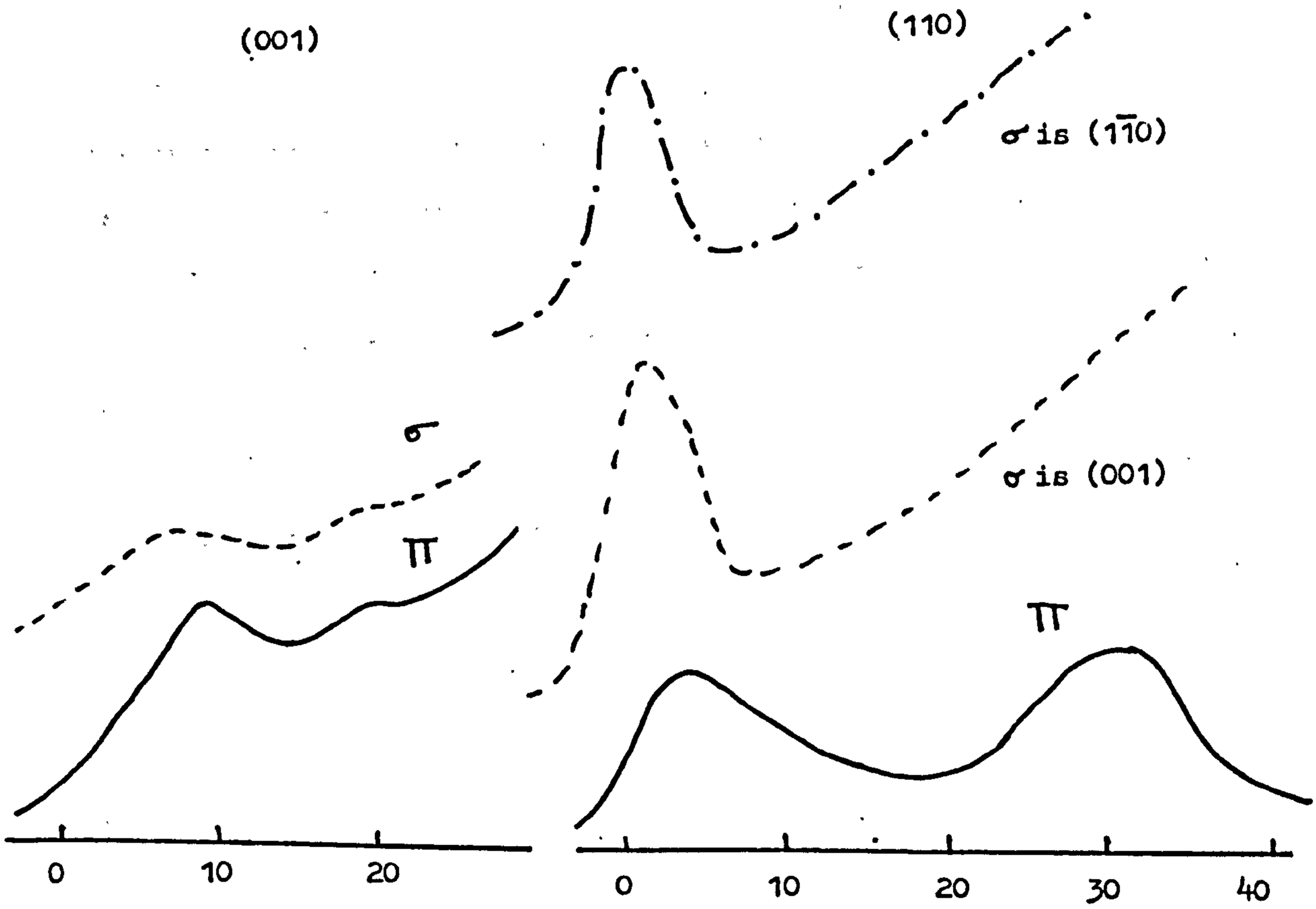

Figure 6.8

some lines, namely $\varepsilon, \gamma, \nu'$, of (110) σ_{001} and ν' of (110) $\sigma_{1\bar{1}0}$ which are predicted to occur are not seen experimentally.This is probably due to thermalisation effects in the split ground state and to the fact that, even at zero stress, the 2.358eV line has quite a large line-width of 5.7meV.The experimental stress split spectra for a stress of 3GPa are shoen in figure 6.8 where it can be seen that the steep background makes observation of small splittings difficult.

The 2.358eV line disappeared after the diamond had been annealed at 1 000^{o}C for 30 minutes; the 2.085eV line also disappeared with this annealing and since this line has also been shown to be an E to E transition at a trigonal centre (Davies and Nazare, 1978) one might

think that these two transitions occur at the same defect centre; but, as with the 1.795eV and 1.945eV lines, more detailed annealing experiments are needed before any definite conclusion about the 2.358eV centre can be established.

In conclusion, then, two hitherto unreported lines seen in type Ib diamond have been analysed using uniaxial stress.The 1.795eV line has been shown to be an A to E transition at a trigonal centre and the 2.358eV line has been tentatively assigned to an E to E transition at a trigonal centre.More work is clearly needed to establish the precise nature of these two centres.

CONCLUSION

The technique of uniaxial stress spectroscopy is now firmly established as a very useful tool for investigating the symmetry and probing the vibronic structure of defect centres in diamond and other materials.The experimental techniques are quite straightforward and definite conclusions can usually be drawn from the results.It is one of the best methods for determining the basic properties of a defect centre and is applicable to many different materials.

Most of the sharp zero-phonon lines and their associated vibronic bands seen in the optical spectra of diamond have been thoroughly investigated.The work in this thesis has therefore concentrated on those lines whose properties are still not fully understood.

Electron irradiation of type II diamonds creates the absorption band shown in figure C1; the main features of this are the GR1 band, consisting of the GR1-8 zero-phonon lines and a very complicated vibronic structure, the TR12 system and the ND1 centre.The GR system and the TR12 centre have been investigated in this thesis.

Although the symmetry of the ground state and the first three excited states of the GR centre had been determined previously (Clark and Walker, 1973; Davies and Penchina, 1974; Walker et al, 1974) it was felt that there was much more information still to be gained from a study of this centre.In the present work the energy of the A_2 vibronic level of the GR ground state was determined.The symmetry of the prominent one-phonon sideband of the GR1 line seen in absorption was also found and this proved to be different from that of the parent zero-phonon line.By obtaining the first high resolution spectrum for the GR centre the ratio of the intensities of the GR1 line at 1.673eV and its satellite line at 1.665eV was found.All these measurements enabled more detailed calculations on the Jahn-Teller properties of

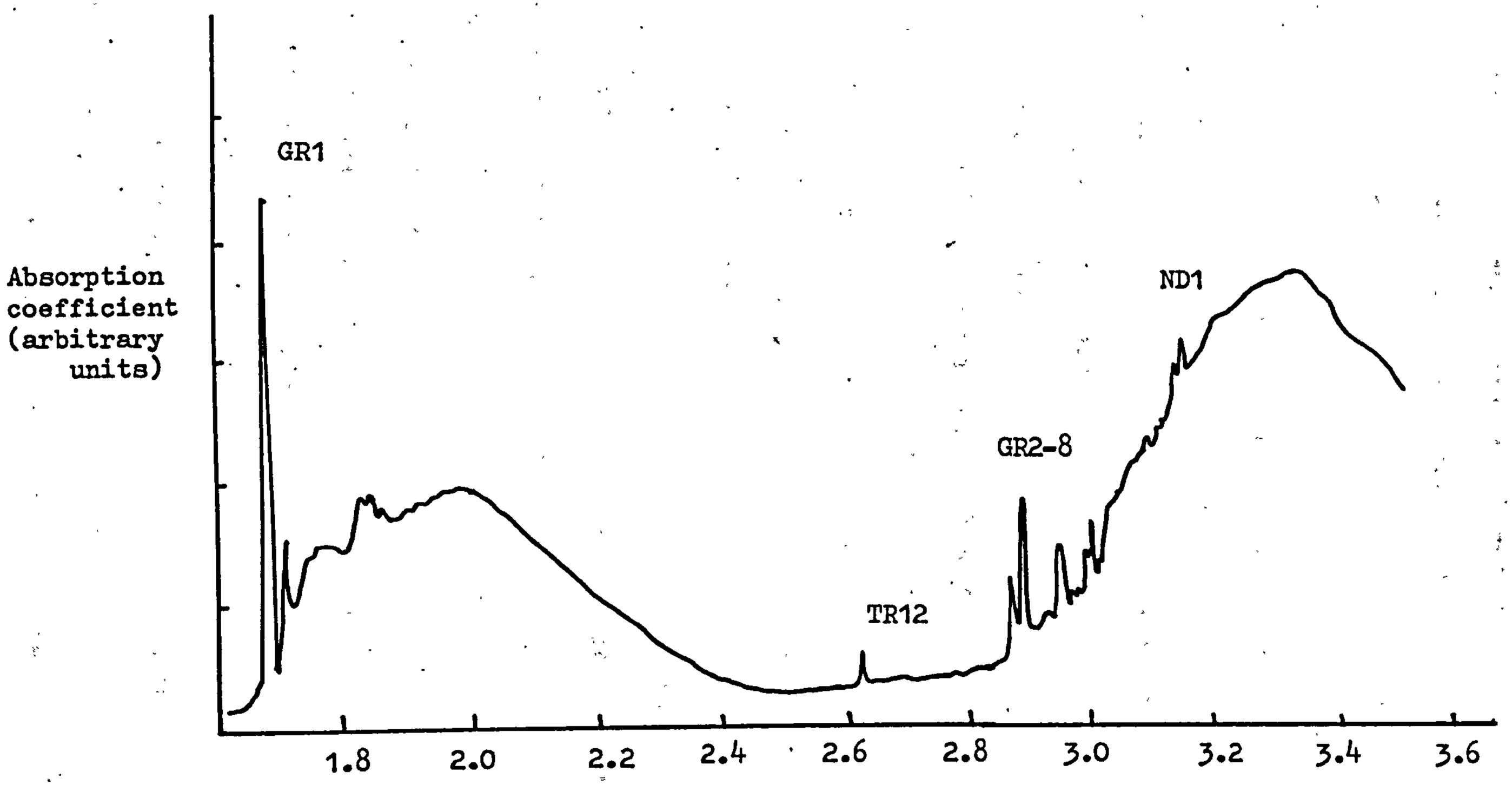
GR1
ND1
GR2-8
TR12
Absorption coefficient (arbitrary units)
1.8
2.0
2.2
2.4
2.6
2.8
3.0
3.2
3.4
3.6
Photon energy (eV)

Figure C1

the centre to be made, yielding more accurate values for the Jahn-Teller parameters than had hitherto been obtained.The symmetries and stress responses of the GR2-8 lines have been determined but the problem of the origin of these sharp lines still remains.

There is still more to be learnt about the GR centre; in particular the GR absorption and luminescence bands have very odd shapes and future work on this centre could be aimed at explaining these.The Jahn-Teller properties of the centre could be clarified further by moment analysis of the GR1 band under uniaxial stress.And theoretically, a model which accounts for both the origin and interesting properties of the GR2-8 lines is needed.

Another main feature of the absorption band of electron irradiated type II diamond is the TR12 centre.Although some earlier work was done on this centre (Walker, 1977) this was concerned only with the TR12 zero-phonon line and was not very detailed.In the present work both the TR12 and TR13 lines were investigated and their piezospectroscopic properties determined.

It is difficult to postulate a model for the TR12 centre since the main effect of electron irradiation of type II diamond is the creation of a vacancy; the GR centre has been identified as the neutral vacancy and the TR12 centre has neither its properties nor those that might be expected of a charged vacancy.The ND1 centre, which is also shown in figure C1, probably involves a nitrogen interstitial but again the TR12 centre shares none of its properties.In this work the symmetry of the centre was confirmed and its stress parameters determined and this should provide the basic information upon which a vibronic model for the centre could be built.

Annealing studies of electron irradiated type Ib diamonds are interesting since sharp lines appear and disappear according to the

temperature at which the sample is annealed.Most of the lines that result from fairly high temperature annealing have been studied and identified (see Chapter VI and figure 6.1) but in a brief survey of the optical spectra of several type Ib diamonds two hitherto unidentified lines were found; these were intense enough to be worth investigating. As the first step towards their complete identification their symmetries have been determined and tentative correlations with two other documented systems made.Annealing studies of diamonds whose precise irradiation histories are known should yield further information on these lines.

REFERENCES

Born,M., and Oppenheimer,J.R., 1927, Ann.Physik. 84, 457.

Chrenko,R.M., Tuft,R.E. and Strong,H.M., 1977, Nature, 270, 141.

Clark,C.D., Ditchburn,R.W. and Dyer,H.B., 1956a, Proc.R.Soc., A234, 363.

" " " 1956b, " " , A237, 75.

Clark,C.D., Kemmey,P. and Mitchell,E.W.J., 1961, Disc.Faraday Soc. 31, 96.

Clark,C.D. and Mitchell,E.W.J., "Radiation Effects in Semiconductors", 1976, Inst.Phys.Conf. ser.31, 45.

Clark,C.D., Parsons,B.J. and Vermeulen,L.A., 1979, J.Phys. C12, 2597.

Clark,C.D. and Walker,J., 1973, Proc.R.Soc.Lond., A241, 443.

Collins,A.T., 1974, Diamond Conference, Oxford (unpublished)

Collins,A.T., 1978a, J.Phys. C11, 1957.

Collins,A.T., 1978b, J.Phys. C11, 2453.

Collins,A.T., 1979, Inst.Phys.Conf. ser.46, 327.

Collins,A.T. and Williams,A.W.S., 1971, J.Phys. C4, 1789.

Condon,E.U., 1928, Phys.Rev. 32, 858.

Coulson,C.A. and Kearsley,M.J., 1957, Proc.R.Soc.Lond., A241, 443.

Coulson,C.A. and Larkins,F.P., 1971, J.Phys.Chem.Solids, 32, 2245.

Crowningshield,G.R., 1958, Gems Gemol., 9, 99.

Custers,J.H.F., 1952, Physica, 18, 489.

Davies,G., 1974, Proc.R.Soc.Lond., A336, 507.

Davies,G., 1977a, in Diamond Research (Industrial Diamond Information Bureau, Ascot)

Davies,G., 1977b, Chemistry and Physics of Carbon, 13.

Davies,G., 1979a, J.Phys., C12, 2551.

Davies,G., 1979b, Solid St.Commun., (in press)

Davies,G. and Hamer,M.F., 1976, Proc.R.Soc.Lond., A348, 285.

Davies,G. and Manson,N., 1979, Diamond Conference, Cambridge (unpublished)

Davies,G. and Nazare,M.H., 1978, Diamond Conference, Oxford, (unpublished

Davies,G. and Nazare,M.H., 1979, Proc.R.Soc.Lond., A365, 75.

Davies,G. and Nazare,M.H., 1980, to be published.

Davies,G. and Penchina,C.M. 1974, Proc.R.Soc.Lond., A338, 375.

de Vos,J.C., 1954, Physica, 20, 690.

Dunn,P., 1976, Diamond Conference, Bristol, (unpublished)

Dyer,H.B. and du Preez,L., 1965, J.Chem.Phys., 42,1898.

Dyer,H.B. and Ferdinando,P., 1966, Br.J.Appl.Phys., 17, 419.

Evans,T., 1973, Diamond Research, Industrial Diamond Information Bureau, Ascot.

Evans,T. and Phaal,C., 1962, Proc.R.Soc.Lond. A270, 538.

Farrer,R.G. and Vermeulen,L.A., 1972, J.Phys., C5, 2762.

Feofilov,C., 1954, Soviet Phys.JETP, 26, 609.

Fitchen,D.B., 1968, in "Physics of Colour Centres", (ed. W.Beall Fowler) Academic Press.

Foy,C.P. and Davies,G., 1979, to be published.

Franck,J., 1925, Trans.Faraday Soc., 21, 536.

Griffiths,J.S., 1964, "The Theory of Transition Metal Ions", Cambridge University Press.

Grimsditch,M.H., Anastassakis,E. and Cardona,M., 1978, Phys.Rev. B18, 901.

Ham,F.S., 1968, Phys.Rev., 166, 307.

Ham,F.S., 1972, "Electron Paramagnetic Resonance", (ed. S.Geshwind) New York: Plenum.

Hoerni,J.A. and Wooster,W.A., 1955, Acta.Cryst., 8, 187.

Hughes, A.E. and Runciman,W.A., 1967, Proc.Phys.Soc., 90, 827.

Kaiser,W. and Bond,W.L., 1959, Phys.Rev., 115, 857.

Kaplyanskii,A.A., 1964a, Opt.Spectry. (USSR), 16, 329.

" 1964b, " " , 16, 557.

Kaplyanskii,A.A., Medvedev,V.N. and Skvortsov,A.P., 1970, Opt.Spectrosc., 29, 481.

Kaplyanskii,A.A., Medvedev,V.N. and Skvortsov,A.P., 1971, Sov.Phys. Solid State, 12, 2867.

Lax,M.E. and Bernstein,E., 1955, Phys.Rev. 97, 39.

Lowther,J.E., 1975, J.Phys., C8, 3448.

Lowther,J.E., 1976, Solid St.Commun. 20, 933.

Lowther,J.E., 1977, Phil.Mag., 36, 483.

Lowther,J.E., 1979, to be published.

Lowther,J.E. and Stoneham,A.M., 1978, J.Phys., C11, 2165.

Maeda,K., 1965, J.Phys.Chem.Solids, 26, 595.

Mainwood,A.M., 1978, J.Phys., C11, L449.

Mitchell,E.W.J., 1965, "Physical Properties of Diamond" (ed. R.Berman) Oxford, Clarendon Press.

Mitchell,E.W.J., 1967, "Science and Technology of Industrial Diamonds" (.ed. Burls), Industrial Diamond Information Bureau, London.

Nedvetskii,D.S. and Gaisin,V.A., 1973, Sov.Phys.Solid St., 14, 2535.

O'Brien,M.C.M., 1964, Proc.R.Soc.Lond., A281, 323.

O'Donnell,K., 1979, Diamond Conference, Cambridge, (unpublished)

Parsons,B.J., 1977, Proc.R.Soc.Lond., A352, 397.

Pryce,M.H.L., 1966, in "Phonons in Perfect Lattices and in Lattices with Point Imperfections", Oliver and Boyd, Edinburgh.

Rutgers,G.A.W., and de Vos,J.C., 1954, Physica, 20, 715.

Sakamoto,N. and Muramatsu,S., 1978, Phys.Rev., B17, 868.

Smith,W.V., Sorokin,P.P., Gelles,I.L. and Lasher,G.J., 1959, Phys.Rev., 115, 1546.

Sobolev,T., 1968, Sov.Phys., Doklady, 12, 665.

Stoneham,A.M., 1975, "Theory of Defects in Solids", Oxford, Clarendon Press.

Stoneham,A.M., 1977, Solid St.Commun., 21, 339.

Sutherland,G.B.B.M., Blackwell,D.E., Simeral,W.G., 1954, Nature, 174, 901.

Tinkham,M., 1964, "Group Theory and Quantum Mechanics", McGraw-Hill.

Walker,J., 1975, Lattice Defects in Semiconductors: Inst.Phys.Conf. ser. 23, 317.

Walker,J., 1977, J.Phys., C10, 3031.

Walker,J., Vermeulen,L.A. and Clark,C.D., 1974, Proc.R.Soc.Lond., A341, 253.

Kannoo M., Stoneham A.M., 1968, J.Phys. Chem.Sol. 29, 1487.

Douglas, I.N., Runciman, W.A., 1977, Phys.Chem. Min. I, 301